POLITECNICO DI TORINO

Department of Electronics and Telecommunications

Master in Biomedical Engineering

Master Degree Thesis

Wearable Microwave Antennas for Brain Stroke Imaging

Supervisors:

Prof. Francesca Vipiana

Dr. Jorge Tobon

Candidate:

Gorana Malesevic

October 2019

Index

Abstract

The following thesis deals with the design and realization procedure of two wearable antenna prototypes, to be included in a microwave system for brain stroke diagnosis and monitoring.

This type of system use one antenna to transmit microwaves into the brain, in order to collect then the field scattered by the tissues with the others antennas of the array. The scattered signal contains the information about the contrast between the electrical properties of the stroke and those of the surrounding tissues, permitting to reconstruct an image of the object. What distinguishes this technique for stroke diagnosis from the others is that it does not use ionizing radiations and it does not involve high costs. Furthermore, it offers the possibility to have a device that is not only transportable, but also wearable. In order to have a wearable device that is also as comfortable as possible for the patient, it must be equipped with flexible antennas, adaptable to the head shape, thus allowing not only the diagnosis of the disease, but also continuous monitoring after its occurrence.

The purpose of this thesis is therefore to investigate the state of the art regarding the materials and technologies used for the production of wearable antennas, to design flexible antennas and to develop a possible procedure for their realization.

During the antenna design phase, the main requirement to be met was to chose materials that have a good compromise between electrical and mechanical properties. In fact, they must allow good bending behavior to the antenna without changing its performance. Taking into account this and others project specifications, two materials were identified to be used as antenna substrate and thus two prototypes, with two different antenna geometries, were developed. Both are wideband monopole antennas, optimized to have 1 GHz as the central frequency of the bandwidth and to work in direct contact with a material that mimics dielectric properties of average brain tissues. The CST Microwave Studio software was used for the design and through a time domain analysis the following

antenna parameters were mainly evaluated: reflection coefficient (s11), electric near-field, surface currents and far-field radiation pattern.

Subsequently, others simulations were done to evaluate the antenna bending and to consider a more realistic operation conditions. For that, the geometry of the object in contact with the antenna in the initial tests (parallelepiped) was replaced with a CAD of the head phantom. This CAD corresponds to the same phantom, 3D-printed plastic object, then used for measurements in laboratory. This involved the insertion of a plastic layer between the antenna and the material representing the brain and consequently changes in the antenna performance. The modifications have been analyzed and a possible solution has been proposed.

The antennas were then built and tested, making measurements of different antenna parameters and in different conditions. This last step was fundamental to obtain a comparison between the simulated and measured data, to understand which critical issues emerge in the construction process and how to overcome or manage them in a future development of the project. Besides this, the thesis proposes an antenna prototype that with subsequent improvements could be used in the mentioned microwave imaging system.

Sommario

La seguente tesi tratta la progettazione e la procedura di realizzazione di due prototipi di antenne wearable, da inserire all'interno di un sistema di imaging a microonde per la diagnosi e il monitoraggio dell'ictus.

Questo tipo di sistema utilizza un'antenna per trasmettere delle microonde nel cervello, per poi acquisire il campo riflesso dai tessuti con le altre antenne dell'array. Il segnale riflesso contiene le informazioni sul contrasto tra le proprietà elettriche dell'ictus e quelle del tessuto circostante, permettendo così di ricostruire l'immagine dell'oggetto. Ciò che distingue questa tecnica di diagnosi dell'ictus dalle altre è che non utilizza radiazioni ionizzanti e non implica costi elevati. Inoltre, essa offre la possibilità di avere un dispositivo non solo trasportabile, ma anche indossabile. Affinchè il device sia indossabile e il più comodo possibile per il paziente, è necessario che esso sia dotato di antenne in grado di adattarsi alla forma della testa, consentendo così, sia la diagnosi della malattia, che il monitoraggio continuo dopo la sua insorgenza.

Lo scopo di questa tesi è dunque quello di indagare lo stato dell'arte per quanto riguarda i materiali e le tecnologie utilizzate per la produzione di antenne indossabili, di progettare delle antenne flessibili e di sviluppare una possibile procedura per la loro realizzazione.

Durante la fase di progettazione dell'antenna il requisito principale da soddisfare è stato quello di utilizzare materiali che avessero un buon compromesso tra proprietà elettriche e meccaniche. Infatti, essi devono permetterle di avere una buona resistenza alla curvatura senza modificare le sue performance. Tenendo conto di questa e altre specifiche di progetto, sono stati individuati due materiali da utilizzare come substrato dell'antenna e si sono sviluppati due prototipi. Entrambe sono antenne a monopolo a banda larga, ottimizzate per lavorare a 1 GHz, in diretto contatto con l'oggetto di analisi, costituito da un materiale con proprietà medie dei tessuti del cervello. Per la progettazione è stato utilizzato il software CST Microwave Studio e con un'analisi nel dominio del tempo sono stati valutati principalmente i seguenti parametri d'antenna: il coefficiente di riflessione

(s11), il campo elettrico vicino, le correnti superficiali e il pattern di radiazione in campo lontano.

Successivamente, sono state eseguite delle simulazioni che verificassero la curvatura delle antenne e altre in condizioni più realistiche, sostituendo la geometria dell'oggetto d'analisi iniziale (parallellepipedo) con il CAD del phantom della testa. Phantom con la stessa geometria di quello utilizzato per le misure in laboratorio, stampato in 3D con materiale plastico. L'inserimento del layer di plastica tra l'antenna e il materiale rappresentante il cervello ha comportato delle modifiche nelle prestazioni dell'antenna. Esse sono state analizzate ed è stata proposta una possibile soluzione.

Le antenne sono state poi realizzate e testate, effettuando le misure di diversi parametri dell'antenna e in condizioni differenti. Quest'ultima fase è stata fondamentale per poter fare un confronto tra i dati simulati e misurati, per capire quali criticità emergono nella fase di costruzione e il come poterle superare o gestire in uno sviluppo futuro del progetto. La presente tesi, inoltre, propone un prototipo di antenna che con successivi miglioramenti potrebbe far parte del sistema di imaging a microonde menzionato.

Ringraziamenti

Il mio percorso universitario sta per concludersi, un percorso che è durato cinque anni. Ora che mi guardo indietro, non mi sembra vero che sono trascorsi così tanti anni e che non dovrò più dare esami e seguire lezioni. D'ora in poi sarà la vita ad insegnarmi il resto, come un po' per volta ha fatto anche negli anni passati, insegnandomi a non mollare mai e a credere sempre di più in me stessa. Così ho scoperto, crescendo, che la forza per superare i momenti più difficili la trovi solo dentro te stesso e quando non basta, nell'abbraccio e nel sostegno dei più cari.

Voglio dunque ringraziare innazitutto i miei genitori che mi hanno permesso di inseguire i miei sogni, sostenendoli sempre, curandosi di loro e di me, proteggendoci. Grazie perché ci siete sempre stati per me, quando avevo bisogno di un aiuto, di un consiglio e di appoggio. Grazie a mio fratello che è stato il mio più grande sostenitore, che è diventato il mio migliore amico e confidente da quando ci siamo separati per la prima volta per i miei studi, capendo quanto fosse forte il nostro legame.

Un grazie grande lo devo alla professoressa Francesca Vipiana che mi ha seguito e consigliato in questi sei mesi di tesi. Grazie per avermi fatto scoprire il mondo della ricerca e per avermi trasmesso la sua passione e determinazione. Grazie al mio correlatore Jorge Tobon, per avermi aiutato sempre quando avevo bisogno e per avermi insegnato che anche un non risultato è un risultato.

Grazie a Emilija, Dako, Milenko e Dragana per avermi sempre sostenuto in questi anni e per aver condiviso con me i momenti più belli e anche quelli più difficili, anche solo ascoltandomi. Grazie a Nikola e Kristina per avermi regalato la loro spensieratezza e il loro sorriso. Grazie a Dajana e a tutti gli zii per avermi sempre incoraggiato. Grazie a tutta la mia famiglia, grande, sparsa per molti paesi, bella.

Grazie a Serena per aver condiviso con me ogni singolo momento di questo percorso universitario, per aver sopportato con me le sessioni d'esame, per l'amicizia sincera in questi dieci anni, un'amicizia che ha sempre superato ogni difficoltà. Grazie per avermi

incoraggiato sempre, per le nostre serate da coinquiline, passate tra gelato, chiacchiere, tisane e tante, ma tante risate.

Grazie a Giuseppe che ha sempre trovato le parole giuste per sostenermi e il tempo per divertirci e scoprire insieme la città che è entrata nei nostri cuori e che piano piano per noi è diventata casa. Mai avrei creduto che il laboratorio di chimica del primo anno di ingegneria mi avrebbe regalato un amico così importante.

Grazie a Vesna e Dejan, due persone speciali, dal cuore grande, che mi hanno sempre capita e sostenuta e che hanno gioito con me per i miei successi.

Grazie a Geni e a Stefano per aver trascorso con me le tantissime ore di lezione di questi ultimi anni, per i tanti progetti portati a compimento insieme; non potevo desiderare compagni di corso migliori. Rimarremo per sempre una squadra fantastica. Grazie infine per aver reso le sessioni d'esame più leggere, per i mille caffè, Milke e Nuvole mangiate insieme davanti alle macchinette del Poli e per le nostre risate, quelle che ormai nascono da uno sguardo e che probabilmente gli altri non capirebbero neanche.

Grazie a Valeria per aver condiviso con me questi mesi di tesi, per aver creduto in me e per avermi spronato nei momenti più difficili. Una persona con cui ricondividerei la scrivania altre mille volte e in cui ho trovato un'amica.

Grazie ad Arianna, Teresa, Alice e Giulia per essere rimaste sempre le amiche su cui so di poter contare, amiche sincere e che vorrò sempre al mio fianco.

Grazie a Milica che ho conosciuto il giorno della mia laurea triennale, quasi per caso, e che ora è diventata una delle amiche più care e speciali che ho.

Grazie infine a Cristina, Federica, Giulia, Angelica, Filippo, Alessandro, Davide e Simone per essere stati compagni di corso che mi hanno reso le giornate di studio e gli esami meno pesanti e con cui ho condiviso i più bei momenti di vita universitaria.

Index Of Figure

Index Of Tables

1. Introduction

1.1 Brain Stroke

1.1.1 Brain Stroke introduction

A stroke is a serious life-threatening medical condition that happens when blood supply to part of the brain is cut off. This situation is caused by a blockage of blood flow or by a rupture of an artery in the brain. The consequence is the sudden death of the brain cells due to lack of oxygen and nutrients. This causes the loss of the abilities controlled by that area of the brain such as memory and muscle control [1]. A stroke is also called CVA, i.e. cerebrovascular accident, or brain attack. There are three main types of stroke, the first two are illustrated in **Errore. L'origine riferimento non è stata trovata.**.1:

- Ischemic stroke: it is the most common type of stroke and is caused by blockage of blood flow in a brain vessel. Usually it is caused by the onset of one of the following problems: blood clots, systemic hypoperfusion (general decrease in blood supply, e.g. in shock), plaques in the cerebral vessels.

- Hemorrhagic stroke: it is characterized by bleeding and results from rupture of a blood vessel. Rupture can be caused by high blood pressure, thinning of the vessel walls, called aneurysm, or by the presence of an arteriovenous malformations (AVMs).

- Transient ischemic attacks (TIAs): also referred to as a mini-stroke, these occur after blood flow fails to reach part of the brain. Normal blood flow resumes after a short amount of time, and symptoms cease [2].
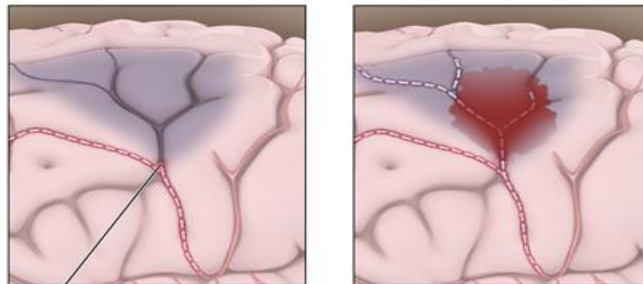
Figure 1.1: Example of an ischemic stroke (left) and an hemorrhagic one (right) [28].

1.1.2 Brain Stroke Consequences And Its Epidemiology

The severity of the damage caused by a stroke depends on its size and the area of the brain affected. The damage varies from a temporary weakness of an arm or leg, to the loss of speech or the permanent paralysis of one side of the body. Some people recover completely from strokes, but more than 2/3 of survivors will have some type of disability [1].

According to a report of the World Health Organization published in 2002, 15 million people suffer stroke worldwide each year. Of these, 5 million die and another 5 million are permanently disabled. The situation has not changed much in the following 14 years, in fact from an analysis carried out in 2016 it emerges that stroke is the second cause of death worldwide and that combined with the ischaemic heart disease accounts for 15.2 million deaths, as can be seen in the graph of Figure 1.2.
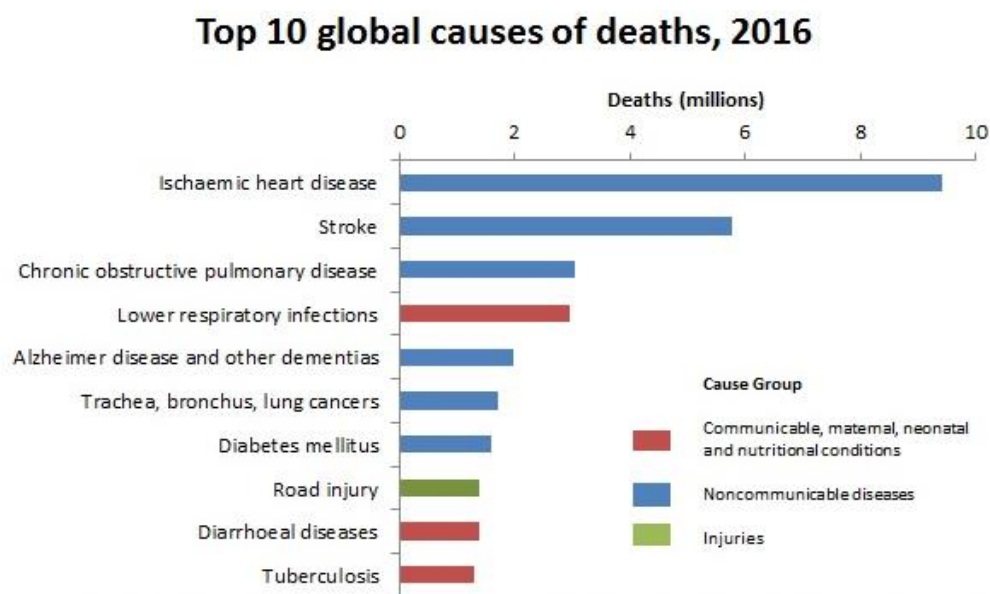
Figure 1.2: Top 10 global causes of deaths in 2016 worldwide, stroke is the second [29].

Such a large number of people suffering from this disease entails also considerable economical impact, in fact it is estimated that worldwide stroke consumes about 2–4% of total health-care costs (in industrialised countries accounts for more than 4%) [3].

In developed countries the incidence of stroke is decreasing in the last decades due to improved management of disease-related risk factors, including hypertension, diabetes, atrial fibrillation, cholesterol and smoking. Despite these efforts, the overall stroke rate

remains high due to the ageing of the population, another problem that health-care systems have to manage. However, it was observed that the mortality due to stroke decreases more rapidly than its incidence, so this means that the percentage of survivors is increasing. This reinforces the need for improved methods to control the disease and places increased demands on health-care and social-care systems. Furthermore, considering that 80% of strokes can be prevented [1] and that the mortality and damage caused by them can be greatly reduced by promptly intervening with the appropriate care tools, it is clear that new technologies are needed for the diagnosis, the treatment and monitoring of this disease.

1.1.3 Medical Rationale

All these motivations lead in one direction, the one with "the aim to further enhance recovery rate and reduce consequences of brain stroke, reason why continuous post-event monitoring of physiological parameters in the acute stage has gained an increasing importance in recent years" [4], [5]. "As a matter of fact, recovery and treatment depend on both early diagnosis as well as close clinical observation, especially during the first few hours after the onset of a stroke" [6]. The sooner the stroke is treated, the less damage it will cause. For strokes caused by a clot it is important to intervene within the first 90 minutes with clotbusting drugs. The diagnosis and the drug delivery could be done in ambulance while patient is still on the way to the hospital, so portability is the main requirement for the new solutions to the problem. Furthermore, there is an increasing need to have a device that does not carry high costs for hospitals, that is not bulky and harmful for the patient. Thus, the requirements that the new stroke diagnosis and monitoring solutions should possess, emerge and they are summarized in Figure 1.3:

Figure 1.3: Requirements that the stroke diagnostic and monitoring systems should satisfy.

In such a framework, the currently adopted techniques for brain stroke diagnosis appear not to be suitable to perform pre-hospital diagnosis and continuous post-event monitoring [7], as can be seen in the analysis done in the Paragraph 1.1.2.

1.1.4 Brain Stroke Diagnostic Techniques

Today there are two principal technologies, based on imaging, that are used for the detection and classification of the brain attack and they are:

- CT (Computerazed Tomography) scan;
- MRI (Magnetic Resonance Imaging) scan;

accompanied by others exams such as electrocardiogram (ECG), blood tests, Doppler ultrasound and arteriography done in order to investigate the possible risk factors and causes. The two scanner are illustrated in Figure 1.4.

Figure 1.4: A MRI scanner (left) and a CT scanner (right) [30].

- **CT scan**

  The first imaging modality employs X-rays source (frequency: $3 \cdot 10^{16}$ Hz to $3 \cdot 10^{19}$ Hz) that rotates around the object to produce cross-sectional images, then joined together to form a 3D reconstruction of the head. Each body layer is divided by the device into elementary volume units (voxel). To obtain the image of the layer the X-ray beam attenuation is calculated for each individual voxel. The different tissues in the human body impose different attenuation to the beam, thus bones absorb the most and look white in the images, soft tissues absorb less and look gray, while air absorbs least and appears black. However, when two different

tissues have a similar absorption coefficient it is difficult to distinguish them. Thus, to analyze cerebrovascular disease the CT imaging is often made through the use of contrast media, which are employed to highlight some structures, like blood vessels, and to perform functional evaluations. This technique nevertheless brings with it a certain number of concerns and risks. The main problem is related to the ionazing nature of the X-rays, in fact they are dangerous for the patient because this type of radiation has enough energy to ionize an atom or a molecule, inducing chemical changes in cells and mutations in the DNA. These type of damages can result in radiation sickness and increase the risk to develop a cancer. Furthermore intravenous contrast agents can lead to anaphylaxis or worsening of renal impairment.

- **MRI scan**

The MRI scans, instead, uses a powerful magnet and RF pulses (commonly in the 1-300 MHz range) to produce images of the anatomy and the physiological processes of the body. The operating principle is based on undergoing the patient to a strong, static magnetic field that induces protons of the tissue water molecules to aligne according to the direction of the field. After that a rotating magnetic field is applied at Larmor frequency, in order to rotate the proton magnetization. They tend to revert to the low-energy state, emitting a radiations that are captured by the scanner. The radiations emitted by the different tissues have different frequency and this difference can be detected to create the image. The MRI technique offers a higher resolution than the CT, managing to distinguish even between a normal and an abnormal tissue, that the CT fails to do. Also this imaging modality sometimes requires the somministration of a dye to make more accurate diagnosis.

Despite the two techniques are now commonly adopted in clinical practice for the CVA treatment, they have drawbacks that push the research to find new solutions, as well as for the reasons seen in Paragraph 1.1.1. The disadvantages of both imaging modality are summarized in Table 1.1:

Table 1.1: Disadvantages of CT and MRI scanners.

CT scan	MRI scan
Not portable	
Expensive	
Bulky	
Often needs contrast agents	
Ionizing radiation	Time consuming (10-30 min)
Does not distinguish well soft tissues	Patients with pacemaker can not be scanned
	Claustrophobia
	Noisy
	Patients must remain very still for a long time

1.2 MWI Technology

As seen in Paragraph 1.1, existing modalities for brain imaging do not solve more and more specific needs. An emerging technology that potentially meets all of the requirements, shown in Figure 1.3, is represented by the MicroWave Imaging (MWI). First experiments based on this imaging method have been done by Larsen and Jacobi as part of a feasibility study in the 1980s, applying it to image perfused organs. Over the years, MWI has advanced significantly with the development of robust imaging algorithms and simple, but fast, data acquisition hardware supported by the advancements made in microelectronics, material science, and embedded systems [8]. These improvements enhanced its application in many pathological cases. In fact today, it is considered as a potential alternative imaging technique to the aforementioned ones because of its numerous benefits and some complementary characteristics with respect to the others methods. The microwave imaging for medical application uses electromagnetic signals in the frequency range of 0.5 – 10 GHz, as shown in Figure 1.5, thus it does not induce ionizing and thermal effects on analysed tissues, in controlled condition.
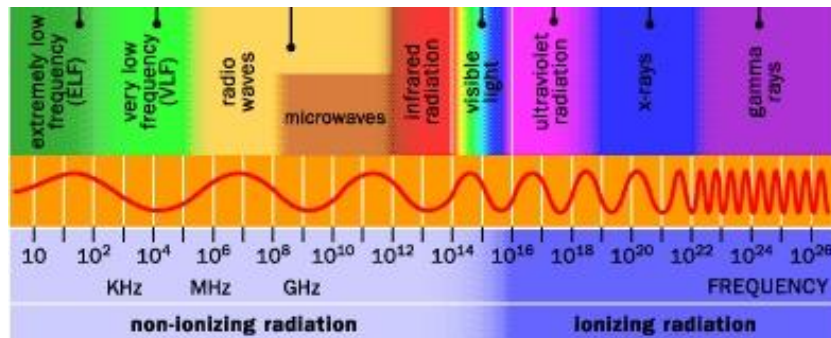
Figure 1.5: Electromagnetic spectrum [31].

1.2.1 Physical Principles Of MWI

The physical phenomenon underlying this technology is that of electromagnetic scattering, that occurs when an electromagnetic field crosses a medium. The interaction between the field and the material results in a field perturbation that brings with itself information about the electric properties of the medium. In particular, the modification depends on the morphology of the target and on the contrast between the electric parameters (relative permittivity and conductivity) of the target and those of the surrounding medium [7]. The scattered signal is measured and a map or image is obtained thanks to a reconstruction algorithm that processes them and extracts information about the target's properties.

The reconstruction algorithms are substantially divided into two categories: qualitative and quantitative algorithms. The quantitative ones usually are based on the inverse EM scattering problem with the aim to reconstruct the distribution of the dielectric properties of the tissues, either in 2D or 3D. Instead, the qualitative ones use radar-like techniques to generate the 2D or the 3D image of the intensity of the scattered signal that shows the location of the strong scatterer as the tumor [8].

1.2.2 MWI System Components

An MWI system consists of the following main parts, as illustrated in the block scheme in Figure 1.6:

1. an array of antennas;
2. a switching matrix;
3. a Vector Network Analyser (VNA);
4. a control unit (typically a computer);
5. a display.

The antennas are located around the object to be imaged and can operate as transmitters (TX) or receivers (RX). Only one antenna transmits the signal at a time: it transmits the RF signal generated by the VNA while the rest of the antennas are connected to the receiver in order to collect the scattered signal.
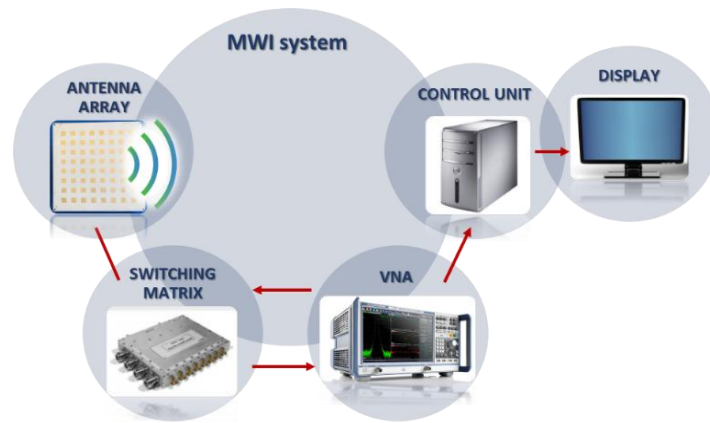
Figure 1.6: Block scheme of the basic setup for microwave imaging system.

The signal is routed to one single antenna at a time by the switching matrix. A complete scan requires iterating until all the antennas are configured as TX. The scattering parameters obtained from a complete scan are stored by the VNA as a NxN matrix [9], where N is the number of the antennas of the system. The file produced by the network analyser is acquired by the computer that processes the information through the reconstruction algorithm and creates the image on the monitor.

The overall design involves others parts, such as, usually, a matching medium that facilitates the coupling of the field with the body, in order to reduce the reflections caused by large differences in electrical properties between the object and the medium in which the antennas are kept, i.e. air. The simplest matching medium is water. Therefore, the microwave imaging equipment consists of few elements that together form an imaging system that are:

> cost-effective and easily maintainable, it usually costs a fraction of the cost of the components necessary for the others diagnostic methods;

> compact and mechanically robust, usually a multi-static measurement configuration is employed, in which the antennas are fixed;

> time-saving, the switching matrix connected to the VNA are extremely fast as a result of electronic or electro-mechanical switching;

> portable and also wearable if the antennas are positioned on a helmet;

> harmless, thanks to the frequency range adopted;

> complementary to the others imaging techniques, that allow in particular for the brain imaging, pre-hospital imaging and post-event continuous monitoring.

1.2.3 MWI For Brain Stroke Diagnosis And Its Others Applications

One of the most widely investigated medical application of microwave imaging is the detection of breast tumor [8], but there are many others medical applications:

- brain imaging for stroke and tumor;
- bone imaging to detect leukemia and osteoporosis;
- heart imaging to investigate the presence of myocardial infarction;
- soft tissues and joint imaging.

The applicability of MWI for brain diseases monitoring and imaging relies on the existence of a significant change in the electric properties of brain tissues when a stroke occurs [7]. In fact, haemorrhagic stroke can be detected thanks to the fact that blood has higher permittivity and condutivity than the grey and white matter, that implies that a contrast can be observed. Also in case of ischemic stroke a contrast exists because the blood clot has lower values of dielectric properties as compared to the brain.

In the last decade many research groups worldwide have worked on the design and development of systems based on microwave technology for brain imaging [10] [11], in fact it has become its second most important application. In particular, two groups have reached good results in developing promising devices that recently have undergone clinical trials: Persson and his colleagues have designed an MWI device at Chalmers University in Sweden and have proven with clinical trials that it can distinguish the two types of strokes, allowing a pre-hospital diagnosis; Semenov and his team works in the field of EMT (ElectroMagnetic Tomography) since 1990s and with EMTensor GmbH located in Vienna, Austria, has developed a device that reconstructed for the first time worldwide the stroke of a patient.

The proposed EMT technologies are very different either for the external aspect, as is possible to see in Figure 1.7, and also for the type of algorithms and approach. The first is wearable and have a small number of antennas (12 patch antennas) [12], the second is not wearable, but transportable, and has 160 ceramic loaded waveguide antennas [13]. This fact demonstrates that the MW technology is a fertile soil for the brain imaging and

that there are plenty of different ideas to enhance the reduction of post-stroke disabilities and consequences.

Figure 1.7: Comparison of two different MWI devices developed for brain imaging: the one on left is a prototype of a Sweden group of reserchers, the one on right is an EMTensor GmbH product [12] [13].

1.3 Thesis Outline

The present thesis deals with the design of wearable microwave antennas for brain stroke imaging. In the first Chapter an introduction to the work is given, exposing the main characteristics of brain stroke disease, the technologies currently used to diagnose it, compared to MicroWave Imaginag technology. In Chapter 2 the main notions of transmission lines and antennas are provided, describing the main antenna parameters to be monitored during its design. In the next Chapter the state of the art regarding wearable antennas are analyzed, identifying the most used materials.

Chapter 4 describes the imaging system in which the antenna to be designed has to be inserted. In it the design specifications and the main steps of the design process are listed. In Chapter 5 and 6 the different design steps for the two antenna prototypes are explained in detail. Here therefore, it is explained how the prototypes satisfy the imposed requirements and which materials and geometries have been chosen.

Chapter 7 describes the phase of realization of the Antenna Prototype 1 and the tests performed in the laboratory to evaluate its performance and its consistency with the simulated data. Finally, Chapter 8 contains the conclusions of the thesis work and the possible future developments of the project.

2. Theoretical Foundations

An antenna is a transducer that is able to transform the signal traveling on a conductor into electromagnetic wave radiated in the space. For the energy transfer to take place three elements are needed:

1. the antenna;
2. the Transmission Line (TL);
3. the signal generator at the required frequency.

This chapter provides an overview of the first two components, discussing the transmission line theory principles and the antenna parameters and properties. In this thesis, the frequency range considered is that of RF (RadioFrequency) that includes the microwave frequency range.

2.1 Transmission Line Theory

In order to radiate an electromagnetic field, the antenna have to be connected to a RF generetor through a transmission line. A transmission line is a component responsible for the transmission of the RF power from the source to the radiating part, in the most efficient way, maintaining as lowest as possible the attenuation of the signal and its distortion, in both directions of the lines.

There are two main types of transmission lines, i.e. coaxial cables and waveguides; in this thesis is considered the first type. The coaxial cable consists of a conductive core, a dielectric material, that isolates it from the third layer constituted by a conductive shielding. There is also an outer protective layer, made usually in PVC, not illustrated in Figure 2.1 (a), where instead are present the others three layer in section. The TL is represented symbolically by two parallel lines, as shown in Figure 2.1 (b), where one line represents the core and the other line the shielding.
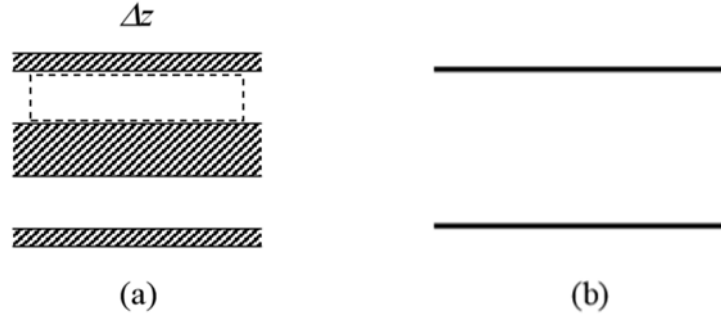
Figure 2.1: a) Portion Δz of the transmission line, shown in section, and b) its corresponding symbolic representation [14].

The voltage and the current along a transmission line are not constant and depend on time and on the longitudinal coordinate *z*, so they are expressed as *v(z,t)* and *i(z,t)*. This is due to the non ideality of the conductor and dielectric materials, in fact there are dissipations and leakages. The voltage and current variations are described by the Telegrapher's equations that have the following general solution:

$$V(z) = V_0^+ e^{-jkz} + V_0^- e^{+jkz} \qquad (2.1)$$

$$I(z) = Y_\infty V_0^+ e^{-jkz} - Y_\infty V_0^- e^{+jkz}$$

where *k* is the phase constant obtained from $k = \frac{2\pi}{\lambda}$, in which λ is the wavelength of the signal. V_0^+ and V_0^- are two arbitrary constants that can be calculated once the load and the source characteristics are known. Instead, the term Y_∞ represents the characteristic admittance of the TL, defined as the reciprocal of the characteristic impedance Z_∞, considered as the input impedance of the transmission line whose length is infinite.

Thus, both *V(z)* and *I(z)* result as a linear combination of two waves, a wave that propagates in the positive direction of *z* (apex +) and a wave that moves in the opposite direction (apex -). They are called forward and backward waves, respectively. When they are both present with the same amplitude, it is said that a stationary wave is moving along the line [14].

12

Consider now a two-port device, i.e. a quadrupole connected to two transmission lines, as the one illustrated in Figure 2.2.
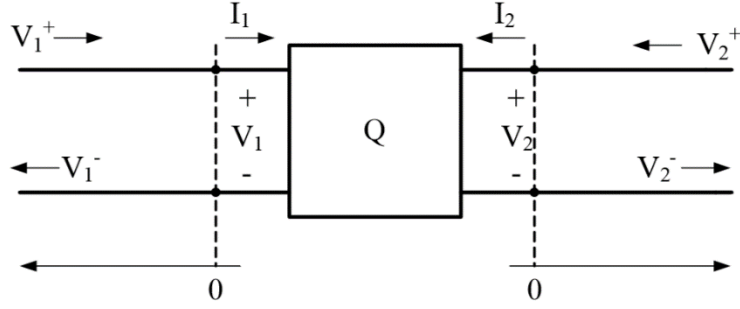
Figure 2.2: Two-ports device with input and output signals.

The charateristic admittance and impedance of one line are obtained as:

$$Y_\infty = \frac{1}{Z_\infty} \tag{2.2}$$

$$Z_\infty = \frac{V^+}{I^+} = -\frac{V^-}{I^-} \tag{2.3}$$

$$V_i = V_i^+ + V_i^- \quad , \quad I_i = I_i^+ + I_i^- \tag{2.4}$$

considering *V(z)* and *I(z)* in *z=0*.

To study the signal power transfer efficiency, from one port to the other of this network, and the reflections present at each port, it is necessary to introduce the power flow waves a_i and b_i (i=1,2), moving like illustrated in Figure 2.3.
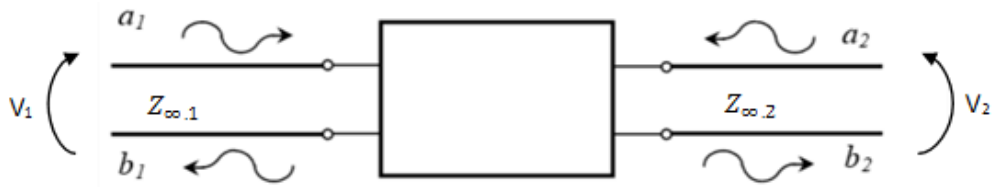
Figure 2.3: Two-ports device and the related incident and reflected parameters.

The latter parameters are defined as:

$$a_i = \frac{V_i + Z_{\infty,i} I_i}{2\sqrt{Z_{\infty,i}}} = \sqrt{Y_{\infty,i}} V_i^+ \tag{2.5}$$

$$b_i = \frac{V_i - Z_{\infty,i} I_i}{2\sqrt{Z_{\infty,i}}} = \sqrt{Y_{\infty,i}} V_i^-$$

13

For two-port device, the scattered power flow waves b_1 and b_2 are expressed as:

$$b_1 = S_{11}a_1 + S_{12}a_2 \tag{2.6}$$

$$b_2 = S_{21}a_1 + S_{22}a_2$$

The scattered waves on the different lines depend on the incident waves at all ports [14]. This system of equations can be expressed in a easier way with a matrix form:

$$[b] = [S][a] \tag{2.7}$$

in which emerges the square *[S] matrix*, called *scattering matrix*. It contains in the main diagonal the reflection coefficient of the i-th port when all the others are terminated (impedance equal to Z_∞) and in the other positions of the matrix, the transmission coefficients of port j to port i. For a generic N-port device the scattering matrix and its S parameters can be written as:

$$S = \begin{pmatrix} S_{11} & S_{12} & \dots & S_{1n} \\ S_{21} & \dots & \dots & S_{2n} \\ S_{n1} & \dots & \dots & S_{nn} \end{pmatrix} \tag{2.8}$$

$$S_{ij} = \left. \frac{b_i}{a_j} \right|_{a_k=0,\, k \neq j} \tag{2.9}$$

In particular, the S parameters contained in the main diagonal are very important during the design of a network. In fact, they rapresent the quantity of reflections present in the considered transmission line, the percentage of the reflected signal with respect to the incident one. So, during the design process is fundamental to maintain the reflection coefficients very low, close to 0 in the linear scale or as negative as possible in dB. In order to obtain that, the load must be matched with the source of power, in particular there must be impedance matching, so that the input impedance of the load (Z_L) is equal to the output impedance of the source (Zg). Otherwise, the mismatching leads to the generation of standing waves which imply that the amplitude of the voltage on the line is no longer constant.

$$S_{11} = 0 \leftrightarrow Z_L = Z_\infty \tag{2.10}$$

Other two relevant parameters for the evaluation of the matching between source and load are:

- Return Loss (RL), that indicates the losses due to the mismatching of the load and is defined in dB:

$$RL = -20log|\Gamma|\ dB \qquad (2.11)$$

$$\Gamma = \frac{V_0^-}{V_0^+} = \frac{Z_L - Z_g}{Z_L + Z_g} \qquad (2.12)$$

where Γ is the voltage reflection coefficient, with similar meaning to the reflection coefficient S, but that consider the amplitudes of the voltage waves instead of the power flow waves. So, a matched load has a Γ = 0 and a $RL = \infty$ (no reflected power).

- Voltage Standing Wave Ratio (VSWR), that measures the quality of the impedance matching between the load and the line:

$$VSWR = \frac{1 + |\Gamma|}{1 - |\Gamma|} \qquad (2.13)$$

When VSWR = 1 means that there is a perfect matching.

The circuit model of the network used in this thesis is illustrated in Figure 2.4, where there are the source of microwaves, the antenna as load and the coaxial cable as transmission line. Usually the antenna is matched to 50 Ω, standardly used as output impedance of the source and as characteristic impedance of the coaxial cable.
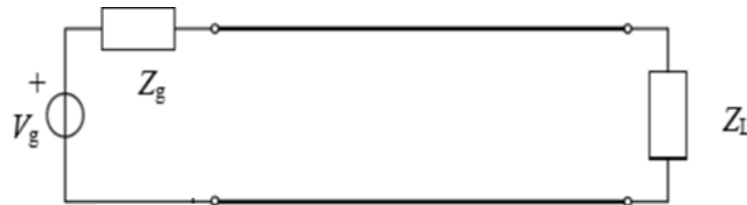
Figure 2.4: Circuit representing a load, e.g. an antenna, connected to its source of power through a TL.

To allow the maximum power transfer and thus satisfy the necessity of impedance matching, different techniques are avaible. The double stub technique is discussed in this

thesis due to the fact that is the one used during the design process of the antennas. "A stub is a short-circuited section of a transmission line connected in parallel to the main transmission line" [15]. An example of two stubs added to a transmission line is reported in Figure 2.5.
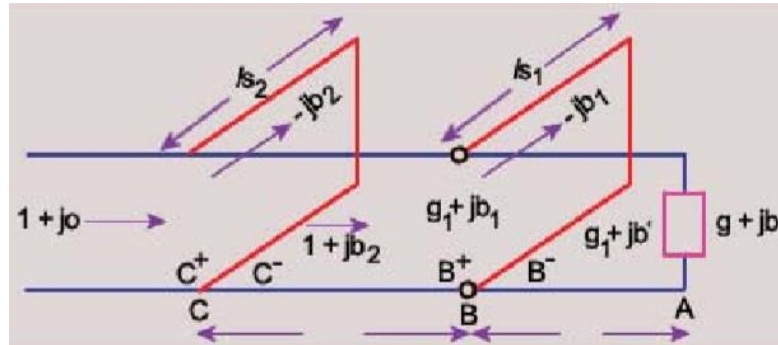
Figure 2.5: Double-stub technique for impedance matching.

Positioning two stubs of appropriate length on the line, at certain distance from the load, it is possible to reach the impedance matching because the impedance seen from the source is not only those of the load but is balanced by that of the stubs. What happens is that the reflected waves from the load and from the stubs completely cancel each other, resulting in no backword signal toward the source.

2.2 Antennas

2.2.1 Antennas overview

The antennas are fundamental in the field of wireless telecommunications. They are able to radiate electromagnetic waves in the medium that surrounds them, transmitting power in certain directions and thus transfering information. An antenna can work as a receiver or as a transmitter. In the last case it is seen as a load for the feeding line, hence its behavior is described through its input impedance, reflection coefficient and radiation pattern.

Depending on the frequency range in which they work and on the applications, antennas may have very different forms. There are several types of antennas and they can be classified by different criteria, the most common are the radiation pattern and the structure.

A possible classification is the following:

- *Omnidirectional antennas*

  They radiate the power homogeneously in the surrounding space and are divided in four main categories:

  - Dipole
  - Monopole
  - Collinear
  - Slotted waveguide

- *Directional antennas*

  They radiate preferentially in one direction and can be of different nature:

  - Sectorial
  - Patch antennas
  - Cantenna
  - Yagi
  - Biquad
  - Dish

2.2.2 Antenna Parameters

The space surrounding an antenna can be divided into three regions, visualized in Figure 2.6: the reactive near-field, the radiating near-field (Fresnel) and the far-field (Fraunhofer). To evaluate some characteristics of an antenna, such as its radiation pattern, it is necessary to consider the electromagnetic field in the far-field, because in the near-field the radiation pattern still varies with distance. In the reactive near-field the antenna does not propagate yet, since the electric and magnetic field are out of phase.
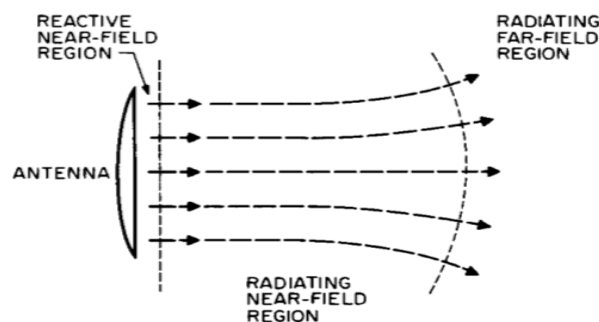
Figure 2.6: Regions in which the space surrounding an antenna is divided.

- *Radiation pattern*

  The radiation pattern of an antenna is a graphical representation of the spatial distribution of the power received from the source and radiated in the surrounding space. It shows the power density per unit solid angle in the different directions, forming a surface whose points are identified by an angle ϑ, an angle φ and by the distance r from the origin, proportional to dPrad/dΩ. The antennas usually have a main direction in which they radiate, this form the main lobe, the lobes in the others directions constitute the side lobes. The radiation pattern can be expressed through different plots, the most used are that in spherical coordinates, but also 2D plots in polar and cartesian coordinates are employed. These three types of graphs are illustrated in Figure 2.7.

  | (a) | (b) | (c) |
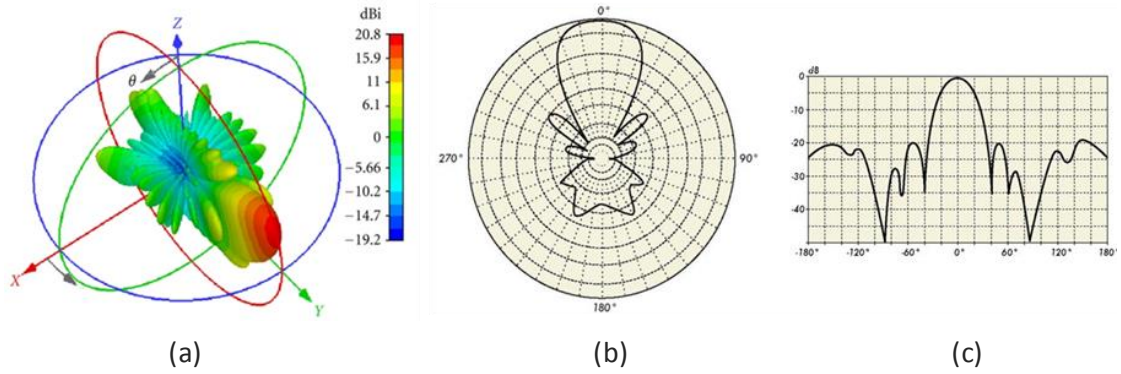
  Figure 2.7: a) 3D representation of a radiation pattern. b) Radiation pattern in 2D polar coordinates. c) Radiation pattern in 2D cartesian coordinate.

- *Directivity*

  The directivity of an antenna is an important parameter that is defined as the ratio between the radiation intensity in one direction and the average radiation intensity over all the directions:

$$d(\vartheta,\varphi) = \frac{\left.\dfrac{dP_{rad}}{d\Omega}\right|_{(\vartheta,\varphi)}}{\dfrac{P_{rad}}{4\pi}} \tag{2.14}$$

$$D = 10log_{10}(\max d(\vartheta, \varphi)) \tag{2.15}$$

  where D is the directivity in dB of the main lobe.

18

- *Gain*

A parameter used instead to measure the antenna performance in terms of radiation efficiency in one direction is the gain, defined as:

$$g(\vartheta,\varphi) = \frac{\left.\dfrac{dP_{rad}}{d\Omega}\right|_{(\vartheta,\varphi)}}{\dfrac{P_{in}}{4\pi}} \tag{2.16}$$

- *Input impedance and antenna radiation efficiency*

When an antenna operates in transmitting mode, it behaves as a load for the source, thus it is characterized by an input impedance, defined as:

$$Z_{in} = R_{in} + jX_{in} \tag{2.17}$$

where the resistive part R_{in} is due to the non ideality of the antenna materials and involves a dissipated power (P_{loss}) lost in heat. The remaining part of the active power (P_{in}) absorbed by the antenna is radiated as P_{rad}. Thus, it is possible to define another parameter, the antenna radiation efficiency:

$$\eta = \frac{P_{rad}}{P_{in}} \tag{2.17}$$

- *Bandwidth*

The bandwidth of an antenna indicates the range of frequencies over which the antenna is able to properly operate. In this range the antenna satisfies a parameter specification, such us generally gain, radiation pattern, VSWR and S11. In this thesis, referring to the bandwidth means considering the frequency range between the two points of S11 which are at -10 dB.
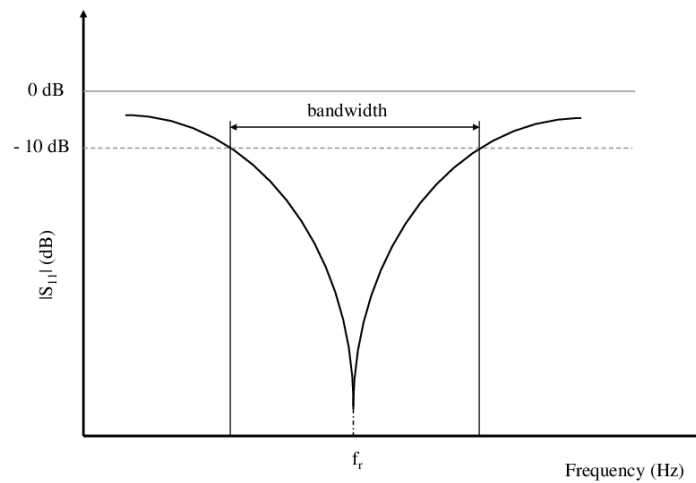
Figure 2.8: An example of an antenna bandwidth.

2.2.3 Planar Monopole Antennas

A planar monopole antenna is constituted by a ground plane and a planar element that radiates the electromagnetic signal. The antenna is fed applaying the driving signal between the ground plane and the planar element. This is the aspect in which dipole and monopole antenna differs the most, in fact to transmit the signal to the dipole antenna it is applayed between two identical conductors. The planar monopole antenna is usually printed on FR4 substrate and present various geometries, such as triangular, rectangular, circular and elliptical disc.

A monopole antenna can be seen as a dipole antenna, with the bottom half of a vertical dipole antenna substituted with the ground plane, thanks to the image charges method. A rapresentation of the situation is shown in Figure 2.8. What changes is the radiation pattern and thus the voltage and energy involved. In particular, the pattern of a monopole with a perfectly conducting, infinite ground plane is identical to the top half of a dipole pattern [16]. However, they both have omnidirectional pattern.
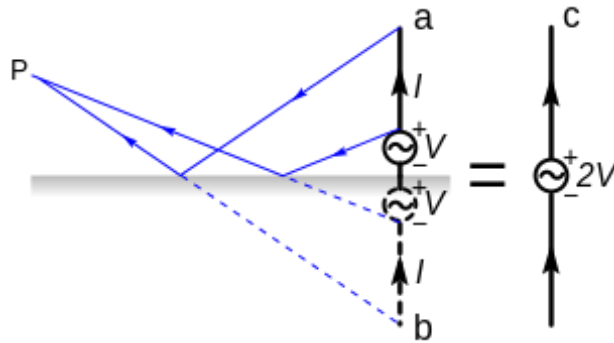
Figure 2.9: Method of image charges applayed to a monopole antenna [16].

This type of antennas are convenient because they have compact and simple structure, easy production processes and wide impedance bandwidth. In the microwave imaging system involved in this thesis, printed monopole antennas are used.

3. Wearable Antennas

3.1 Introduction

The purpose of this thesis is to design a flexible antenna prototype for the MiBraScan brain imaging and monitoring system which will be described in detail in the Chapter 4. The antenna to be designed must therefore be flexible, while retaining the same performance as the antennas currently used in the imaging system. The current antennas are monopole wideband antennas printed on a rigid substrate of FR4, surrounded by a matching medium that allows them to obtain a better impedance matching with the tissues of the brain to be analyzed. Almost all the systems currently in development use the matching medium, as it has been seen in the Chapter 1. Since the matching medium is often thick several centimeters and since there are many antennas that constitute the system, the result is a portable imaging system, that is however bulky and not comfortable. Thus, wearable and on-body matched microwave diagnostic systems could pave the way to providing an effective and continuous patient monitoring system in the future.

Wearable antennas for diagnostics offer many advantages over the conventional rigid antennas such as:

- conformality and comfortability;
- flexibility that facilitates the wearability, the embedding and the portability;
- better response to mechanical solicitations;
- they works in close proximity to the head and does not need matching medium;
- "a configuration of rigid antennas arranged around the head creates asymmetrical distances between the antennas and the skin of the head which will result in an undesired reflection that might lead to poor imaging" [11];
- development of more compact diagnostic systems.

3.2 State Of The Art

Analyzing state-of-the-art literature it can be seen that two routes have been substantially taken to reach the goal of antenna flexibility, both for diagnostic imaging applications and for wireless applications, in which the antenna interacts with the tissues of the human body to send useful information about the body to a receiver.

The two strategies are summarized in the diagram of Figure 3.1 and can be expressed as following:

- Fully textile antennas, in which only textile materials are used, both for the conductive parts and for the substrate;
- Non-textile antennas, made with non-textile materials, thus polimers, plastics and metals;

The hybrid approach is rarely used and consists of using textiles for the substrate and conventional metals for the conductive parts. The two strategies are discussed in the following paragraphs of this chapter, reporting the most used materials for the two techniques. These materials are illustrated in Figure 3.1.
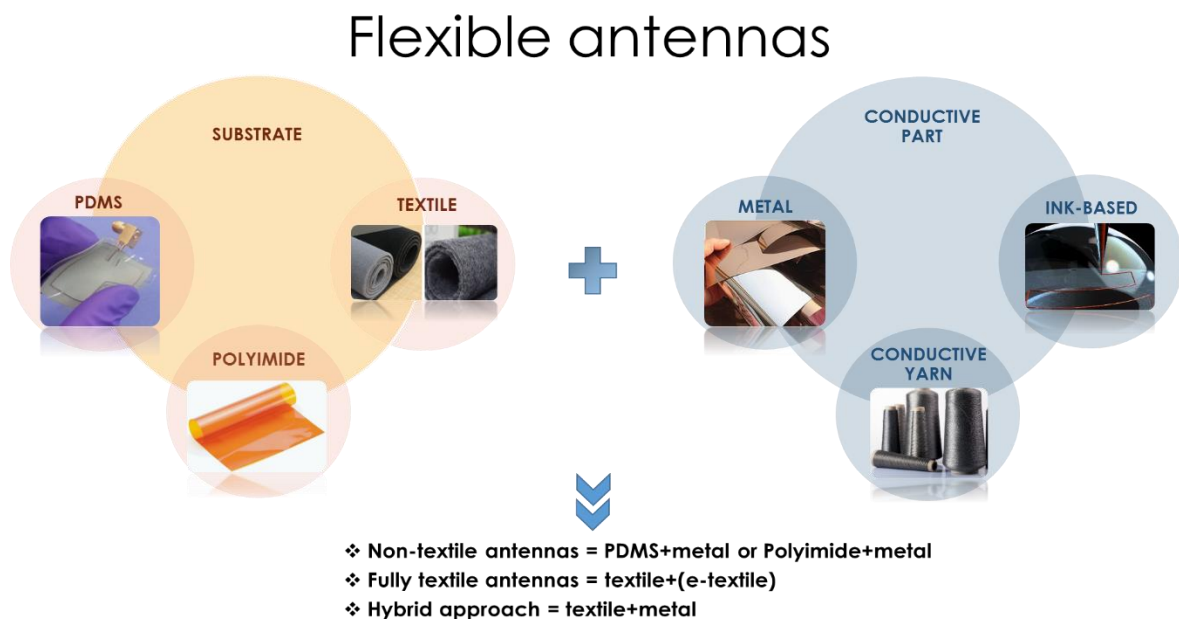
Figure 3.1: Currently used materials for the realization of wearable antennas and strategies adopted.

3.2.1 Fully Textile

Wearable antennas made of textile materials can be grouped together in the cases described below.

Embroidered with pure metal fibers weaved

This type of antenna has the conductive part made of twisted metal wires. However, they have two negative aspects: overall antenna performance strongly affected by the direction of the stitches at high frequencies, reduced flexibility of the final antenna and breakages of the threads issues.

E-threads

A solution proposed to the issues of the previous antenna type is constituted by the e-threads, i.e. electro-threads, that are conductive threads realized in different manner:

- *polymer-based conductive yarns*: are easy to process because their mechanical properties are similar to traditional embroidery threads.
- *metalized textile fibers*, obtained using two tecniques:
  1) the conductive coating/plating is applied on the surface of a non-conductive textile after the weaving process;
  2) conductive fibers are incorporated (via interweaving) in the textile structure.

NWCFs-based (New Waste Calcining Facility based)

This type of antennas are made of conductive fibers casually arranged and bonded together. They are manufatured with the same methods used for the e-threads and have the same properties, but unlike e-threads, NWCFs are not affected by fraying. They have some advantages: cost-effective and time-saving fabrication technique that is industrially scalable, suitable for fabricating antennas with complicated geometries.

Inkjet based

This type of antenna realize the conductive parts, printing them with inkjet printers. In this way the assembling issues are overcomed, but with this technique there is a limitation in the achievable resolution, which strongly depends on the surface roughness

of the substate. Thus, this antenna type is suitable only for wearable applications up to 3 GHz.

Example of fully-textile antenna

An example of fully-textile antenna used for the monitoring of the progression of neurodegenerative diseases is represented by the one developed by Saied et al. (see Figure 3.2). It operates in the frequency range 1-4.2 GHz and is made of: felt (εr= 1.55 , tanδ= 0.068) for the substrate and conductive textile (Shieldex Zell, adhesive with heat) for the conductive parts [17].
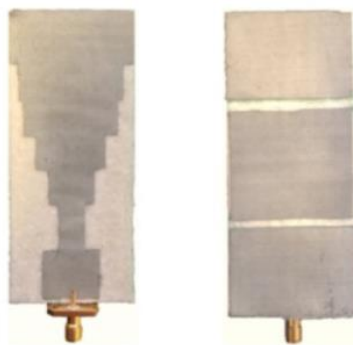
Figure 3.2 Fully-textile, directional, wideband antenna developed by Saied et al. for brain imaging [17].

3.2.2 Non-Textile

The most used materials for non-textile wearable antennas are the PDMS (Poly DiMethyl Siloxane) and the PI (PolyImide). Also other rubbers and polimers are adopted, like the Urethane rubber. The main properties of the PDMS are:

- thermally stable, flexible and has homogenous properties;
- low-cost features, simple fabrication process;
- easy to manipulate.

It has the drowback of having low permittivity, which limits the size miniaturization and the impedance matching with biological tissues. This disadvantage however is overcomed by using fillers that increase the permittivity, like the graphite.

The Polyimide is characterized by the following properties:

- flexible and thermally stable over a wider range of temperatures than PDMS;

- breaking strength is surprisingly high and the elongation is about 70%;
- good chemical resistance;
- excellent adhesion to copper foil;

Its disadvantage is that it has low permittivity and actually it can not be filled with other powders or materials in order to increase the permittivity. Thus its performance has to be further studied and tested for the brain imaging, to evaluateif its usage is suitable for this application. The permittivity of the PI and of the PDMS are reported in Table 3.1.

As conductive parts, the noon-textile antennas use the conventional silver and copper layers.

Table 3.1 Relative permittivity of PI and of PDMS.

Material	εr
PDMS	2.8
PI	3.5

Examples of non-textile antennas

A first example of a non-textile antenna is that of Abbosh et al. [11] designed for head imaging. They develop an antenna whose substrate is made of PDMS loaded with graphite and Al2O3. The radiating part and the ground plane instead is made with copper foil. In their study the antennas demonstrate good bending properties and radiating capabilities. Popovic and her colleagues studied the usege of the PI substrate for breast cancer detection [18]. A Kapton Polyimide isolation superstrate was also adopted to isolate the whole antenna arrey. They have obtained promitting results and very good antennas flexibility. These two antenna examples can be seen in Figure 3.3.
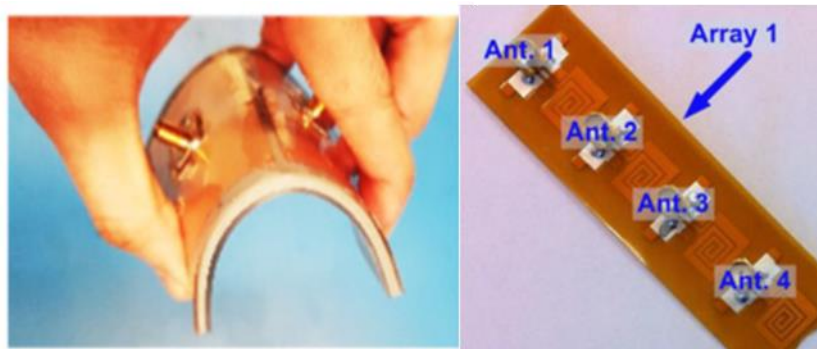
Figure 3.3 Two antenna array prototypes: (left) PDMS based antennas and (right) PI based antennas [11], [18].

4. Design Specifications and Main Steps

4.1 MiBraScan System Overview

The specific MWI system considered in this thesis is "MiBraScan – Microwave Brain Scanner for Cerebrovascular Diseases Monitoring" [19]. It is a research project of national significant interest, supported by the Italian Minister for Education, University and Research (MIUR). The main innovative characteristics of this device are those described in Table 4.1.

Table 4.1 Tools of MiBraScan and its related features.

TOOLS	FEATURES OBTAINED
front-end electronics	portable
low-cost involved technologies	cost-effective
non-ionizing radiations and low power equipment	non-invasive
tailored processing algorithms and proper hardware implementation	real-time imaging
additional images supplied	support to diagnosis
stroke time evolution tracking	bedside continuous monitoring

The hardware system of MiBraScan is reported in Figure 4.1 and consists of five main elements: antennas array, switching matrix, VNA, control unit and monitor.

Figure 4.1: MiBraScan main hardware components [20].

Initially, the object of study consisted in a 3D-printed cylindrical phantom made of acrylonitrile butadiene styrene (ABS), filled with a liquid that mimics the brain [20]. It was surrounded by 12 antennas, placed on the perimeter of a circular support. Thus it was carried out 2D measurements, at different levels of the phantom height. The currently used phantom is a 3D-printed realistic head phantom, adopted in order to consider more realistic condition. It was made with a particular resin starting from the geometry of a CAD that mimics the head shape. Also the number of antennas is now different, in fact the array consists of 24 antennas placed around the head phantom like illustrated in Figure 4.2 (a). They, together with their coupling medium (black blocks in figure 4.2 (a)), form the helmet.

To find the best spatial distribution of the antennas around the phantom and the most appropriate number of antennas, it was made a study [7]. From it emerges that the optimal number of probes is 24, good compromise between measurements' resolution and SNR of the acquired signal, while the best configuration is that shown in Figure 4.2 (b), where the antennas are uniformly spaced over the considered surface and whose orientation and exact positioning is quite irrelevant on the performance of the reconstruction algorithm, that is robust on this front [21].
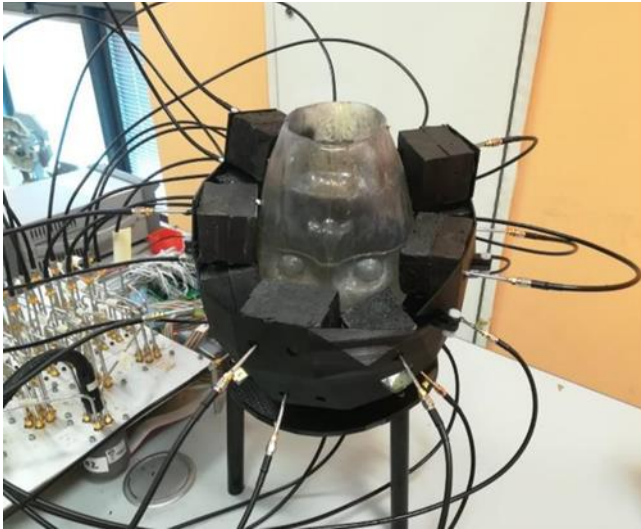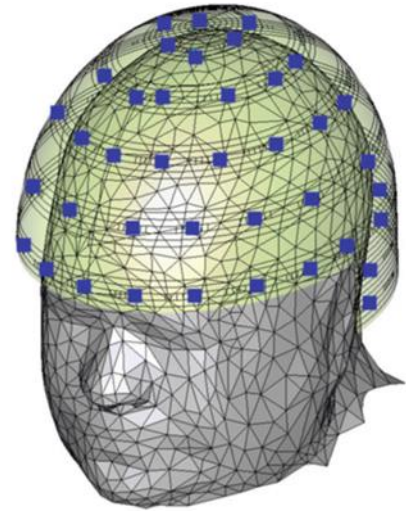
| (a) | (b) |

Figure 4.2: (a) 3D-printed currently used head phantom and helmet containing the 24 antennas [22]. (b) Antennas spatial distribution [7].

The 24 antennas are connected to a two port VNA through a 24x2 switching matrix, that is "built of electromechanical coaxial switches and semi-rigid coaxial cables to minimize

losses and maximize path isolation" [22]. One antenna at a time acts in TX mode, while the others are receiving the scattered signal. The data acquisition is over when all the antennas (in fixed position) have been in transmitting mode. This type of acquisition results in a multi-static multi-view scattering matrix, used then for the image reconstruction.

The reconstruction algorithm adopted in MiBraScan is the Truncated Singular Value Decomposition (TSVD) that uses the differential data matrix (difference of the scattering matrices measured at two different instant of time) in order to reconstruct the image.

The matching medium used is a mixture of urethane rubber and graphite powder, with a permittivity of ε_{mm} = 23.1 and a conductivity of σ_{mm} =0.3 S/m, at the operating frequency of 1 GHz.

4.2 Design Specifications

The Paragraph 4.1 provides an overview of the environment wherein the wearable antenna, subject of this thesis, had to be inserted. The characteristics of the specific imaging system and its medical application determine the specific requirements that the antenna must satisfy. The project specifications for the design of the present wearable antenna are reported in Table 4.2 and concern substantially three aspects: the working frequency band, the substrate material, the type of antenna and its size.

Table 4.2 Antenna design specifications.

Working frequency band	
Resonance frequency	1 GHz
Bandwidth (-10 dB)	> 500 MHz (wideband)
Passband |S11|	below -10 dB
Substrate material	
Thickness	< 10 mm
Flexibility and robustness to bending	
Compatibility with human tissues	
Antenna type and its size	
Planar monopole antenna	
Length L	48 mm
Width W	30 mm

4.2.1 Working Frequency Band

To assess the optimal frequency range to be used in brain stroke imaging one needs to consider two important factors: the spatial resolution obtainable and the penetration depth of the probing field. As a matter of fact, the smallest variations in millimeters that can be detected is inversely proportional to the frequency of the incident wave, as also the penetration depth of an electromagnetic radiation in a human tissue decreases, as the frequency used increases. Furthermore, as the working frequency increases, the SNR (Signal to Noise Ratio) of the scattered signal decreases. The penetration depth of the probing wave is strictly related to the amount of incident power that penetrates into the head. It is necessary to maximize this amount in order to have an adequate scattered signal. So the goal is to use the highest possible frequency, which, however, allows for sufficient signal penetration depth and a reliable SNR.

Another fact to be taken into account is the presence of diverse tissues into the head, with different electrical properties and thickness. This involves a layered structure of the head, with at least five discontinuities as illustrated in Figure 4.3. So, the wave radiated by the antenna has to go across the following tissues: skin, fat, bone, CSF (CerebroSpinal Fluid) and brain.
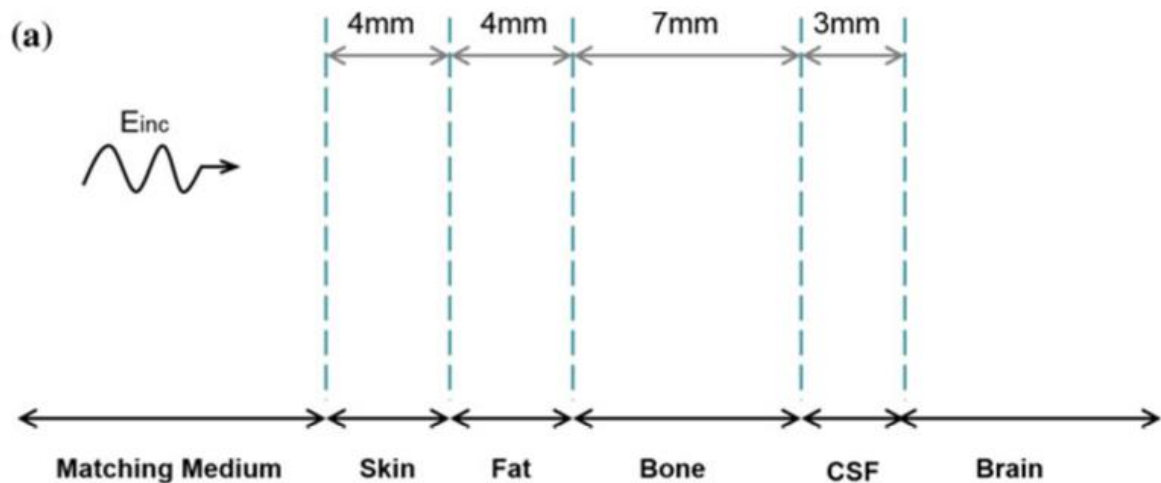
Figure 4.3: Planar layered structure of the head with the different tissues [7].

This layered structure has been studied by Scapaticci and his colleagues during the development of the MiBraScan system. In particular, they have simultaneously assessed

the effect of the frequency and of the permittivity of the matching medium on the transmittance T [7], defined as below:

$$T = 1 - |\Gamma|^2 \tag{4.1}$$

where Γ is the reflection coefficient, defined in Equation 2.12 and having in this case the following expression:

$$\Gamma = \frac{Z_{head} - Z_{mm}}{Z_{head} + Z_{mm}} \tag{4.2}$$

Z_{mm} = impedance of the matching medium

From this study emerges that a forbidden band of frequencies exists. Like it is possible to see in Figure 4.4, in the 1.5-2.5 GHz range the transmittance coefficient is lower than 0.5, independently from the value of matching medium permittivity. So this band is not suitable for brain imaging, as confirmed by other studies, including that of Semenov and Corfield [23], where the matching medium was not considered. Instead, they have estimated the attenuation of the incident signal as a function of frequency.
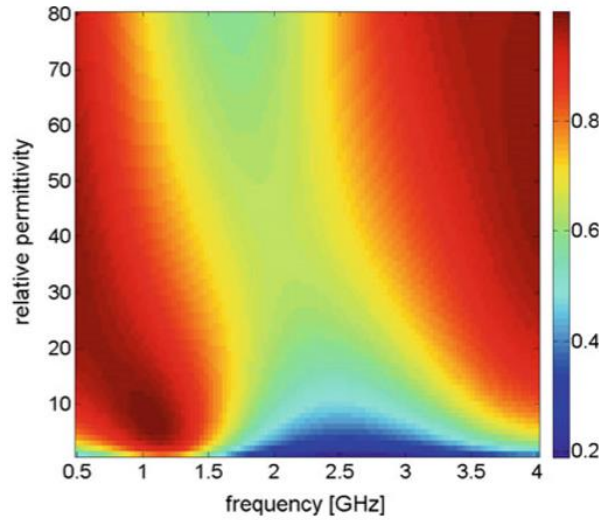
Figure 4.4: Effect of frequency and permittivity of the matching medium on the transmittance [7].

The present antenna had to be designed without matching medium, to be on-body matched, but the forbidden band exists independently of its presence and characteristics, thus, the present wearable antenna has been designed to work in the frequency band 0.5-1.5 GHz, with a bandwidth as wide as possible, centered at 1 GHz.

4.2.2 Substrate Material

In Chapter 3 the characteristics that a wearable antenna, and in particular its substrate, must possess in order to be used in the imaging of human tissue have been explained. The properties that the antenna substrate must have are substantially:

- flexibility and robustness to mechanical solicitations, like bending;

- compatibility with human tissues;

- thickness lower than 10 mm in order to guarantee the flexibility of the antenna, because even the most flexible of the materials loses its ability to bend if it is very thick. This thickness constraint reflects also the need of having a wearable antenna, thus not bulky.

These properties determine the design requirements for the antenna substrate.

4.2.3 Type of Antenna and its Size

Another constraint is represented by the size and the type of the antenna. In fact, in order to maintain the same configuration and number of antennas of the current MiBraScan system, it was chosen to not change the width and the length of the antenna substrate, that are respectively W=30 mm and X=48 mm. The antennas used in the current version of the imaging system are planar wide-band monopole antennas, printed on a FR4 substrate with thickness of 1.6 mm.

4.3 Design Strategy

4.3.1 Choice of the Substrate Materials

The wearable antenna design has been carried out starting from the requirements reported in the previous paragraph. In order to fulfill them, a detailed investigation of the materials currently used for wearable applications of wide-band antennas (Chapter 4) has first been done. Among all the materials analysed, two materials has been chosen as antenna substrate:

1. *Antenna Prototype 1:* Urethane rubber loaded with Graphite;

2. *Antenna Prototype 2:* Polyimide.

Such a choice has been made to analyze and compare two materials, with not only different characteristics, but that follow two different approaches to reach the objectives set by the project specifications:

1. *Antenna Prototype 1:* exploits a higher permittivity of the substrate to have a better coupling of the probing signal with the brain tissues, reserving less flexibility;
2. *Antenna Prototype 2:* focuses on flexibility and reduced thickness, without achieving a high level of coupling as the material's permittivity is low.

The reasons why the two materials meet the project requirements are explained below.

Urethane rubber loaded with Graphite

The first approach consists in satisfying the materials' requirements, reported in Table 4.2, adoperating materials that allow to realize a better impedance matching between the radiated field and the brain. To do this, it has been decided to use materials whose electric and mechanical properties are well known. In fact, it has been chosen those used by the MiBraScan team as a coupling medium. The mentioned materials are mixtures of urethane rubber and graphite powder, in different weight-ratio, as it is possible to see in Table 4.3, for a sample of 40 g.

Table 4.3 Mixtures for antenna substrate with different weight-ratio of graphite and rubber.

Name	Urethane rubber	Graphite powder
G20%	32 g	8 g
G25%	30 g	10 g
G30%	28 g	12 g
G35%	26 g	14 g

The urethane rubber is part of the rubber family and thus have high elasticity, what differentiates it from the others rubbers is its high resistance to abrasion, atmospheric agents and the mechanical strength, as shown in Figure 4.5 [24]. Moreover it maintains the same properties in a fairly wide range of temperatures (from -20 °C to 70 °C) and is suitable to be placed in contact with human body, also when it is filled with graphite.

Item	Weak ←							→ Strong
Mechanical Strength	Silicon	Low Elastic	Butyl	Ethylene	Nitrile	Fluorine	Chloroprene	Urethane
Weather Resistance	Nitrile	Low Elastic	Chloroprene	Urethane	Butyl	Silicon	Ethylene	Fluorine
Abrasion Resistance	Silicon	Low Elastic	Butyl	Ethylene	Chloroprene	Urethane	Nitrile	Fluorine

Figure 4.5: Comparison of the urethane rubber properties with those of the others rubbers [24].

The permittivity and the conductivity of the mixtures has been measured, reporting the values present in Figure 4.6 and Figure 4.7. From the graphs of these figures it is possible to notice that with the increase of graphite concentration, the materials have an increasing permittivity and conductivity and therefore a better coupling with the brain ($\varepsilon_b = 40$). But what has also been observed, after the realization of some test samples, is that the increase in the quantity of graphite leads to a decrease in the flexibility of the material. Despite this, all of the four materials (G20, G25, G30, G35) are potentially enough flexible for the application, thanks to the good elongation properties of the rubber. Therefore, what has been mainly evaluated during the design phase is the influence of the graphite on the mechanical properties and the optimal thickness (anyhow lower than 10 mm), in order to establish the best material.
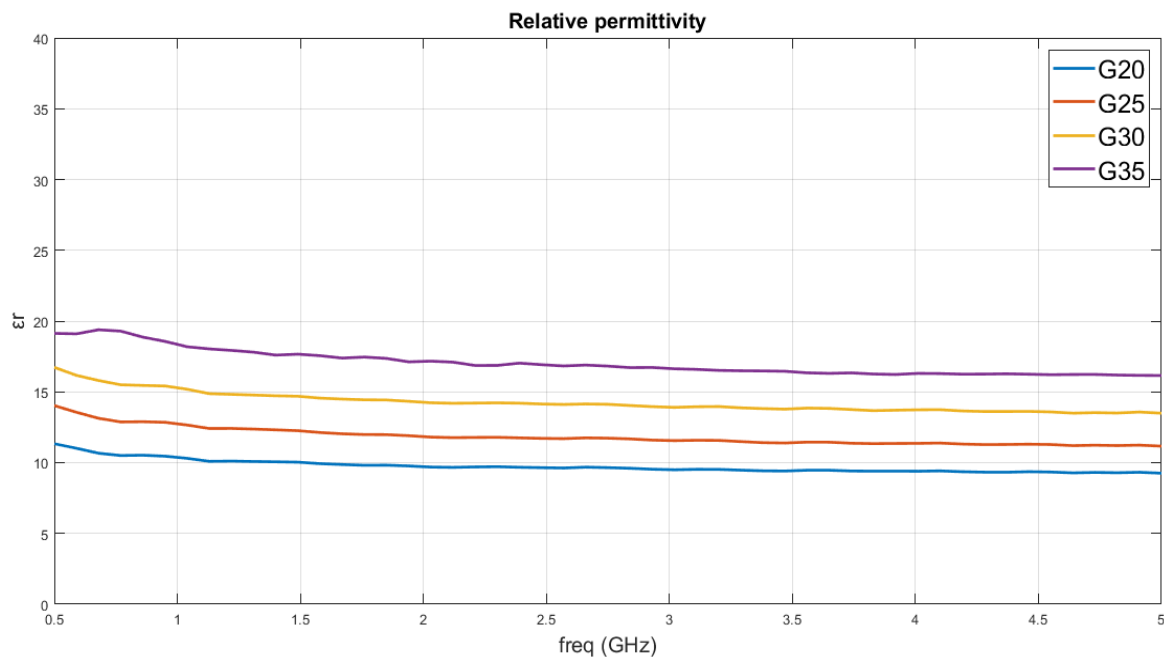
Figure 4.6: Relative permittivity of the four mixtures.
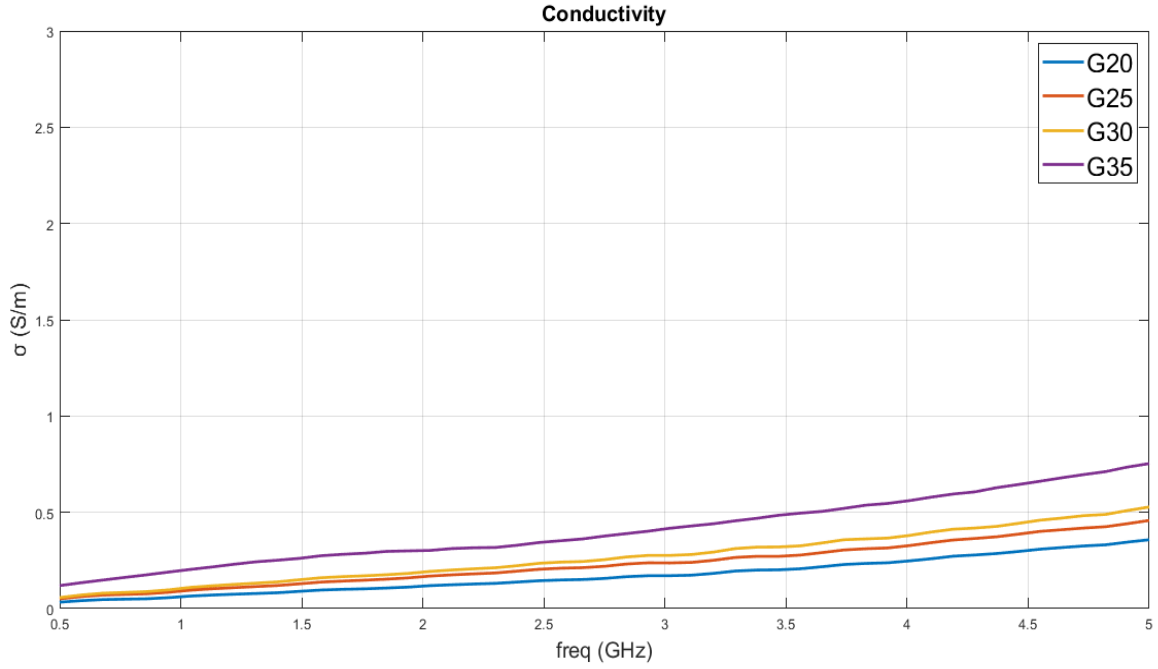
Figure 4.7: Conductivity of the four mixtures.

Polyimide

The Polyimide has been chosen for its good mechanical properties, already discussed in Chapter 3. The advantages of this material allow to it to satisfy the project specifications:

- thickness of 150 µm;
- ultra-high flexibility and bending capabilities;
- thermal stability until 232 °C;
- good chemical resistance and compatibility with human body.

The Polyimide used for the simulations has ε_{PI} = 3.4 and tangent loss of 0.0027 .

4.3.2 Design Steps

The project requirements concerning the working frequency band and the antenna type and its size has been met following a procedure that was outlined step by step during the design phase. A procedure that was built up testing several routes, discarding the more intricate and inefficient ones and noting those that with a few steps allowed to reach more significant results.

The procedure, reported in Figure 4.8, includes the following steps:

1) *Model construction*: costruction of a head model that reflects its characteristics (volume and average electric properties) and importing of the rigid antenna's CAD, modeling the currently used antenna in the MiBraScan system.

2) *Parameterization*: the second step consists in the assignment of a parameter for each relevant dimension of the antenna geometry and of the head model.

3) *Assignment of initial values*: an initial value in millimeters is assigned to each created model parameter and each material is characterized with its ε and σ.

4) *Optimization*: the central part of the antenna design is the one that involves the antenna geometry parameters' tuning in order to analyse the antenna performance and to find the parameters' values that lead to the best results. This phase may also include the variation of the materials properties. The performance are evaluated through the simulations in CST MWS, done with the antenna in direct contact with the head model. In this step is fundamental to change one parameter at a time, to see the performance changes introduced only by that variation, and to make gradual changes. At the end of the optimization process an antenna prototype that meets all the design requirements are obtained.

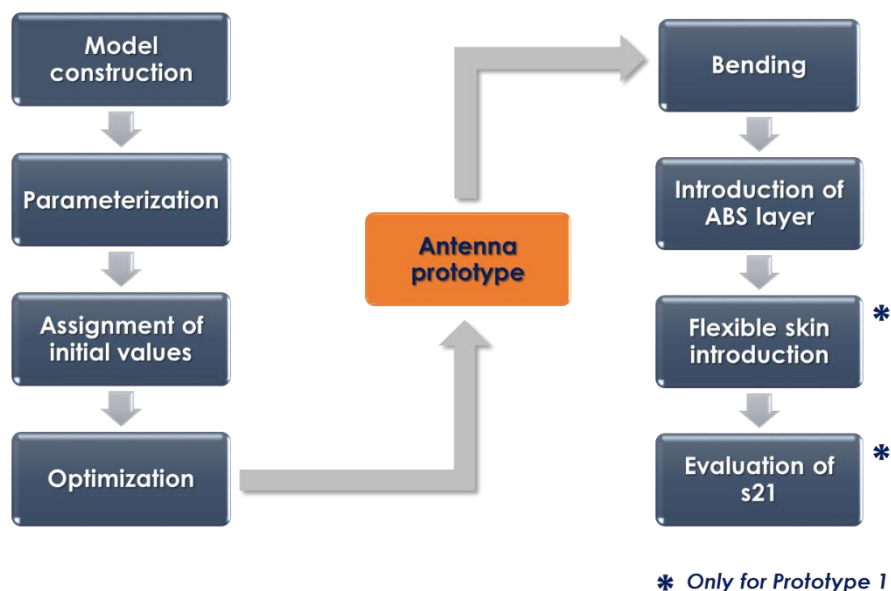Figure 4.8 Main steps of the design process.

5) *Bending*: the antenna prototype before being realized has to undergo to the second part of the design process that puts the antenna in a more realistic condition. In fact, the antenna is firstly subjected to the bending tests. Two types of tests are

done: bending on cylinders with different radii and bending on the CAD of head phantom, that mimics the head shape.

6) *Introduction of ABS layer*: if the prototype successfully overcome the bending test, then there is the substitution of the material of the outer phantom layer, with the material really used to make the phantom, i.e. Acrylonitrile Butadiene Styrene (ABS). The previous material has the same properties of the phantom interior, that is the average electrical properties of the brain. Instead, the plastic layer has very different dielectric properties thus it increases the reflections and interferes with the transmission. This test is crucial to investigate the variations in the antenna performance because the real phantom is made of ABS.

7) *Flexible skin introduction:* to improve the antenna radiation capabilities after the introduction of the ABS layer, different solutions are tested. They all consists in a flexible skin that plasticizes the external shell of the phantom, what changes are the materials and the thicknesses. The best solution is applied.

8) *Evaluation of s21:* the last test consists in the evaluation of the transmission capabilities of the designed antenna, using the antenna and phantom model obtained at step 7. This means simulating the condition in which two antennas are applied to the phantom and excited one at a time. Two different configurations of the antennas are tested.

4.3.3 CST Microwave Studio

The design of the two antenna prototypes has been done using the CST Microwave Studio (CST MWS), a layout window of it is shown in Figure 4.7. It is a featured software for the 3D analysis, design and optimization of electromagnetic components and systems in the high frequency range. CST MWS provides different simulation techniques, the one used in this work is the Time Domain Solver (TDS). The TDS excites the computational volume (space considered for the simulation containing the model) using a port that transmits a time domain signal. In particular, in this work waveguide ports and a Gaussian pulse are used. The pulse numerically propagates throughout the different medium, losing its energy. Part of its energy will be radiated, dissipated by the lossy materials and absorbed by other ports. The simulation stops when the energy decays to a convergence level defined by the user.
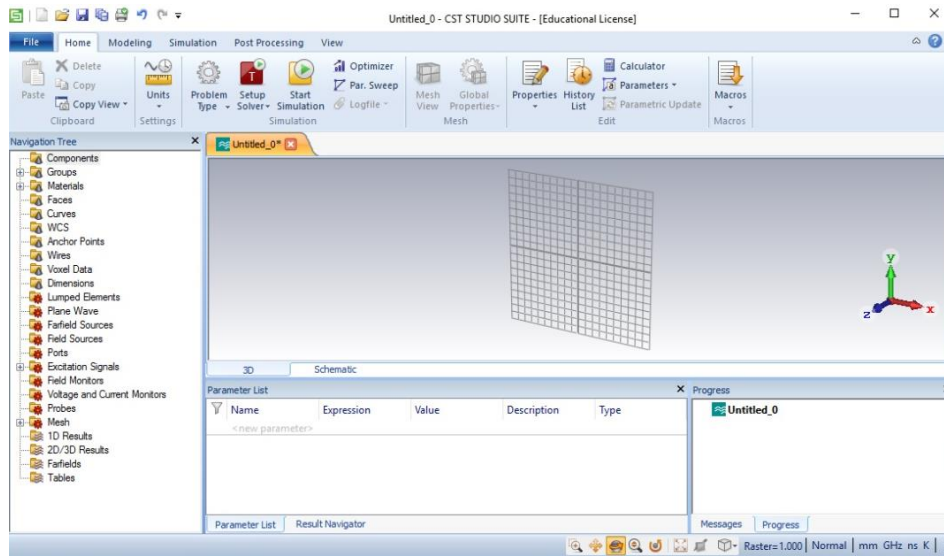
Figure 4.9: Layout window of CST MWS simulation program.

The computational volume is divided into many hexahedral mesh cells (in general $\Delta x \neq \Delta y \neq \Delta z$). The electromagnetic field is calculated in each mesh cell (discrete location) at discrete time instant. To obtain a good discretization and an accurate reconstruction of the fields, at least 10 mesh cells per wavelength must be used. In Figure 4.8 are reported the basic definitions of the hexahedral mesh adopted in this thesis.
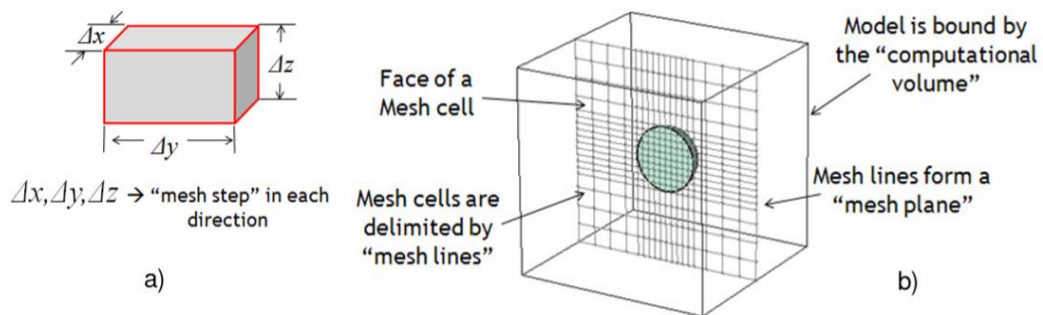
Figure 4.10: Basic definitions for the a) single mesh cell and b) for the hexahedral mesh.

5. Antenna Prototype 1

5.1 Design Process

5.1.1 Model construction, its parameterization and assignment of initial values

The first step of the design process consists in the modeling of the environment in which the antenna works and in the modeling of the antenna too. At each relevant dimension of the antenna geometry and head model is then assigned a parameter and an initial value in millimeters. Each material is also characterized with its ε and σ.

Antenna model

The initial antenna model was already available and consisted in the currently used rigid antenna model of the MiBraScan system. Thus, it has been only imported in the CST MWS. The antenna of the MiBraScan system consists in a wide-band monopole antenna, printed on a FR4 substrate. The top side contains a transmission line with a double stub matching circuit and the triangular shaped radiating part, as shown in Figure 5.1 (a). The bottom side is made of a ground plane that terminates close to the beginning of the radiating trangle, as illustrated in Figure 5.1 (b) [20]. The antenna is fed with a coaxial SMA feed, perpendicular to the antenna plane.
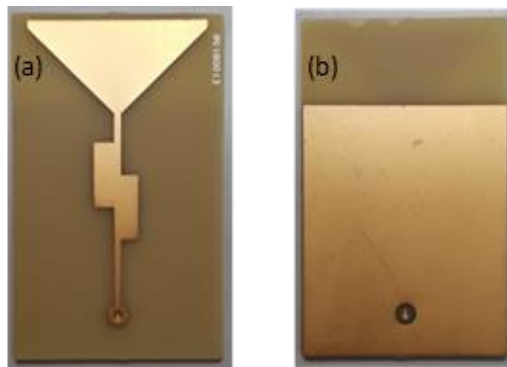
Figure 5.1: (a) Top side of the MiBraScan antenna and (b) its bottom side.

The sizes of this antenna has been saved in order to constitute the starting values of the antenna geometry parameters, see Table 5.1. The parameters of the geometry are indicated in Figure 5.2 and the antenna model are shown in Figure 5.3.
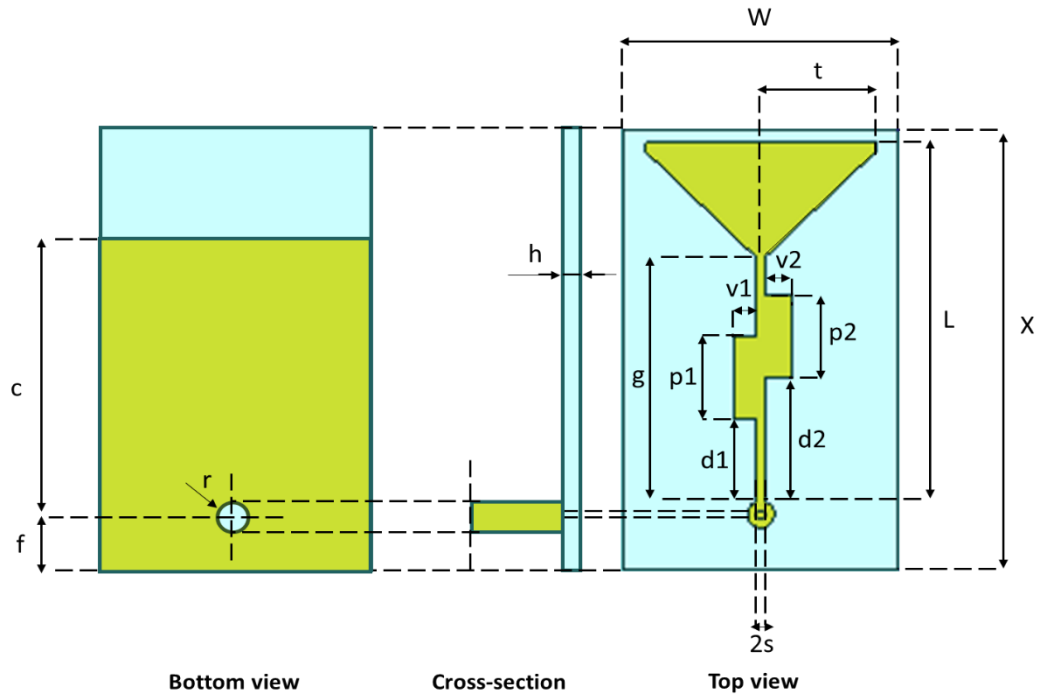
Figure 5.2: Bottom view, cross-section and top view of the rigid antenna model with the assigned parameters.

Table 5.1 Initial values of the antenna geometry parameters.

Parameter	Size (mm)	Parameter	Size (mm)
X	48.00	v1	2.44
W	30.00	v2	2.90
h	1.60	d1	9.09
r	1.60	d2	13.59
f	6.00	g	28.00
c	29.40	t	12.64
		s	0.50
		p1	9.00
		p2	9.00
		L	40.50
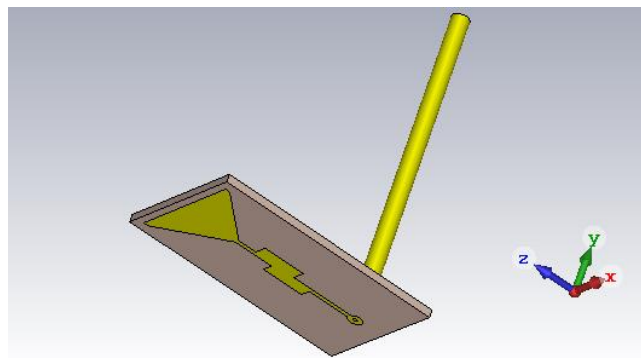
Figure 5.3: Antenna model in CST MWS.

The materials assigned to the antenna components are those listed in Table 5.2, where can be seen that as initial material for the substrate is used the G20 as it is the most flexible. In the optimization phase it will be compared with the others materials to determine which one gives the best results for the specific system.

Table 5.2 Materials assigned to the antenna prototype 1 components.

Component		Material	Properties
Radiating part and TL		Copper annealed	σ = 5.8e+07 S/m
Ground plane		Copper annealed	σ = 5.8e+07 S/m
Substrate		G20	ε = 10.5 and σ = 0.01 S/m (1GHz)
Coaxial SMA feed	Core	Copper annealed	σ = 5.8e+07 S/m
	Dielectric	PTFE	ε = 2.1
	Outer layer	Copper annealed	σ = 5.8e+07 S/m

Head model

To model the head a parallelepiped is used in order to start the design with a simple geometry (see Figure 5.4). The values assigned to the parallelepiped parameters are reported in Table 5.3. Its volume is similar to that of the head and it is filled with a material that has the averaged permittivity and conductivity of the different brain tissues, called in this work *average_brain*. It is characterized by ε_b = 43 and σ_b = 0.7 S/m at 1 GHz, the behavior at the others frequencies are illustrated in Figure 5.5. In this way the antenna will be optimized while it is in direct contact with the head model.
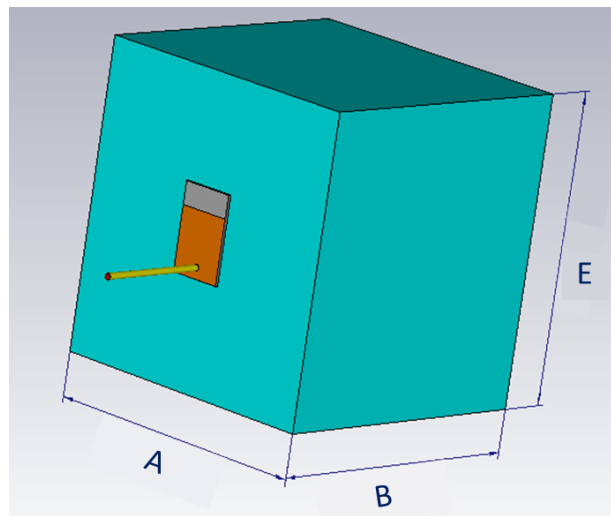
Figure 5.4: Head model (parallelepiped) and antenna model.

Parameter	Size (mm)
A	160.00
B	160.00
E	168.00
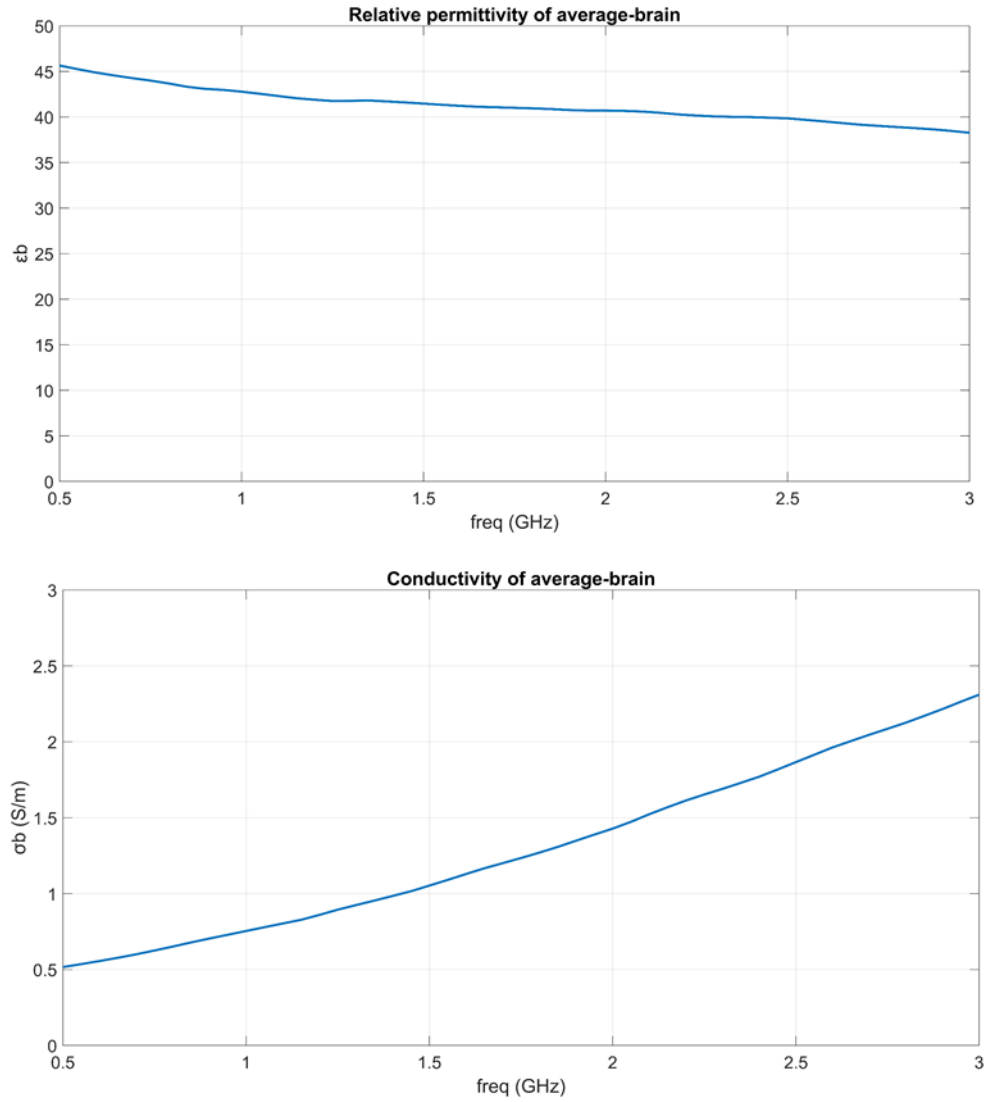
Figure 5.5: Relative permittivity and conductivity of the average_brain.

5.1.2 Optimization

A monopole antenna with a triangular radiating part does not have precise formulas that correlate the main dimensions, such as the width of the triangle and the length of the transmission line, with the electrical properties of the substrate and its thickness, as

happens for example for a rectangular microstrip patch antenna. Therefore, in order to optimaze the antenna parameters general considerations about the monopole antennas behavior has been followed, together with the observation of the results obtained from the sweep of the parameters on CST MWS.

1. *Sweep of h parameter*

The first parameter that has been considered for the optimization was the thickness of the antenna substrate, indicated as h. The sweep of parameter h ranges from 1.6 mm, thickness of current MiBraScan antenna, to 10 mm, the limit imposed by the flexibility requirement. In Figure 5.6 are reported the trend of |S11| at the different h values.

The value of h that has been chosen as the best is 5.0 mm because it allows to have a resonance frequency close to 1 GHz (1.13 GHz) with acceptable value of |S11| peak (-14.48 dB) and moreover it is a value of thickness that allows flexibility and an easier realization in the laboratory. Lower thicknesses are difficult to obtain.
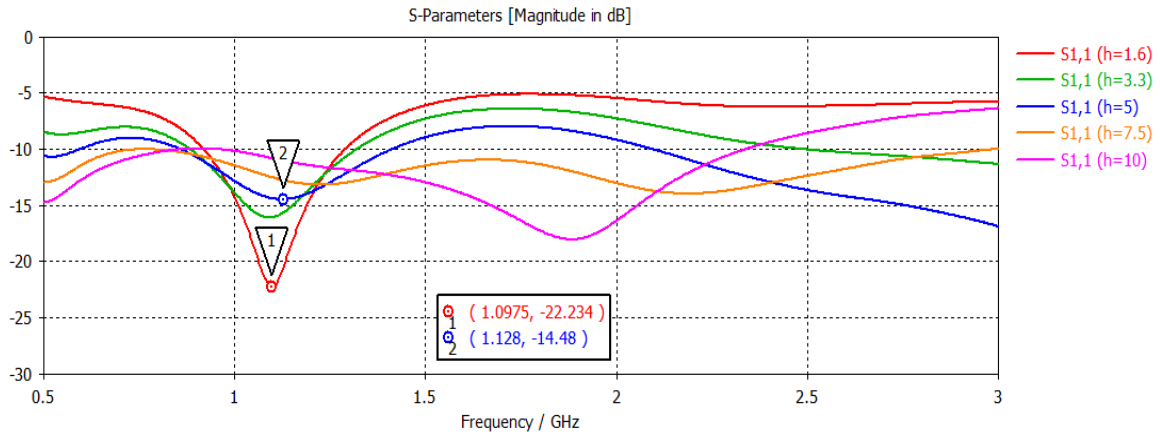
Figure 5.6: Simulated sweep of the parameter h of the antenna made in G20.

2. *Others parameters modifications*

To understand the influence of the others parameters modifications on the antenna |S11|, different simulations has been done. The relative versions of the antenna with the changed parameters are reported in Table 5.4 and the plot of the reflection coefficient is illustrated in Figure 5.7. In the last mentioned figure it is possible to see that the parameters that mainly influence the antenna behavior are the parameters s, d1 and d2. This is in agreement with the fact that the position of the two stubs on the transmission line and the width of the line, are important factors to reach the impedance matching and

therefore a good s11. The version of the antenna that is closer to the design requirements is the fifth (ver5), so it will be used for the continuation of the study.

Table 5.4 Changed dimensions of some of the antenna parameters.

Parameter (mm)	v1	v2	s	d1	d2
Version 1	2.44	2.90	0.50	9.09	13.59
Version 2	**4.00**	**6.00**	**1.00**	9.09	13.59
Version 3	4.00	6.00	**2.00**	9.09	13.59
Version 4	**2.94**	**3.40**	2.00	9.09	13.59
Version 5	0.50	1.00	2.00	**14.50**	**16.00**

Figure 5.7: Simulated influence of changes of the antenna's dimensions on its performance.

3. Comparison of the four urethane rubber-graphite mixtures

Now it is necessary to shift the antenna resonane frequency closer to 1 GHz, thus the antenna performance has been analyzed using the four different substrate mixture: G20, G25, G30 and G35. The simulated s11 is reported in Figure 5.8. It can be noticed that G30
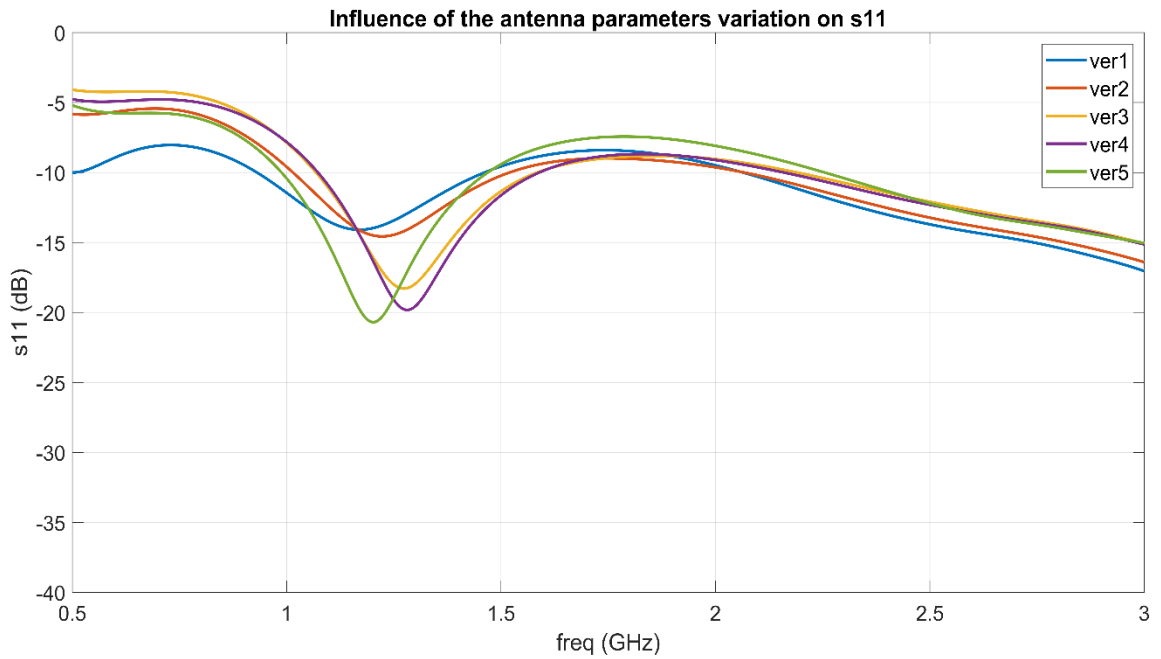
is closer to 1 GHz than G25, but it is less flexible than G25 and has a smaller bandwidth. Therefore, G25 has been chosen as the final choice for the substrate of Antenna Prototype 1 (ε = 12.66 and σ = 0.09 S/m).
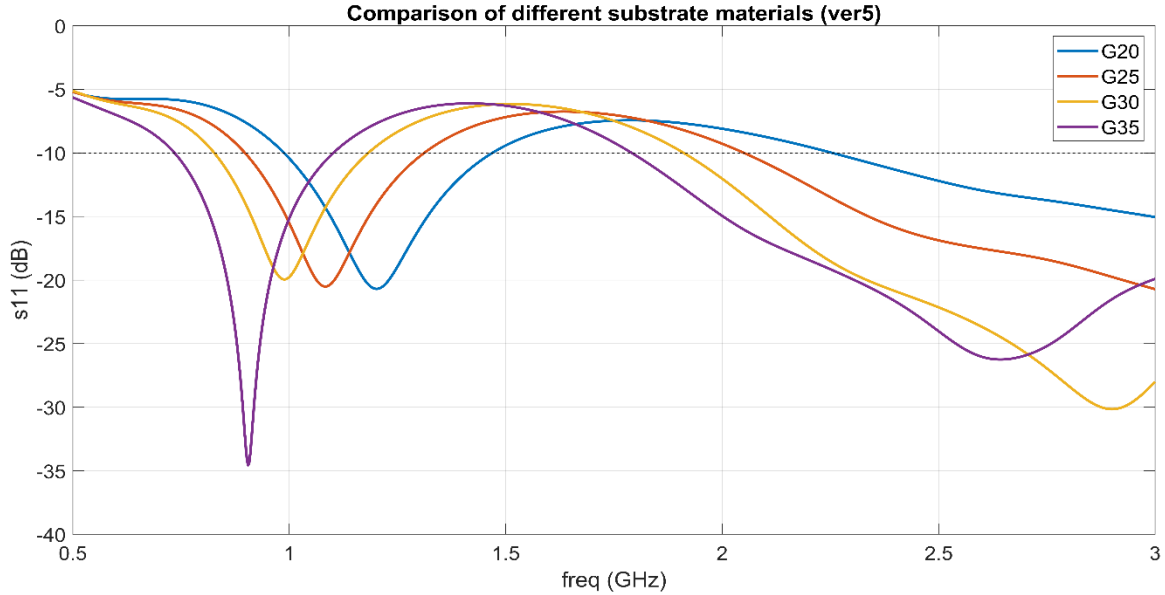
Figure 5.8: Comparison in performance of the four rubber-graphite mixtures (antenna version 5).

4. *Modification of parameters c, p1, p2*

The next tuned parameters has been c, p1 and p2, starting from the version 5 of the antenna whose substrate is made of G25. The tuning of the parameters is reported in detail in Table 5.5.

Table 5.5 Tuning of antenna parameters c, d1 and d2.

Parameter (mm)	c	p1	p2
Version 5	29.40	9.00	9.00
Version 6	**35.00**	9.00	9.00
Version 7	35.00	**6.00**	**6.00**

The obtained s11 are shown in Figure 5.9, in which can be seen that the increase of the ground length and the decrease of the stubs length lead to an improvement of the antenna performance, in fact the amount of reflected signal decreases, reaching an s11 of -45 dB at the resonance frequency of 0.96 GHz.

44
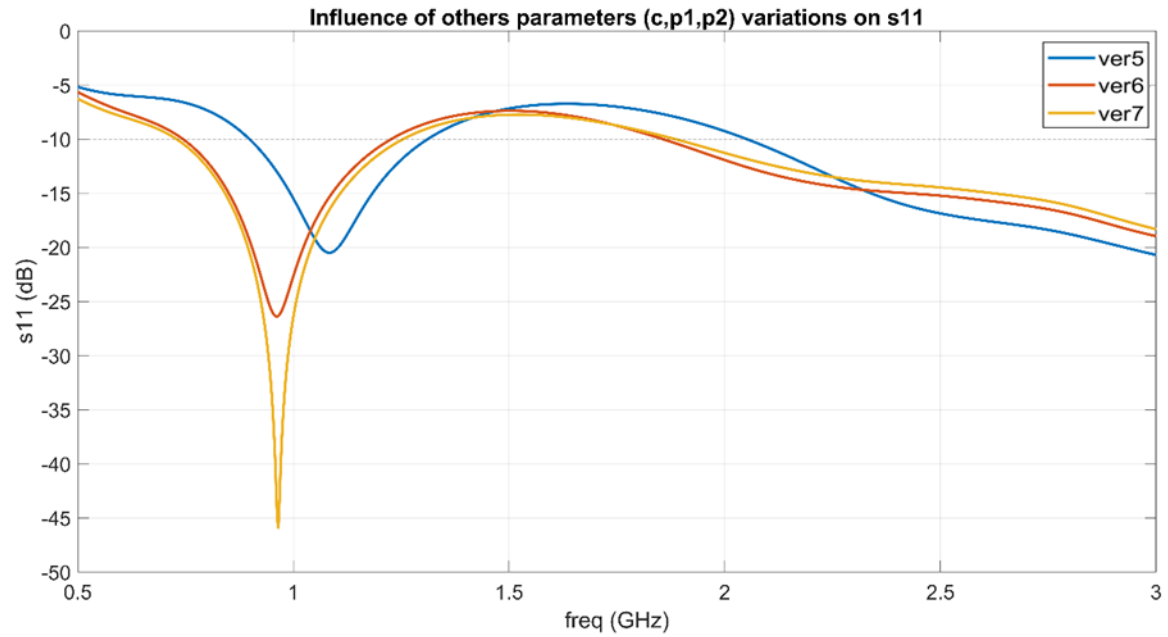
Figure 5.9: S11 signal modifications due to the last parameters changes.

5. *Properties of the final version of the antenna*

The version 7 of the antenna is its final version (see Figure 5.10) because it fullfills all the project specifications, in fact it has the following characteristics:

✓ Resonance frequency at around 1 GHz with a bandwidth of 523 MHz;

✓ Passband s11 of -45 dB;

✓ Substrate thickness of 5 mm, made of flexible and biocompatible material;

✓ It is still a monopole antenna with external dimensions: 48x30 mm.
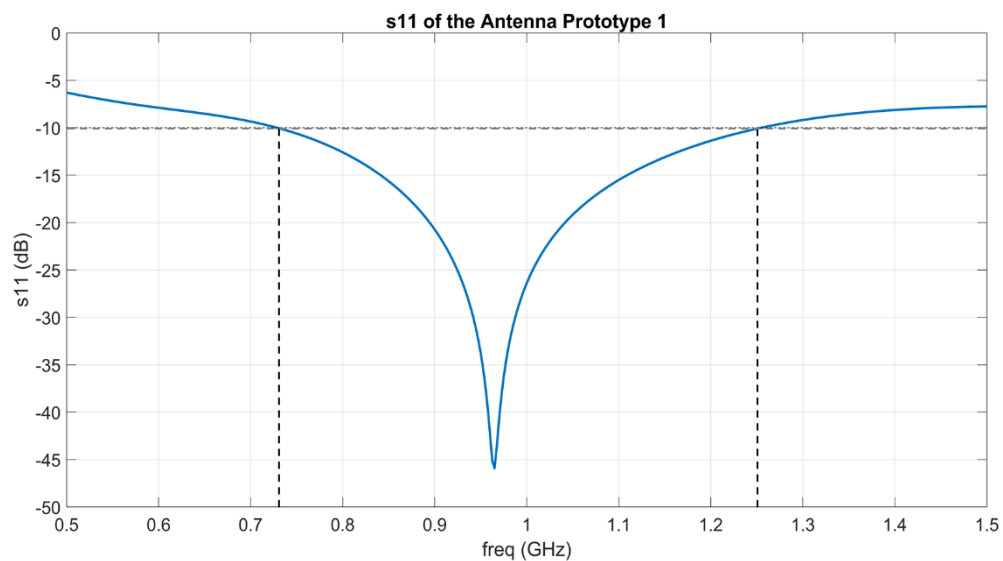
Figure 5.10: Simulated s11 signal of the Antenna Prototype 1.

45

The final antenna geometry is shown in Figure 5.11 and the geometry parameters' values are indicated in Table 5.6. As can be seen in the Figure 5.11 the overall antenna geometry has became thicker, this was also wanted in order to facilitate the antenna production, as it will be built manually.
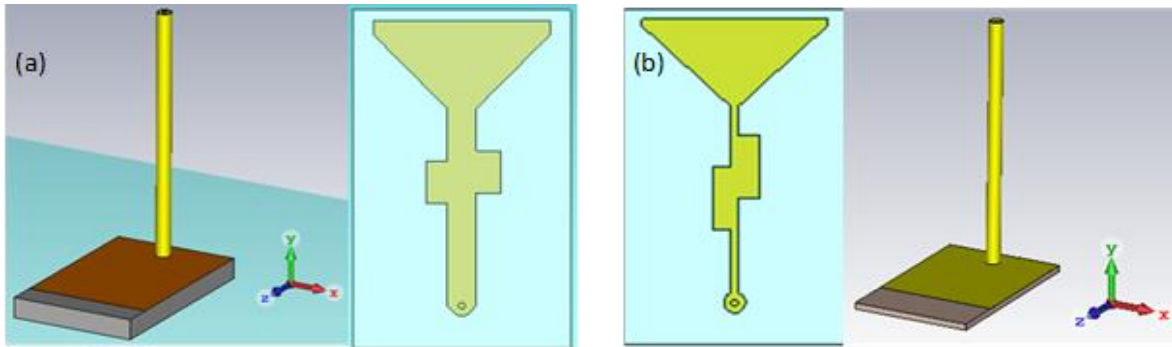
Figure 5.11: Antenna prospective and bottom views, before (b) and after the optimization (a).

Table 5.6 Antenna Prototype 1 final dimensions.

Parameter	Size (mm)	Parameter	Size (mm)
X	48.00	v1	2.94
W	30.00	v2	3.40
h	5.00	d1	14.5
r	1.60	d2	16
f	6.00	g	28.00
c	35.00	t	12.64
		s	2.00
		p1	6.00
		p2	6.00
		L	40.50

During the optimization phase has been evaluated others antenna parameters, besides the s11, such as:

➢ the electric field inside the head and the antenna (E field);
➢ the surface current on the antenna;
➢ the radiation pattern;
➢ the phase of the s11 signal.

They have not been reported for the others antenna version because they would not have helped to understand the consequences of the applied changes as much as the s11 signal. The antenna behavior and characteristic parameters are reported in Figure 5.12 and 5.13.
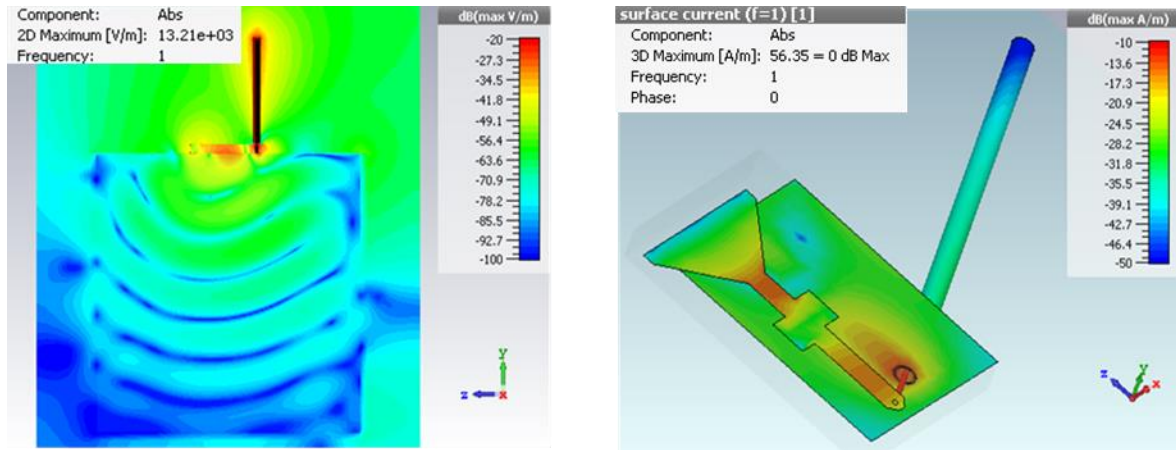
Figure 5.12: Antenna radiated electric field (left) and the surface current (right).
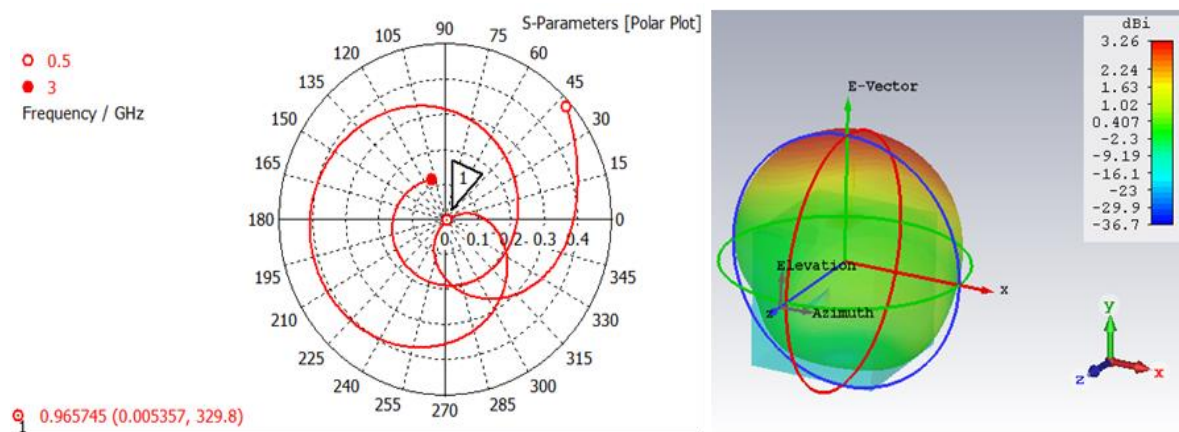
Figure 5.13: Antenna the polar plot of s11 (left) and the radiation pattern (right).

The E field is expressed in dBmax, this means that the colormap is made so that the red color corresponds to the maximum field value in that section (13.21 x 10^3 V/m). As can be seen the maximum quantity of the electric field is concentered in the coaxial cable and in the antenna region, but the fields reaches also to penetrate in the head for some centimeters. The surface current is also satisfactory because in time it propagates like a sinusoidal wave, pulsing from the feeding point to the antenna radiating part (3D maximum equal to 56.35 A/m). The radiation pattern observed in far field is almost omnidirectional as expected. Finally, the s11 signal has a god polar plot that confirms that the resonance frequency is not fictitious but really existing.

5.1.3 Bending

Once that the Antenna Prototype 1 has been obtained, it has been subject to bending tests, in order to verify the antenna's ability to flex. It has been done two type of test:

- Bending on cylinders with decreasing radius;
- Bending on the CAD model of a head phantom.

Bending on cylinders with decreasing radius

To test if the antenna is able to bend enough to adhere to the patient's head, simulations has been initially performed using cylinders with radius ranging from 100 mm to 30 mm, considered the lowest value of bending radius on a human head. The cylinder has been filled with the *average_brain* material. The results of the simulations are illustrated in Figure 5.14, where it can be observed that the bending does not induce strong differences in the antenna performance.
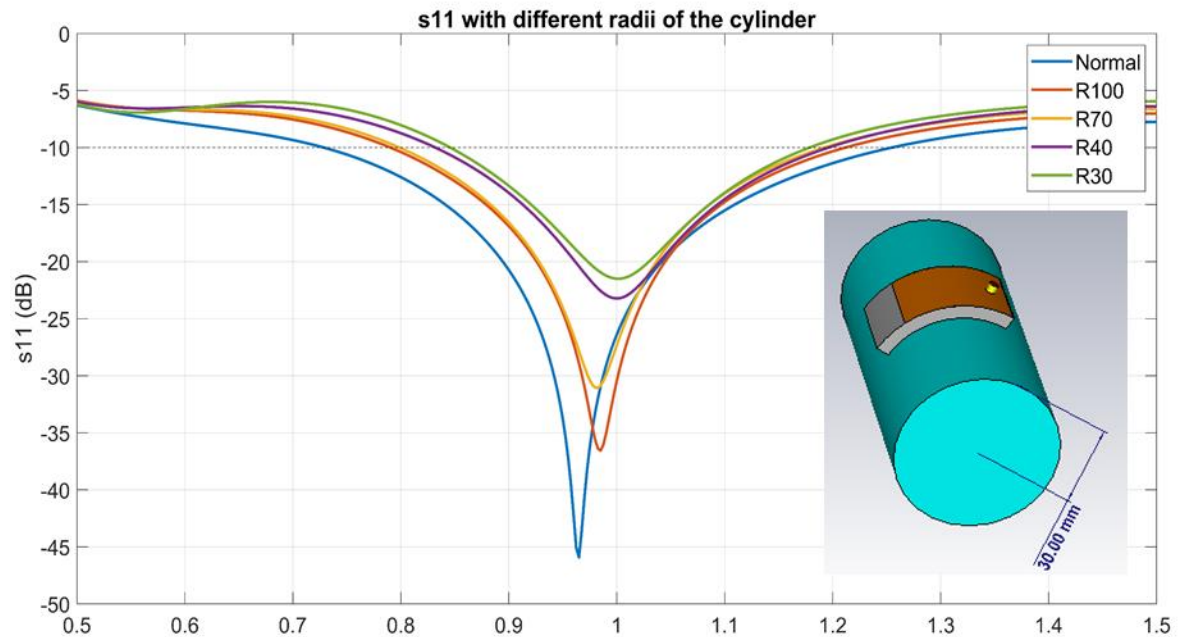
Figure 5.14: Results of the antenna bending on cylinders of different radii.

Bending on the CAD model of a head phantom

In order to consider a more realistic situation, in this second part of the antenna design, it has been introduced the CAD model of a head phantom that mimics the head shape. To be able to bend the antenna on the imported CAD of the head phantom, a cylinder of 100 mm radius, 50 mm high, has been made. It has been intersected with the geometry of the

phantom and, eliminating the non-useful parts, the model shown in Figure 5.15 has been obtained. The phantom model has been imported as an open discretized surface, thus a volume has been created closing the open surface in correspondence of the neck with an elliptical planar surface. The inner volume of the model and also the outer shell have been filled with the material *average_brain*, in order to simulate the antenna in the most realistic condition in which the antenna is in direct contact with the patient's head.

Figure 5.15: Head phantom model in which is indentified with red lines the structure that supports the antenna bending.

In Figure 5.16 the two antenna conditions are compared, when it is normal and when it is bended. One can see that there is no significant variation of the antenna performance.
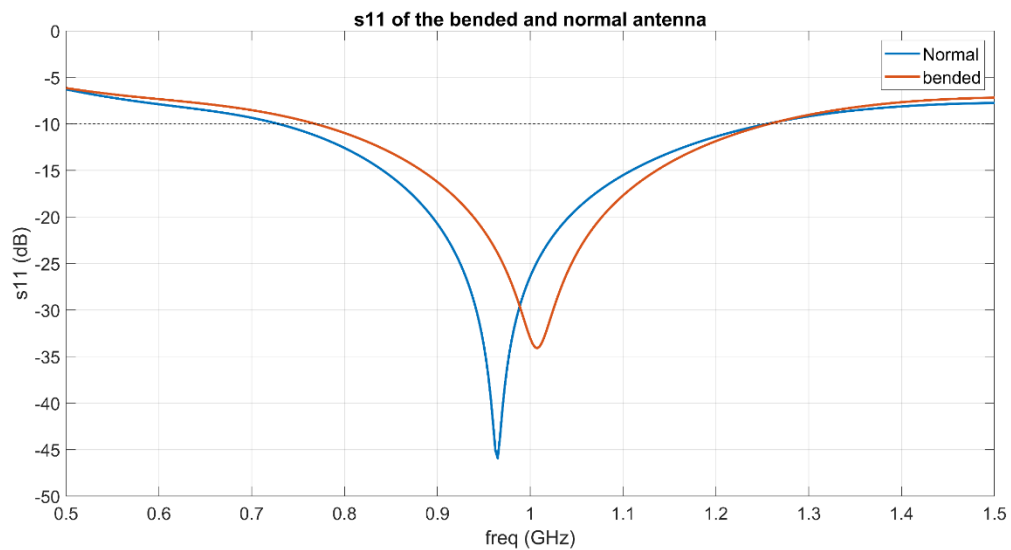
Figure 5.16: Comparison of the normal antenna and the one bended on the phantom model.

The antenna E field continues to be satisfactory, with a good penetration depth, and also the surface current has acceptable behavior, as can be seen in Figure 5.17.
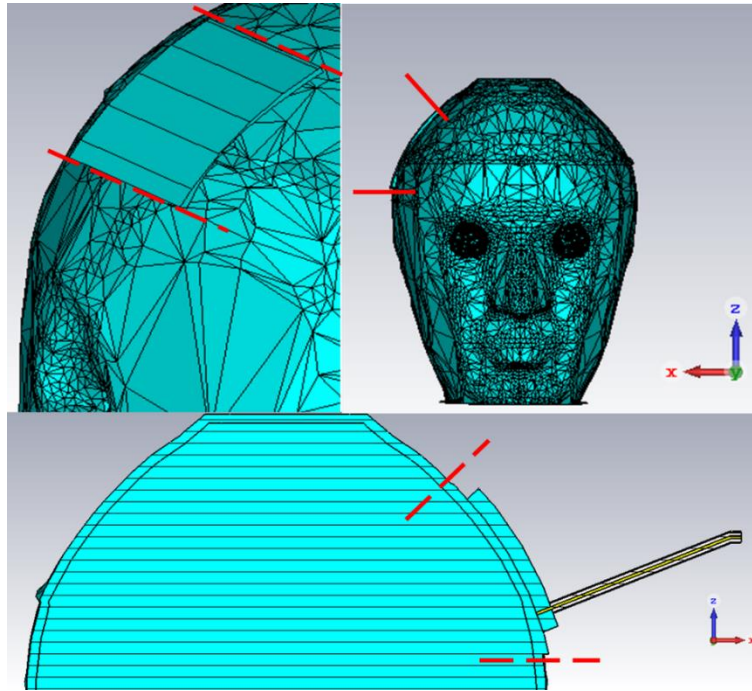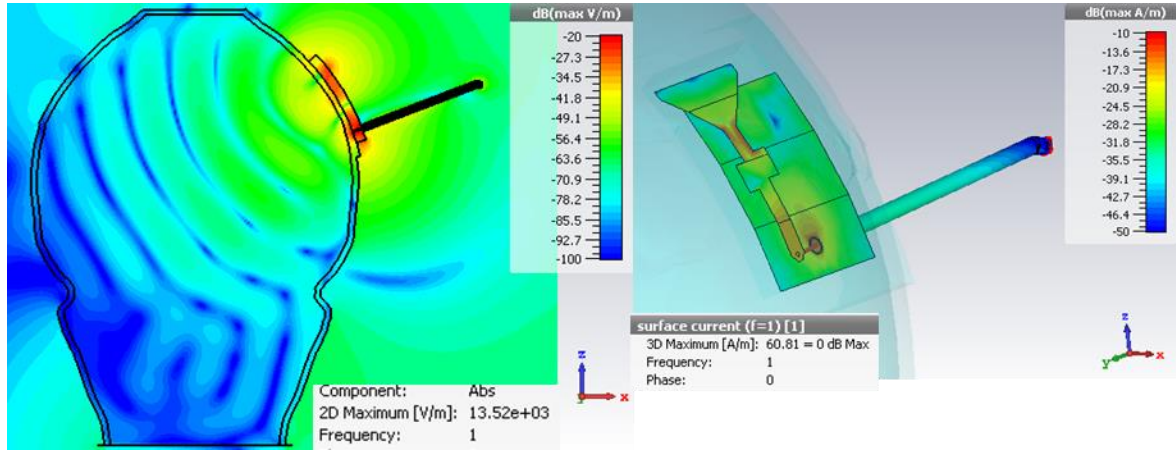

Figure 5.17: Bended antenna: (left) electric field distribution in the head phantom and (right) surface current colormap.

5.1.4 Introduction of ABS layer

Now that the antenna has overcomed well the bending test, it has been chosen to take in account a practical fact, that is the presence of a plastic layer between the antenna and the liquid that mimics the brain in laboratory, since the antenna, once that it has been produced, has to be tested on a head phantom made of Acrylonitrile Butadiene Styrene (ABS). Simulating this condition will allow to make a comparison between the simulated and measured antenna performance, in the same conditions. Furthermore, it will be possible to assess any issues of the measurement set-up. The ABS material is characterized by $\varepsilon=3$ and $\sigma=0.004$ S/m at a frequency of 2.45 GHz and has a similar values in the frequency range of interest in this thesis (0.5 – 1.5 GHz). The different layers are illustrated in Figure 5.18 and the comparison of the two s11 is reported in Figure 5.19.
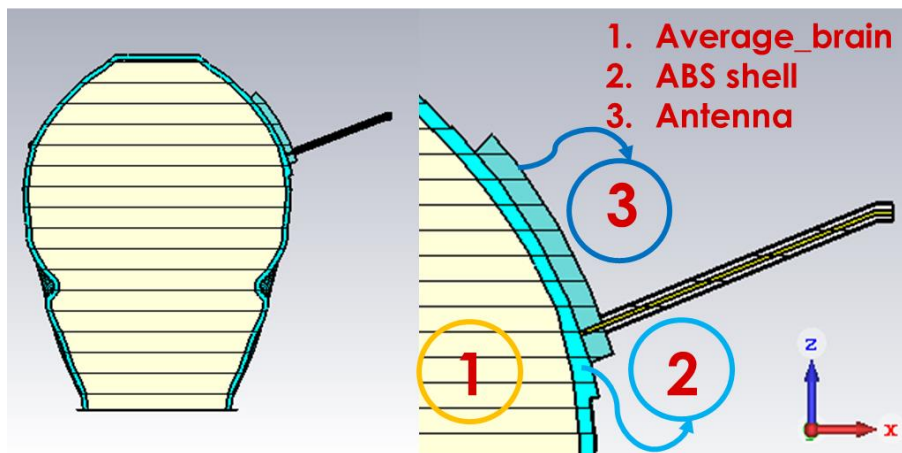
Figure 5.18 Representation of the 3 layers of the measurements set up.
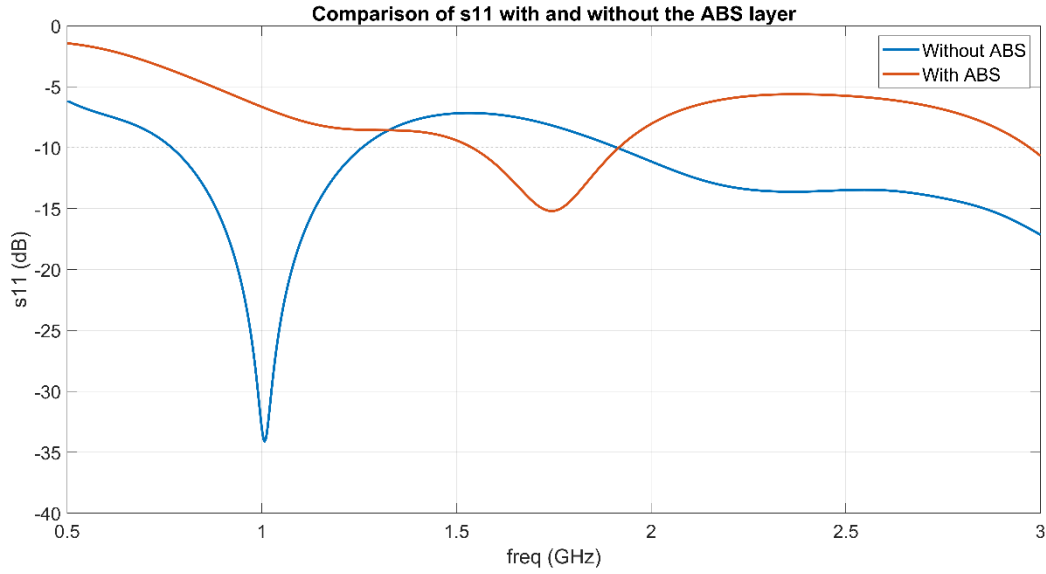
Figure 5.19 Comparison of the two situation: outer shell made of ABS and made of avergae_brain.

As can be seen in Figure 5.19 the behavior of the antenna changes drastically with the introduction of the ABS material. A similar result was expected as the permittivity and the conductivity of the ABS are far from the dielectric properties of the different biological tissues. Moreover, the outer shell of the phantom is relatively thick (≈8 mm) and also this contributes to worse the antenna performance. The head phantom is reported in Figure 5.20. Also the team that is in charge of producing the phantom considered in this thesis (and to which the used CAD belongs) states that "it has been experimentally and numerically shown that due to the high dielectric contrast with respect to the various biological tissues, the ABS walls perturb the field significantly" [25].
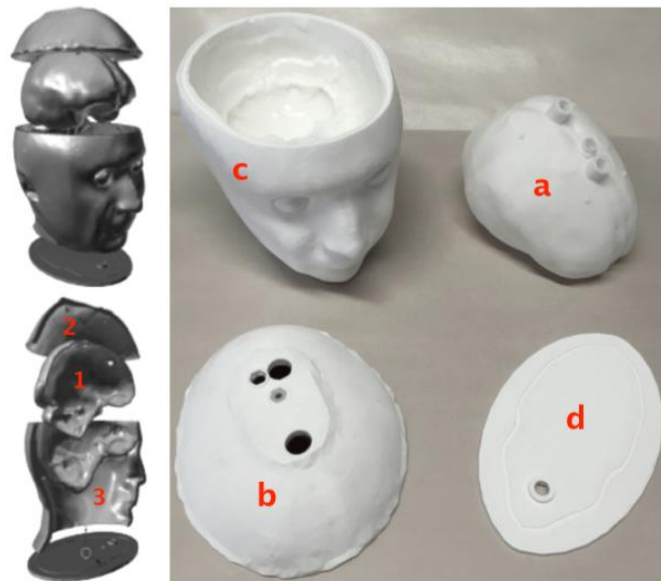
Figure 5.20 The different parts of the used head phantom. In (c) it can be seen the thickness of the shell [25].

51

As a possible solution to this problem the team has proposed two solutions: produce the phantom in conductive ABS ($\varepsilon_r \approx 10$ and $\sigma \approx 0.4$ S/m at 2.45 GHz) or to plasterize the outer shell of the phantom with flexible skin-mimicking mixtures. The first option is not feasible because "a printable material whose parameters are close to that of the brain is still to be found" [25]. Thus, the second option has been chosen and it has been simulated with CST MWS.

5.1.5 Flexible skin introduction

To evaluate the possible solution to the leakages and field perturbation issues generated by the phantom material, it has been simulated the insertion of a flexible skin-mimicking layer between the antenna and the phantom. The model of this situation is represented in Figure 5.21.
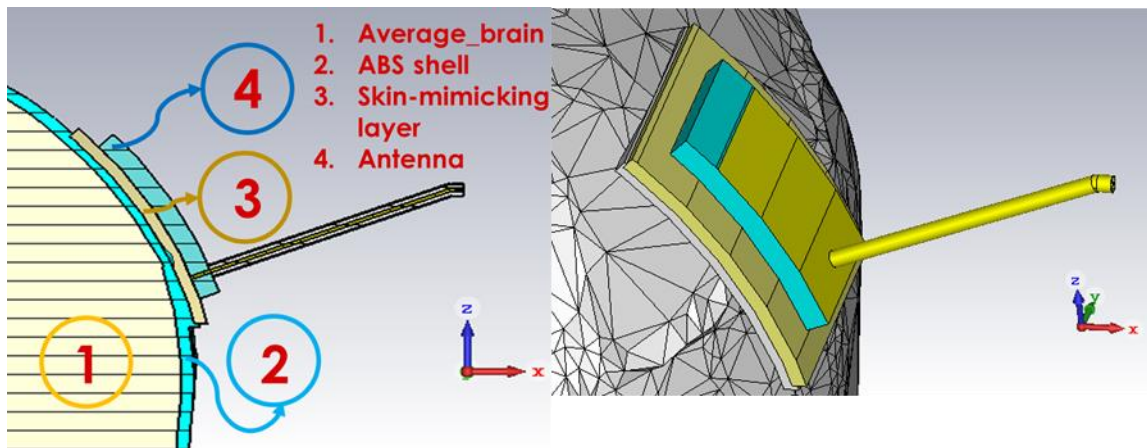

Figure 5.21 Section and perspective views system with the introduction of skin-mimicking layer.

In order to find an adequate material for the skin-mimicking layer different simulations have been done. The inserted material has to improve the impedance matching of the proposed antenna with the *average_brain,* mitigating the negative effect of the ABS shell. So a material with intermediate dielectric properties, similar for example to those of the bone, is required ($\varepsilon_r \approx 12$ and $\sigma \approx 0.2$ S/m at 1 GHz). G25 meet this requirement, therefore it is analyzed with two different thickness, 2 mm and 4 mm. Also G35 is evaluated in order to see if a material with a higher permittivity and conductivity than the bone, has better outcome. The results are shown in Figure 5.22. How it is possible to see the s11 signals improve (better peak depths) and a new resonance frequency appears. The material that represents a good trade-off between flexibility and performance is G35 with 2 mm of thickness.
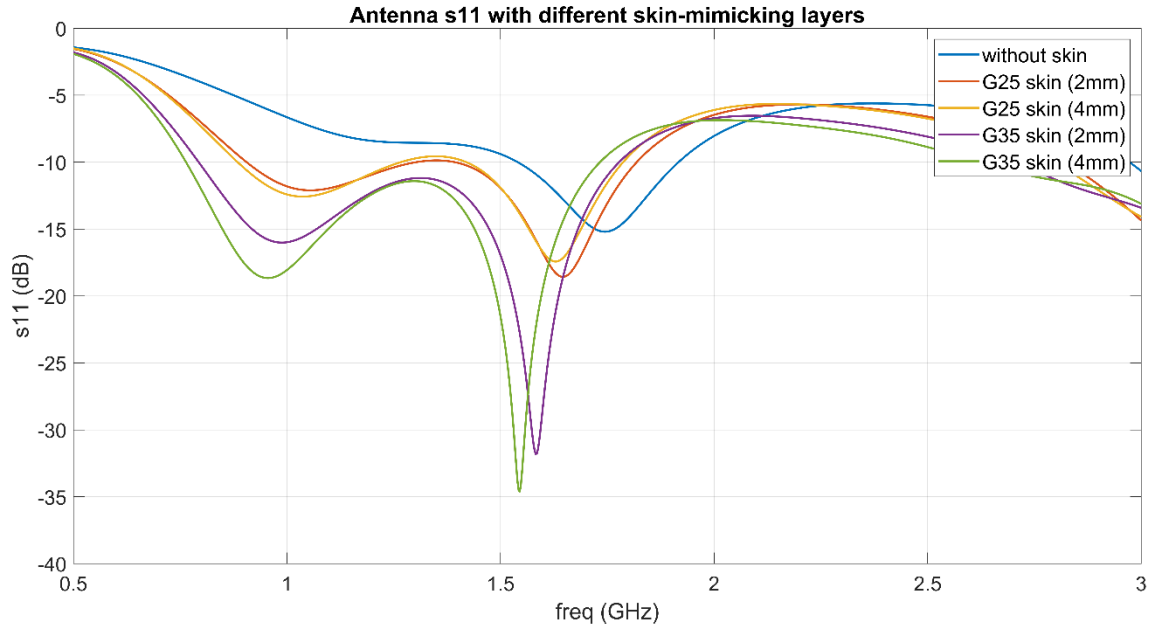
Figure 5.22 Comaprison of the antenna s11 without and with different skin-mimicking layers.

For all the materials, the second resonance is not so close to 1 GHz, while the first peak is a weaker resonance but in close proximity to 1 GHz. That the two peaks are two resonances are also demostrated by the polar plot of the G35_2mm s11 in Figure 5.23. In this figure it is possible to see that the s11 has a phase of 0° when its magnitude is about 0.2, closing almost in a circle and forming the first resonance, while the second is obtained with an even lower s11, close to 0 , with a node positioned in the center of the chart.
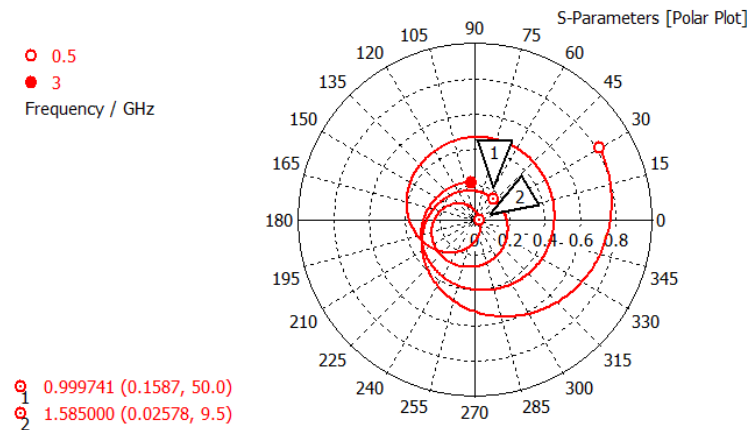
Figure 5.23 S11 polar plot of the antenna with skin layer made of G35_2mm.

Figure 5.24 compares the E field distrubutions in these three situations:

a) Antenna bended on the head phantom made of average_brain;

b) Antenna bended on the head phantom, whose outer shell is made of ABS;

c) Skin-mimicking flexible layer inserted between the antenna and the head.

53

It can be observed that the introduction of the ABS layer decreases the penetration depth and increases the reflections in correspondence of the shell. Instead, the skin_mimicking layer allows again a better penetration. This means that the skin-mimicking layer insertion is a good solution to the phantom material related issues.
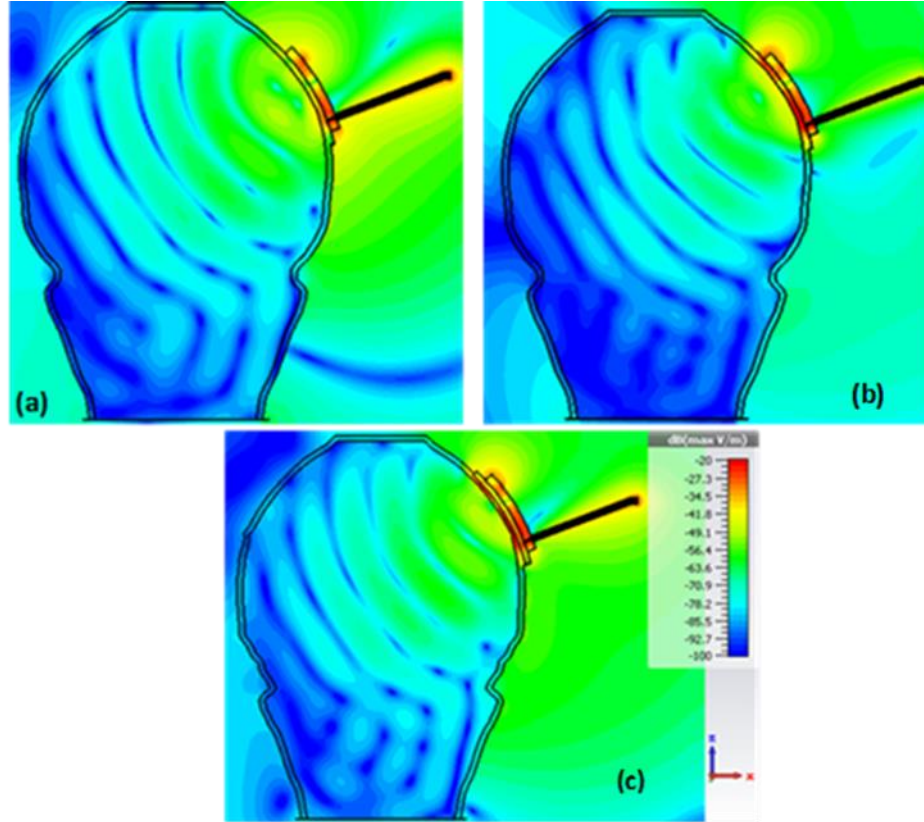
Figure 5.24 E field distribution: (a) without ABS, (b) with ABS and (c) with ABS and skin layer.

5.1.6 Evaluation of s21

The last design step consists in the calculation of the transmission coefficients (s21 and s12) of two antennas equipped with the flexible skin layer (G35_2mm), in order to further evaluate the potential of the skin-mimicking solution. In particular, the s21 signal has been calculated in four different conditions:

1. Maximum attenuation and only the average_brain material in the head;
2. Maximum attenuation and a PEC sphere inside the brain;
3. Lower attenuation and only the average_brain material in the head;
4. Lower attenuation and a PEC sphere inside the brain;

Maximum attenuation is the condition in which the two antennas are positioned on the opposite sides of the head, symmetrically. In this case the radiated field will be attenuated the most. Instead, lower attenuation means that the two antennas are closer to each other, one positioned laterally on the head and one on the top. The sphere made of PEC material has a radius of 10 mm and it serves to investigate the ability of the two designed antennas to detect the presence of an object in the brain, like a stroke could be. The simulation is not done with a sphere with blood electric properties because in the measurements phase a metallic sphere will be used. The positions of the antennas and of the PEC sphere are illustrated in Figure 5.25.
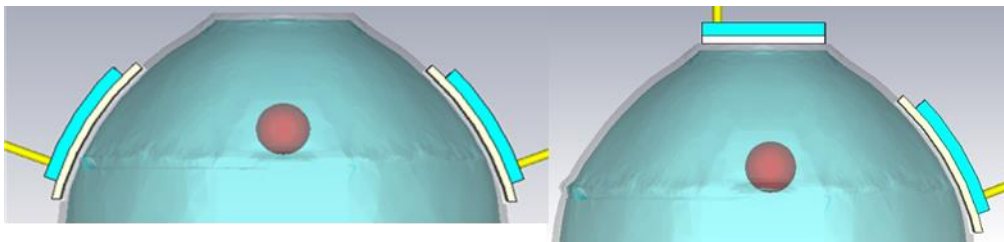
Figure 5.25 Representation of the two simulated conditions: (left) maximum attenuation condition and (right) lower attenuation condition. The presence of the PEC sphere is considered for both the case.

The s11, s22, s21, s12 signals has been obtained from the simulations for all the four conditions. In Figure 5.26 are reported the reflection and transmission coefficients for the maximum and lower attenuation conditions in presence of the metallic sphere.
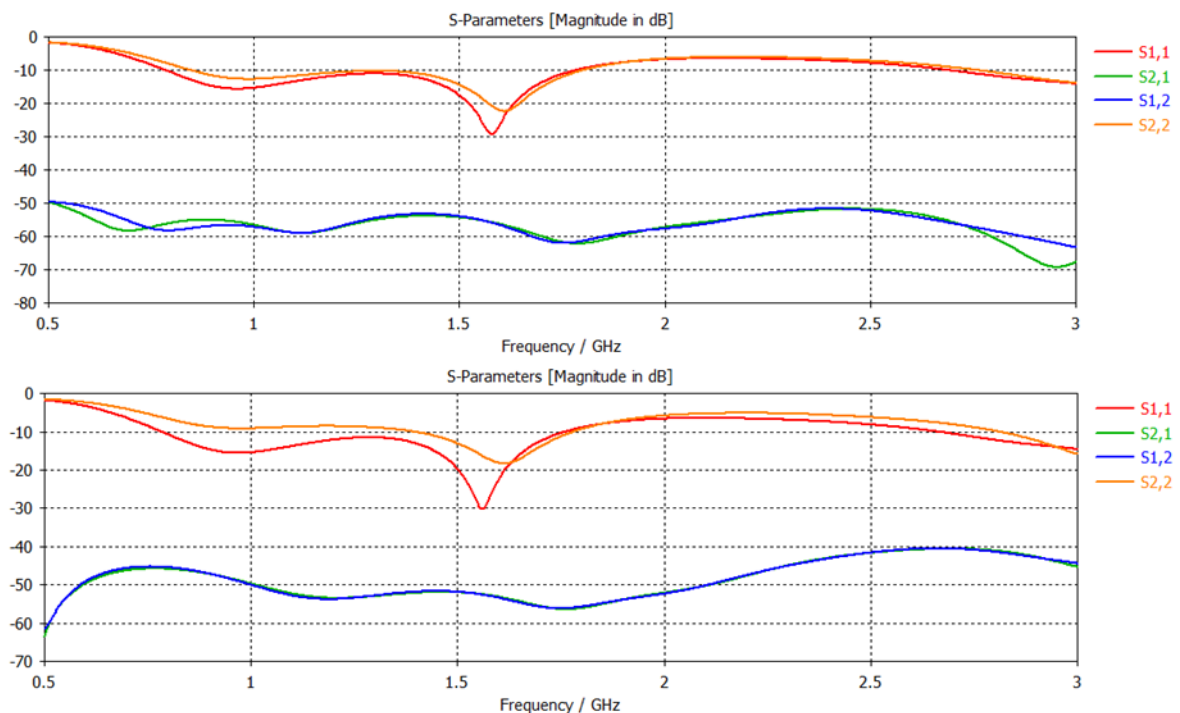
Figure 5.26: S11 plot in presence of the metallic sphere for the (top) maximum attenuation condition and (bottom) for the lower attenuation condition.

It can be seen in the aforementioned figure that the s11 and s22 signals are more similar in the case in which the two antennas are more distant, suggesting that there is more interference and noise when the two antennas are closer. The s21 and s12 signals are almost coicident and they have a value of about -50 dB in both cases. It is acceptable as a value for information transmission, but the closer it is to 0 dB the better.

In order to evaluate instead the ability of the two antennas to perceive the presence of the object, the differential signal is needed. It has been done the difference between the s21 in presence of the PEC sphere and the s21 in its absence. To do ths the two s21 signals has been transformed in linear in Matlab and then the difference has been performed. This differential signal has been again expressed in dB and plotted in Figure 5.27, for the lower and maximum attenuation conditions. To have a good Δs21 it has to not exceed -100 dB. Thus, the postioning wih lower attenuation has, as expected, a better differential signal. This means that these two antennas detect better the presence of the ictus inside the brain.

Figure 5.27 Difference signals of the s21 with and without a sphere of blood.

5.2 Conclusion

The Antenna Prototype 1 has been designed successfully, achieving the objectives set as project requirements. It resonates at around 1 GHz with a s11 of - 45 dB at the resonance

frequency and a bandwidth of 0.5 GHz. Furthermore, the flexibility of its materials has been demonstrated. It has been then investigated the consequences, on the antenna performance, of the material of which the phantom used in the laboratory is made. From the study has emerged that the ABS plastic material drastically worsens the antenna performance. Therefore, a possible solution has been studied, introducing a flexible skin-mimicking layer between the antenna and the head phantom, in order to increase the antenna matching. The solution proved to be effective, in fact the antenna improved its s11 and s12, but the resonance frequency has been shifted to around 1.5 GHz.

6. Antenna Prototype 2

6.1 Design Process

The design process for the Antenna Prototype 2 has followed the same design steps of the Antenna Prototype 1, but the first three steps coincide substantially, since the starting antenna and head models have been the same. In fact, it has been imported into CST MWS the antenna model of the MiBraScan system and the parameterization made for Prototype 1 and the initial values of the parameters has been maintained. Therefore, for the parameterization refer to the Figure 5.2 and 5.4, instead for the initial values to the Table 5.1 and 5.3. The unique difference in this phase is the material chosen for the substrate and thus its electrical properties. For this second antenna prototype the Polyimide has been chosen, with the electrical properties reported in Table 6.1.

Table 6.1 Materials assigned to the antenna prototype 2 components.

Component		Material	Properties
Radiating part and TL		Copper annealed	σ = 5.8e+07 S/m
Ground plane		Copper annealed	σ = 5.8e+07 S/m
Substrate		Polyimide (PI)	ε_r = 3.4 and tanδ = 0.0027 (1GHz)
Coaxial SMA feed	Core	Copper annealed	σ = 5.8e+07 S/m
	Dielectric	PTFE	ε = 2.1
	Outer layer	Copper annealed	σ = 5.8e+07 S/m

In order to simulate the antenna with the substrate in Polyimide, whose thicknesses is less than 1 mm, it was necessary to thicken the number of meshcells in the area of the substrate with respect to the Antenna Prototype 1. An enlargement of the simulated system mesh (lateral section) is illustrated in Figure 6.1.
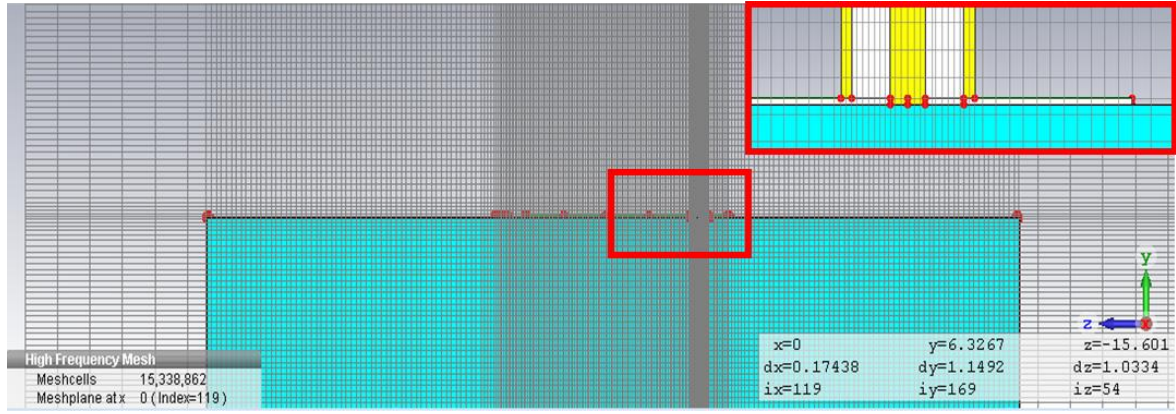
Figure 6.1 Zoom in of the simulated system mesh, in which it is possible to see that there is a higher number of lines, and thus of meshcells, in the region of the antenna substrate due to its small thickness.

6.1.1 Optimization

- *Sweep of h parameter*

The fist parameter that has been optimized is the thickness of the substrate. The production of this second antenna has been thought to be delegated to an external company due to the very low thickness of this material and the precision required. The thickness optimization has therefore been constrained by production limits, in fact the companies produce flexible substrates in Polyimide with a standard thickness of 25 μm and 50 μm, providing other non-standard thicknesses, up to a maximum of 150 μm. Thus, the simulations has been done strating with the initial value of h=1.6 mm down to 0.15 mm. The resulting s11 signals are shown in Figure 6.2.

Figure 6.2 S11 of the sweep of parameter h, from 1.6 mm down to 0.15 mm.

Observing the Figure 6.2 it is possible to see that the resonance moves toward higher frequencies as the thickness of the substrate decreases. It has been not considered lower

values of h because it would have been more difficult to shift the resonance towards 1 GHz with the optimization process. Moreover, it is important to notice that the bandwidth of the antenna decreases with the decreasing of the substrate thickness and this represents a negative aspect of the ultrathin antennas.
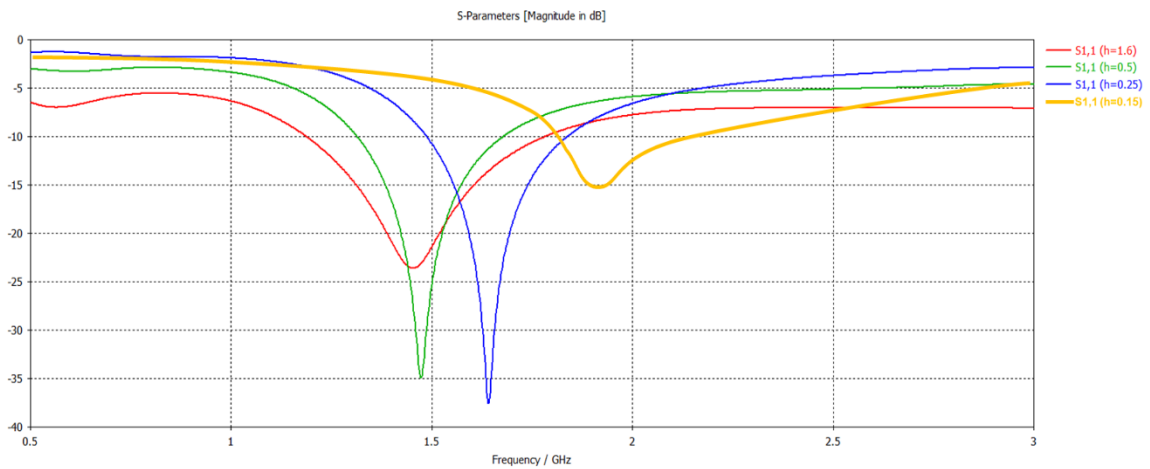
- *Others parameters modifications*

Cosidering the s11 signal with h=0.15 mm, others parameters have been modified. Through the simulations it has been observed that by decreasing the width of the stubs and icreasing the length of the ground, i.e. decreasing v1, v2 and increasing c, two resonances appeared, one close to 1 GHz and the other close to 2 GHz. Therefore, a tuning of the parameters has been carried out in order to obtain an accentuation of the first resonance and an attenuation of the second or modification that does not compromise the first. The more relevant tuning are reported in Table 6.2 and the related changes induced on s11 are illustrated in Figure 6.3.

Table 6.2 Dimensions tuning of some of the antenna parameters.

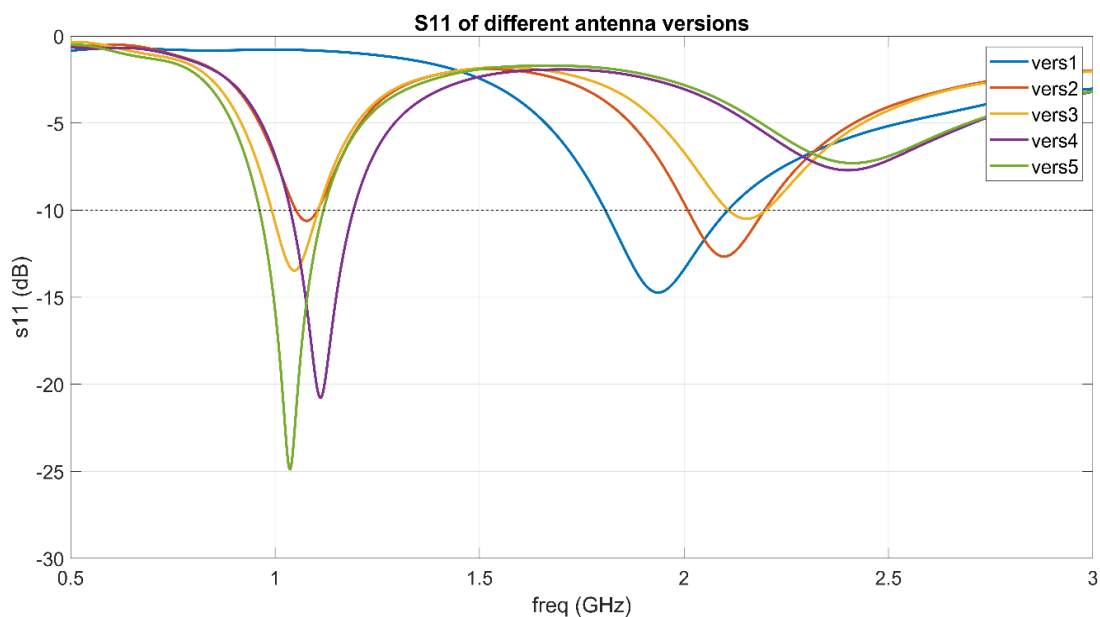| Parameter (mm)	v1	v2	c	p1	p2	s	d1	d2
Version 1	2.44	2.90	29.40	9.00	9.00	0.50	9.09	13.59
Version 2	1.00	1.50	36.00	9.00	9.00	0.50	9.09	13.59
Version 3	0.50	1.00	36.00	9.00	9.00	0.50	9.09	13.59
Version 4	0.50	1.00	38.00	9.00	9.00	0.62	9.09	13.59
Version 5	0.50	1.00	38.00	4.00	4.00	0.62	14.50	15.00

Figure 6.3 Simulated s11 signals of different antenna versions.

As it can be seen in Figure 6.3 for the version 4, the further increase of c and the increase of s has led to the first peak to be accentuated, but the increase in s has also involved the shift of the first resonance towards right. Therefore, in version 5 the parameters d_1 and d_2 have been increased, as they involve a shift to the left of the resonance. Furthermore, the length of the stubs has been decreased to augment the peak depth.

- *Properties of the final version of the antenna*

The final antenna version is version 5 with the dimensions reported in Table 6.3 and the geometry shown in Figure 6.4.

Table 6.3 Final Antenna Prototype 2 dimensions.

Parameter	Size (mm)	Parameter	Size (mm)
X	48.00	v1	0.50
W	30.00	v2	1.00
h	0.15	d1	14.50
r	1.60	d2	15.00
f	6.00	g	28.00
c	38.00	t	12.64
		s	0.62
		p1	4.00
		p2	4.00
		L	40.50

It has the following characteristics:

✓ Resonance frequency at around 1 GHz;

✓ Passband s_{11} of -25 dB;

✓ Ultrathin substrate (150 µm), made of flexible and biocompatible material;

✓ It is still a monopole antenna with external dimensions: 48x30 mm.

Thus the antenna meets almost all project requests, except for having a wide band (> 500 MHz at 1 GHz), in fact it has a bandwidth of 160 MHz at 1 GHz, as can be seen in the Figure 6.4. Despite this, the subsequent design steps has been carried out because in any case the antenna has a quite good radiated electric field and penetration depth, and an almost omnidirectional radiation pattern. These antenna characteristics, the surface current and the s_{11} polar plot are reported in Figure 6.5.

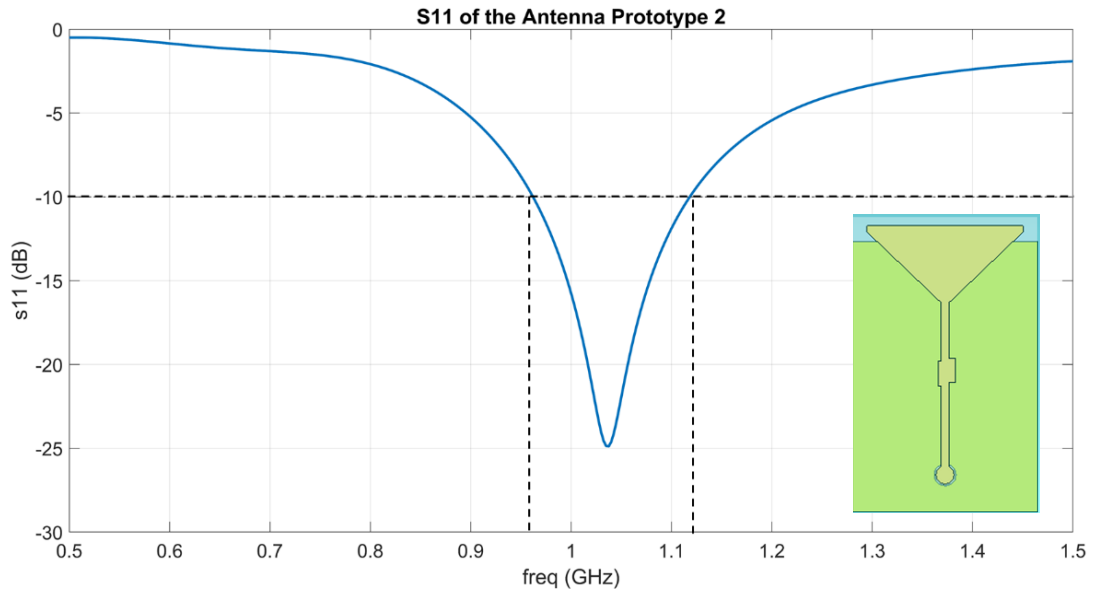Figure 6.5 S11 plot of the Antenna Prototype 2, whose final geometry is shown in the right angle.
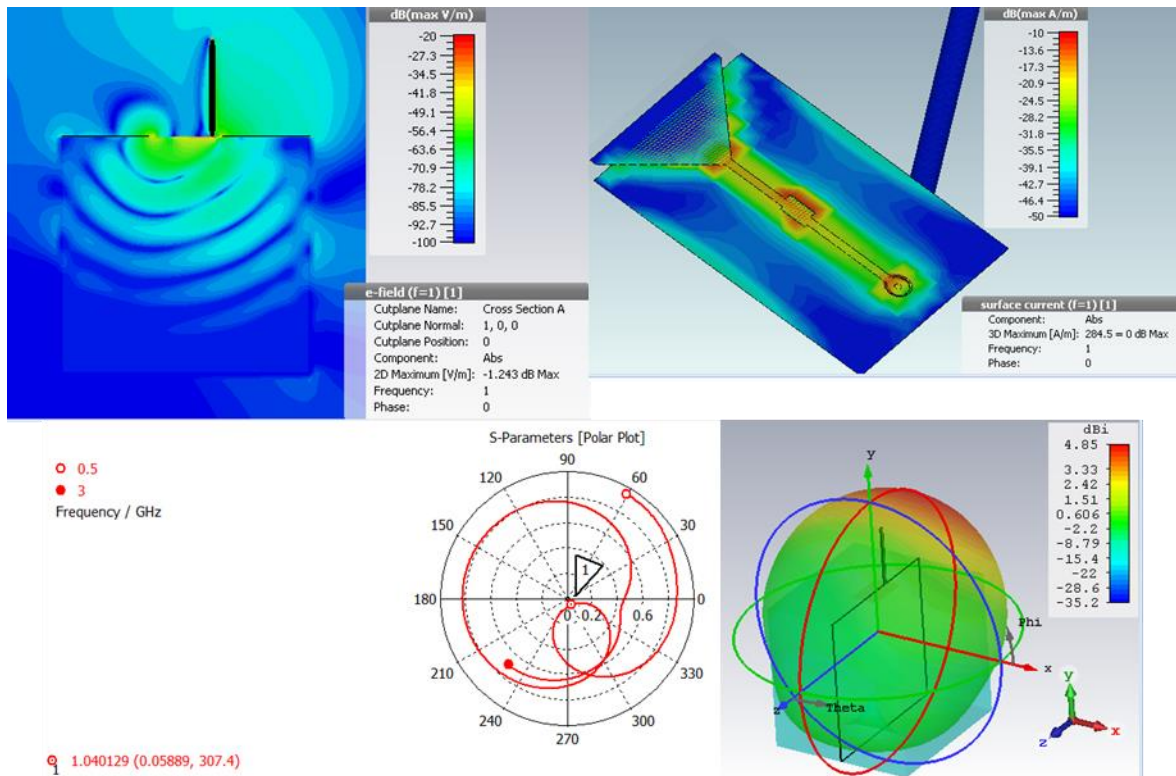

Figure 6.4 Antenna Prototype 2 characteristics: E field, surface current, s11 polar plot and radiation pattern.

6.1.2 Bending

The bending test in this case was performed directly on the CAD of the phantom head (see Figure 6.6), without using the cylinders, as the material is very flexible having a

thickness of 150 μm and in literature there are many studies that already demonstrates the excelent Polyimide bending capabilities [26], [27], [18]. The head phantom has been filled with *average_brain* liquid like for the Antenna Prototype 1. The antenna has successfully passed this test, obtaining an excellent correspondence between the s11 before and after the bending, as can be seen in Figure 6.7, and quite the same E field distribution.
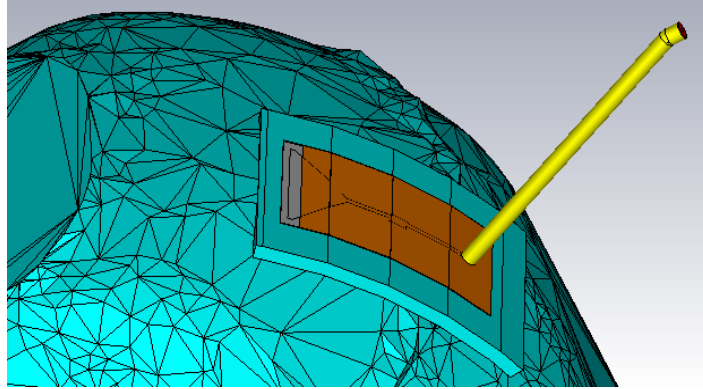

Figure 6.6 Simulated bending condition for the antenna with Polyimide substrate.
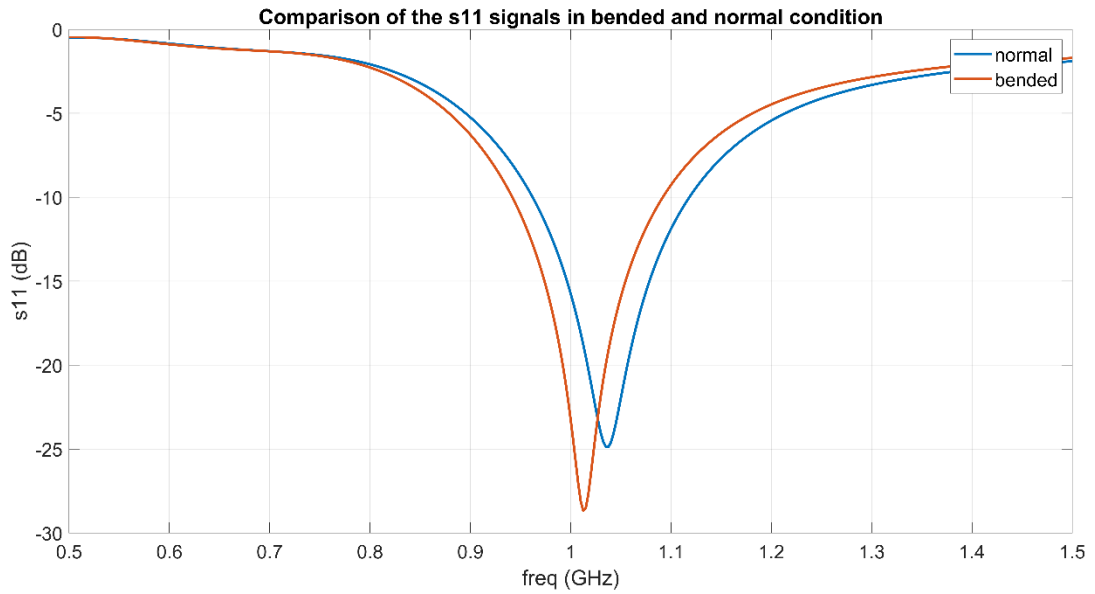
Figure 6.7 Simulated s11 of the antenna in bended and normal condition.

6.1.3 Introduction of ABS layer

At this point it has been simulated the realistic condition in which the outer shell of the phantom is made of ABS, like has been done for the Antenna Prototype 1. The model of

this condition is raffigured in Figure 6.8 and the resulting s11 of the antenna are reported in Figure 6.9.
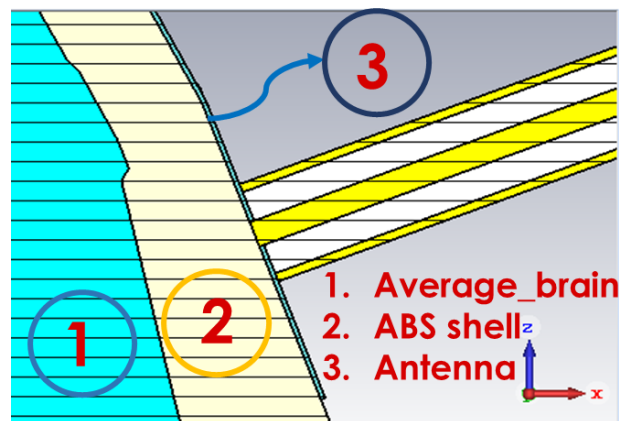
Figure 6.9 Raffiguration of the simulation condition in which the outer shell of the head phantom is made of ABS.
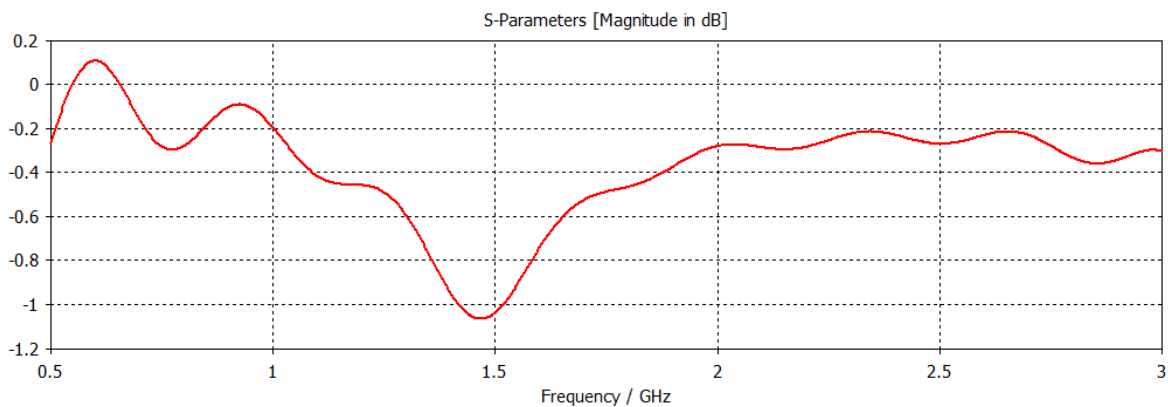
Figure 6.8 S11 plot of the Antenna Prototype 1 after the introduction of the ABS layer of the phantom.

In Figure 6.9 it is possible to see that s11 signal of the antenna becomes close to 0 dB over the entire frequency range, making the antenna unusable for imaging. This problem has persisted trying to put a layer of material with greater permittivity and conductivity, such as the G25 and G35.

6.2 Conclusion

The Antenna Prototype 2, whose substrate is made in Polyimide, has been designed successfully to work at 1 GHz optimizing the parameters of its geometry, obtaining a resonance peak at -25 dB. It has also shown to have excellent flexibility. However, this solution has been discarded for a series of disadvantages:

- it is not wideband (160 MHz of bandwidth);

- no longer able to radiate signal when a plastic shell is placed in front of it, even placing a skin-mimicking layer to increase the impedance matching;

- thickness difficult to simulate;

- high costs of production if you want to use thicknesses different from the standard one.

This type of solution is therefore considered not to be suitable for further analysis in the laboratory on the phantom head. At this point, for brain imaging applications, it is believed that it is better to prefer antennas whose substrate is made of material that allows the antenna to have a better coupling in impedance with the analyzed tissues.

7. Antenna Prototype 1 Realization And Measurement Results

7.1 Antenna Realization

7.1.1 Antenna components preparation

The Antenna Prototype 1 has been realized starting from the preparation of its metallic parts, that are the ground plane and the transmission line with the radiating part. The final dimensions of the antenna, reported in Table 5.6, has been rounded to 1 mm (e.g. v1 =2.94 mm has become v1=3 mm) because the antenna has to be realized manually with a cutter that does not have such high accuracy. To realize these elements adhesive copper has been used. An example of cutted copper elements is shown in Figure 7.1.
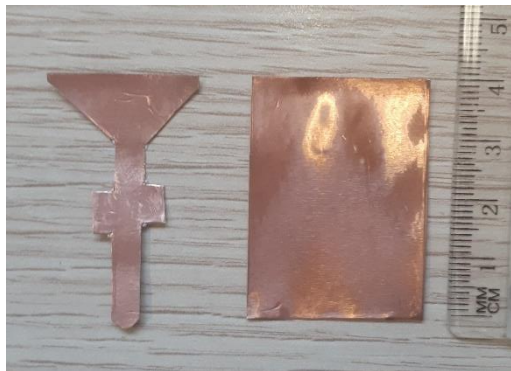
Figure 7.1 Example of antenna conductive parts realized with adhesive copper: (left) transmission line with the stubs and the radiating triangle, and (right) the ground plane.

Subsequently, the substrate was produced using urethane rubber and graphite powder mixture. Four substrate samples has been realized at a time because four plastic molds has been manufactured with a 3D printer. The plastic molds are rectangular with the same inner dimensions as the substrate, i.e. 30x48 mm. They are composed by two L-shaped parts in order to facilitate the detachment of the substrate from the mold, once they are dry. Thus, 40 g of G25 mixture has been prepared. The amounts of urethane rubber and graphite has already been reported in Table 4.3. To obtain the urethane

rubber two parts have to be mixed together, called part A (yellow color) and part B (dark orange color). To have the quantity of urethane rubber indicated, 50% by mass of part A and 50% by mass of part B was used. As reported in Table 4.3, 30 g of urethane rubber and 10 g of graphite has been used for the preparation of four substrates, 5 mm thick. The 3D printed molds and the three materials to mix are illustrated in the photography of Figure 7.2.
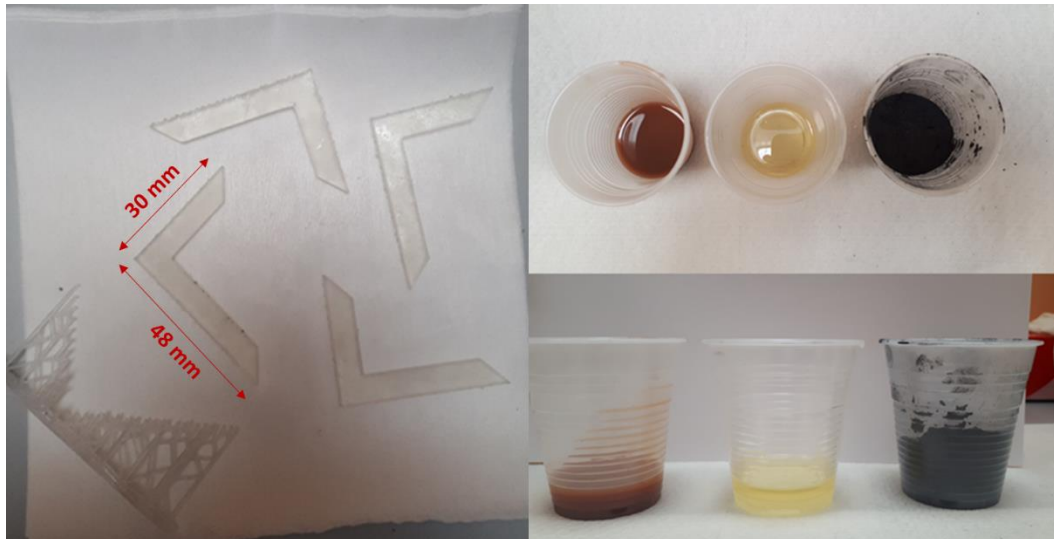
Figure 7.2 (left) The 3D printed L-shaped molds for the substrate and (right) the three materials need to obtain the G25 mixture, in order: part B (dark orange), part A (yellow), graphite powder (black).

To obtain the mixture, first part A has been mixed with part B for 3 min to make them react and then the graphite powder has been gradually added. The result is a liquid mixture that tends to polymerize quickly. So the mixture was poured into the molds, where the ground planes has been already placed. After a few minutes the top part of the antenna has also been placed on the substrate. The material has been left to dry for several hours (see Figure 7.3).

Also 2 cm thick sample of G25 has been realized (see Figure 7.3.) in order to make the measurment of the manufactured mixture permittivity and conductivity. For this scope a Agilent 85070E dielectric probe kit has been used. The results of the measurements will be shown in the Measurements and Results paragraph.

In Figure 7.3 it is also possible to see a a sample of dried substrate without copper that is bent. The high flexibility of the G25 can be noted.

Figure 7.3 (left) Pouring of the liquid G25 mixture in the mold for the 2 cm thick sample. (middle) Finished antenna sample left to dry. (right) Already dried substrate sample without copper that is bent.

7.1.2 Welding of the feeding line and realization of the insulation layer

For the feeding line it has been used a semi-rigid coaxial cable that has been soldered to the SMA connector at one end, in order to allow the connection with the Vector Network Analyzer (VNA) port, and at the other end to the antenna ground (its outer shell) and to the antenna transmission line (its core). The antenna soldered with the feeding line is shown in Figure 7.4 in the lateral and bottom views.

Figure 7.4 (left) Lateral view of welded antenna prototype 1. (middle) Bottom view of the welded antenna prototype 1. (right) Detachment issue of the copper from the substrate.

In the mentioned figure it is also reported (right) an issue that has emerged during the realization phase. The issues consists in the fact that the copper of the antenna tends to

break away from the substrate and to wrinkle when the antenna is bent. During bending it has been also noted that the ground, which covers almost the entire upper surface of the substrate, also tends to wrinkle and stiffens the antenna. To overcome this problem the antenna has been covered with a 1 mm thick layer made of urethane rubber (part A mixed with part B) on both sides, as can be seen in Figure 7.5. Here can also be observed (right) how the bending capability of the antenna returns to be good, without having anymore problems of copper detachment.

Figure 7.5 (left) Covering of the antenna with urethane rubber layer on both sides. (middle) Lateral view of the finished Antenna Prototype 1. (right) Finished antenna bending.

7.2 Phantom preparation

In order to make comparisons with simulated data, measurements with the head phantom has been made. The phantom version used is the one shown in Figure 7.6, following that shown in Figure 5.20, with same thickness of the wall (about 8 mm) and also made in ABS. It was filled with a liquid, which corresponds to the *average_brain* material in simulation, that mimics the electrical properties of the brain. To prepare it Triton X-100-water mixtures with NaCl (salt) has been used. In particular, it has been prepared with the following concentrations:

- 38% of Triton X-100 (volume concentration in water);
- 72% of water;
- 5.2 g/L of NaCl.

Figure 7.6: 3D printed head phantom used for the measurements made of ABS.

7.3 Measurements and Results

To test the performance of the manufactured antenna and compare them with the simulated ones, different measurements has been done:

- in the air;
- placing the antenna on the surface of the liquid that mimics the brain or slightly dipping it into the liquid;
- using the head phantom, and doing measurements with a single antenna and with two antennas, in different positions.

7.3.1 Measurements in air and in contact with the average_brain liquid

The first measurement has been that of the s_{11} of the antenna in the air using the P9373A Keysight Streamline Series USB Vector Network Analyzer and then the s_{11} has been measured in the case of the antenna in direct contact with the brain liquid. In order to do the last mentioned test, a plastic glass with a 4 cm radius and a height of 12 cm has been used. It has been filled with the mixture of Triton X-100-water and salt, in the proportions indicated above to mimic the electrical properties of the brain. The results obtained are reported in Figure 7.7. Here it is possible to see that there is a good agreement between
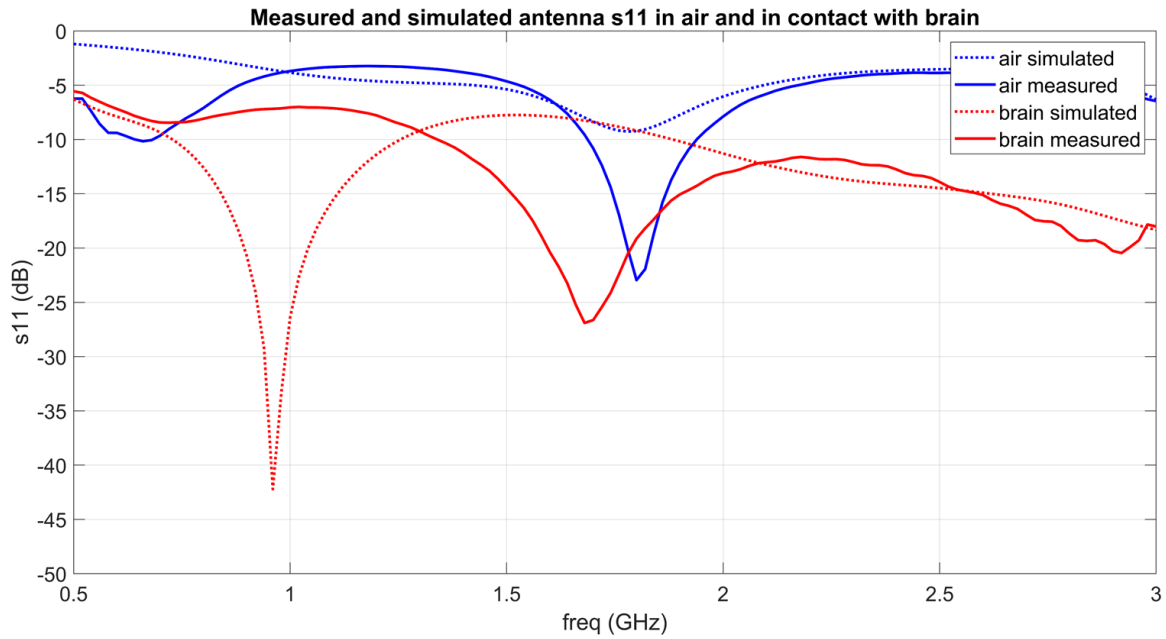
Figure 7.7 Comparison between measured and simulated s11, in air and in brain.

the measured and simulated data in air, in particular the manufactured antenna works even better than the simulated one. Instead, there is less agreement dipping the antenna in the liquid, in fact the measured antenna has a resonance at 1.68 GHz while the simulated at around 1 GHz. In order to understand the reason of this difference others simulations have been done, simulating the brain and the substrate of the antenna with the measured values (see Figure 7.8) and considering the geometry of the brain liquid container, as shown in Figure 7.9.
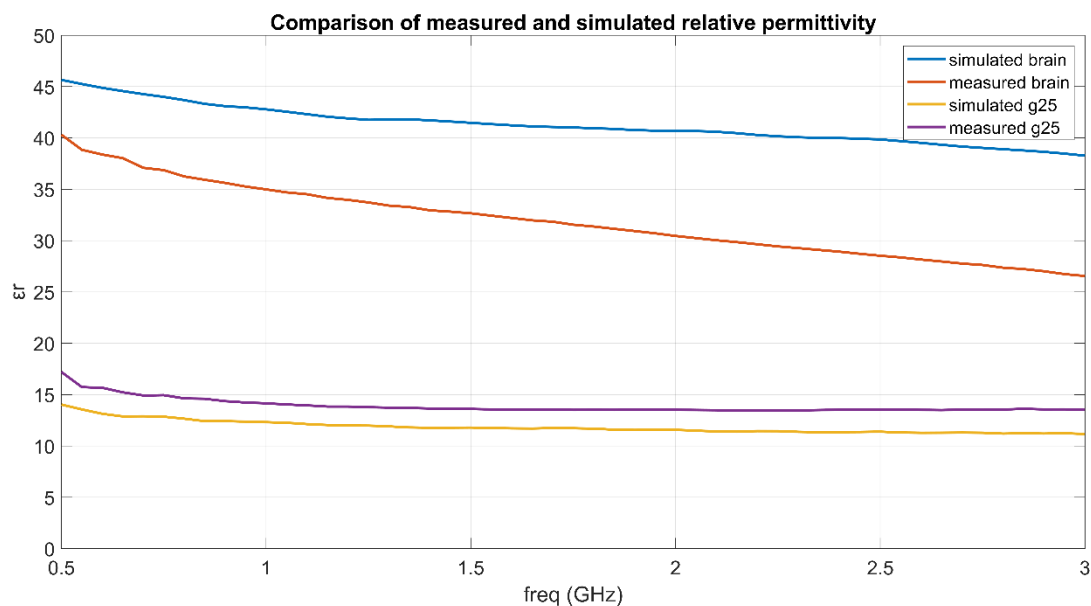

Figure 7.8 Comparison of the simulated and measured permittivity of G25 and of the brain liquid.
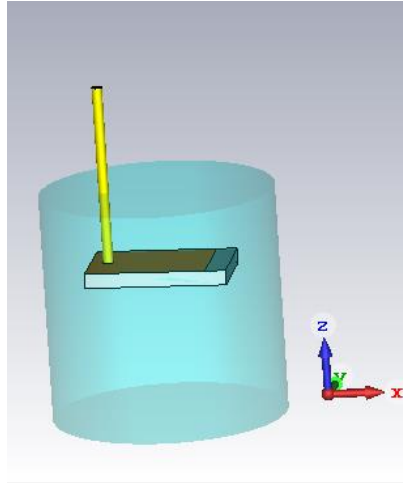
Figure 7.9 Simulation of the antenna immersed slightly in the brain liquid container. Condition that reflects better the measuring one.

Thus the *average_brain* has been simulated with a lower value of permittivity (εr=35 at 1 GHz), while for the substrate the same properties has been mantained (G25 properties). The results are reported in Figure 7.10, where it can be seen that the antenna does not resonate at 1.68 GHz as the measured one, but has two resonances, one at 0.6 GHz and one at 1.2 GHz.
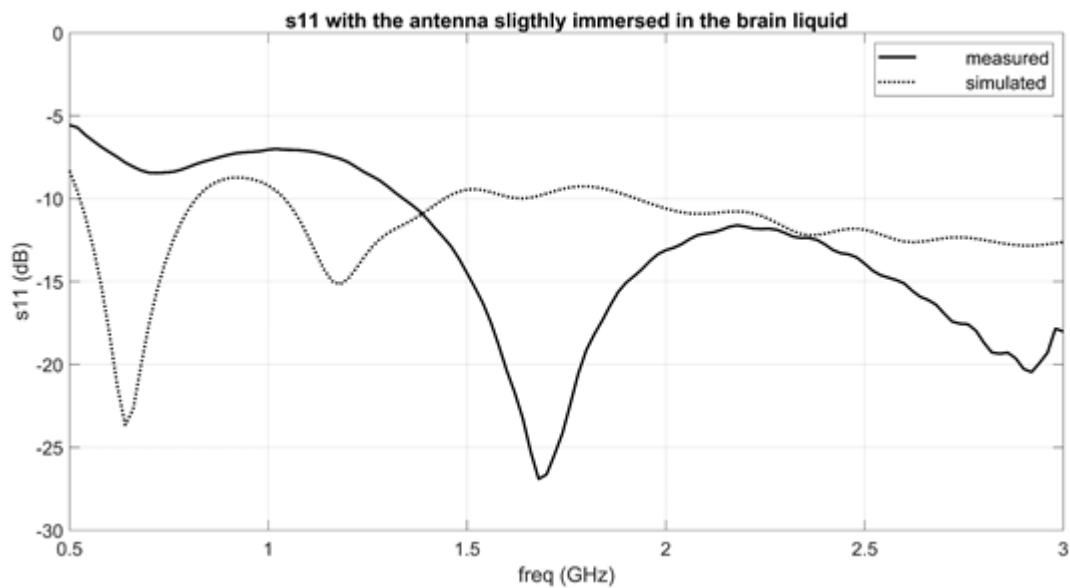
Figure 7.10 Comparison of the meaured and simulated s11 in the case in which the antenna are sligthly immersed in the brain liquid.

Many tests have also been done and what it has been seen is that it is possible to obtain the correspondence with the simulated data in the case of direct contact with the brain, that is to have resonance at 1 GHz, as shown in Figure 7.11. However, this can only be achieved by keeping the antenna in a certain position with respect to the liquid. Therefore, these results leads us to deduce that the antenna is very sensitive to what is

present in its near field and this type of measurement is problematic, not easily reproducible and repeatable, since the s11 is very variable, depending on the relative position between the surface of the antenna and the surface of the liquid and if it is immersed or not. Taking also into account the inaccuracies in the realization it can be considered that this antenna measurement is acceptable.
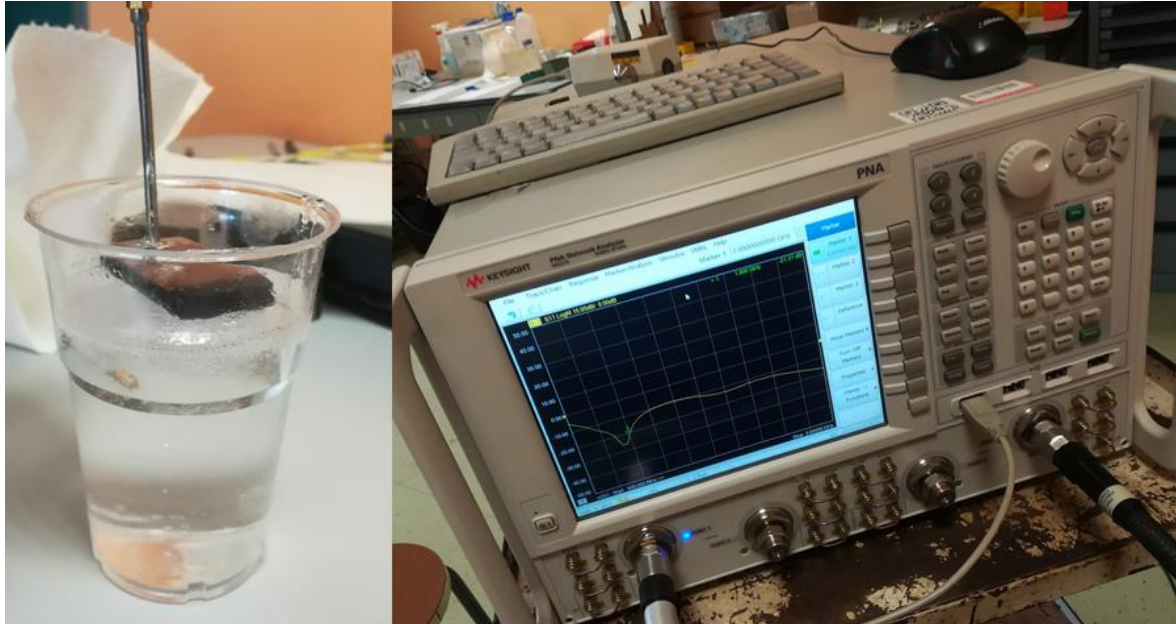

Figure 7.11: Measurement set up for evaluating the s11 on the antenna in direct contact with the brain liquid, contained in a plastic glass. As the VNA shows the antenna has a resonance at 1 GHz.

7.3.2 Measurements with the head phantom

The measurements with the phantom head has been performed with the measurement set up shown in Figure 7.12, consisting of the head phantom, the coaxial cables, the antennas and of the VNA. Measurements of the reflection and transmission coefficients has been performed in the following cases:

1. a single antenna with and without skin-mimicking layer made in G35 (2 mm thick);

2. two antennas placed on opposite sides of the head to measure performance in the case of maximum signal attenuation, in presence and in absence of the metal sphere;

3. two less distant antennas, one placed laterally and one at the top of the phantom, to measure performance in the case of lower signal attenuation, in presence and in absence of the metal sphere.

Figure 7.12 Example of a measurement set up.

1. *Single antenna measurements*

Placing the antenna in contact with the plastic material of the phantom and fixing it, first without inserting the skin-mimicking layer in G35 and then with it (see Figure 7.13), we obtain the results depicted in Figure 7.14, where the measured data are compared with simulated ones, showing that there is agreement.
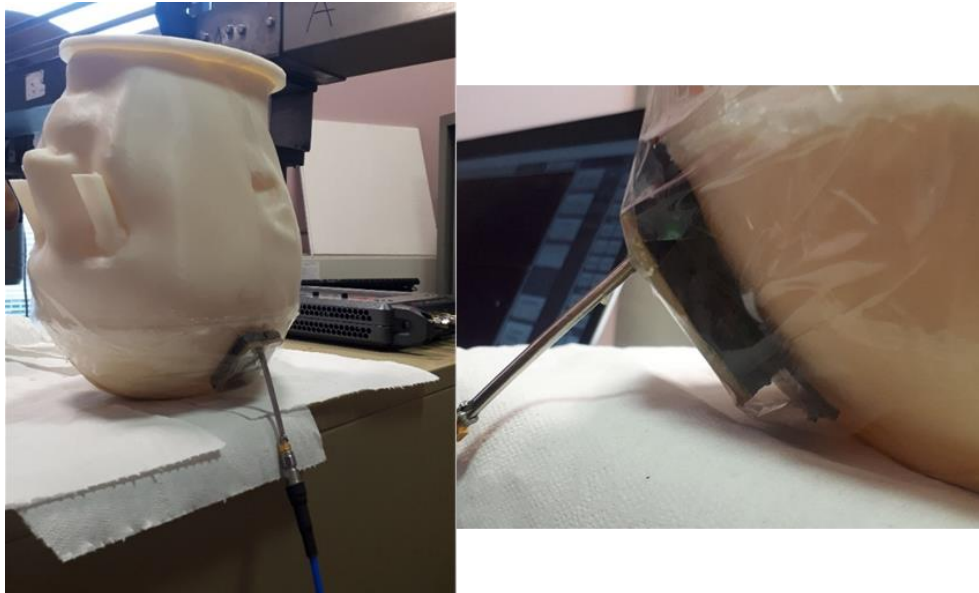

Figure 7.13 Single antenna measurement set up: antenna bended on the phantom without (left) and with (right) the G35 skin-mimicking layer.
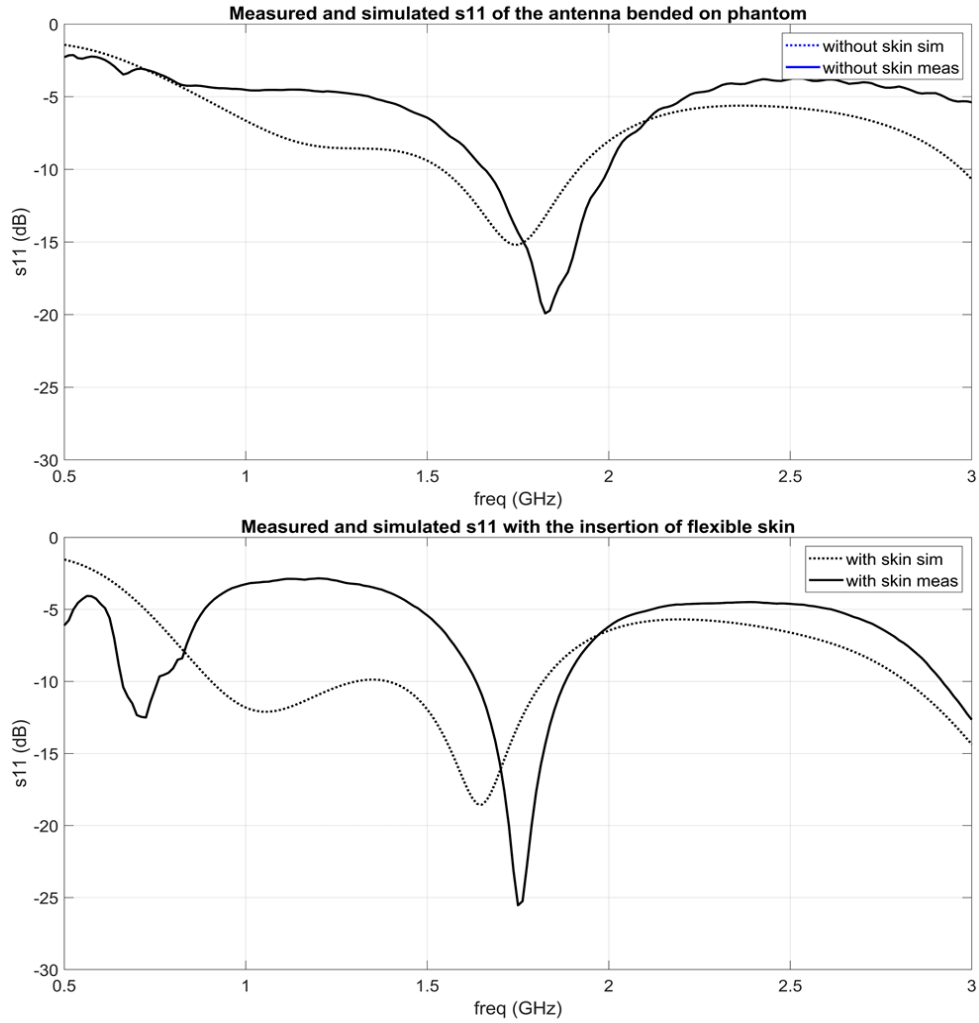
Figure 7.14 Comparison of the measured and simulated s11, with and without the skin_mimicing layer.

2. Measurements with two antennas – maximum attennuation positioning

Since the antenna has showed a better s11 thanks to the insertion of the skin-mimicking layer, the measurements of the transmission coefficient (s21 and s12) has been carried out with and without the metal sphere immersed in the brain mimicking liquid. In the case of two antennas placed at the sides of the phantom, symmetrically (see Figure 7.15), it has been obtained the s21 plot represented in Figure 7.16.
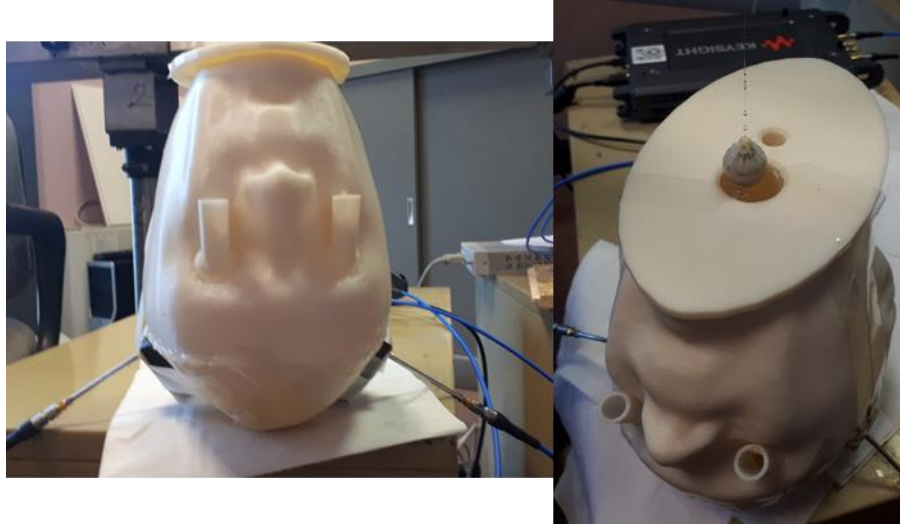
Figure 7.15 Simulation set up for the maximum attenuation case.

From the mentioned plot it can be seen that there is a good correspondence between the measured and simulated data, thus the antenna works well, with a s21 ranging from -50 dB to -65 dB.
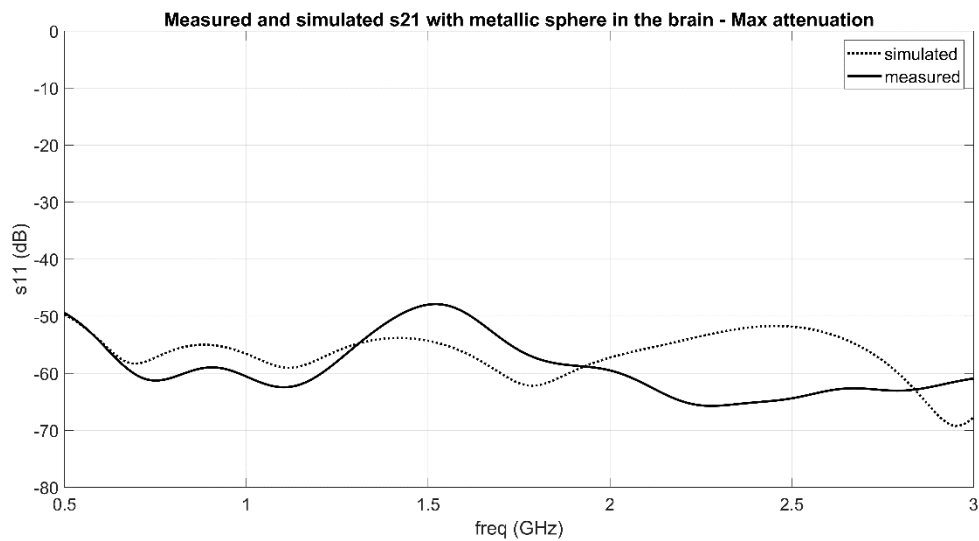
Figure 7.16 Comparison of the measured and simulated s21 with the metallic sphere in the brain, in the case of maximum attenuation.

3. *Measurements with two antennas – lower attennuation positioning*

The measurement set up for the lower attenuation case, is shown in Figure 7.17. The two antennas are closer to each other and the measured s21 signal, in the case of presence of the PEC sphere, is reported in Figure 7.18. Also in this condition there is a good agreement with the simulated data.

Figure 7.17 Measuremet set up for the lower attenuation case.
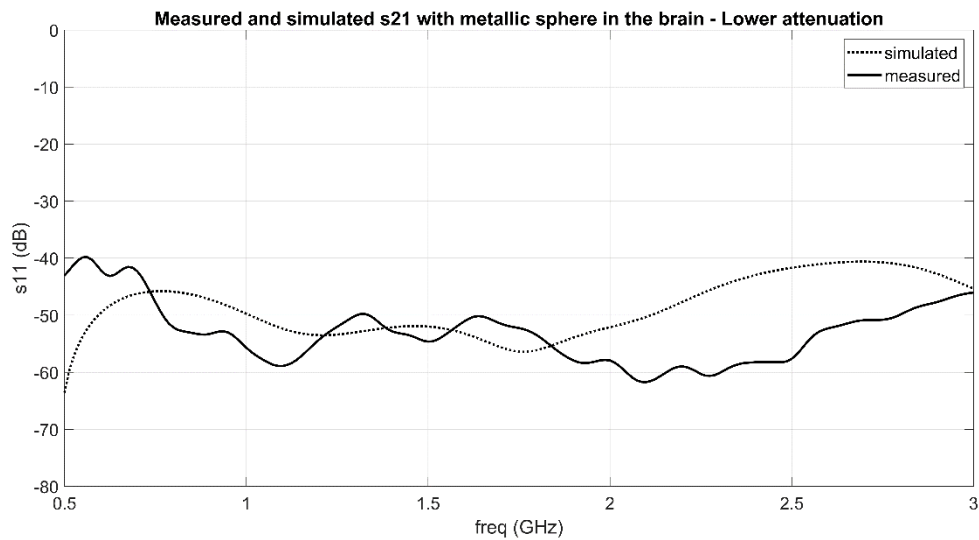
Figure 7.18 Comparison of the measured and simulated s21 with the metallic sphere in the brain, in the case of lower attenuation.

In Figure 7.19, instead, it is possible to see the diffential signal of the s21 in the two conditions, without and with the metallic sphere. It is compared to the simulation, showing a good agreement and a quite better performance, with an averaged value of – 70 dB in the range of interest (0.5-1.5 GHz).
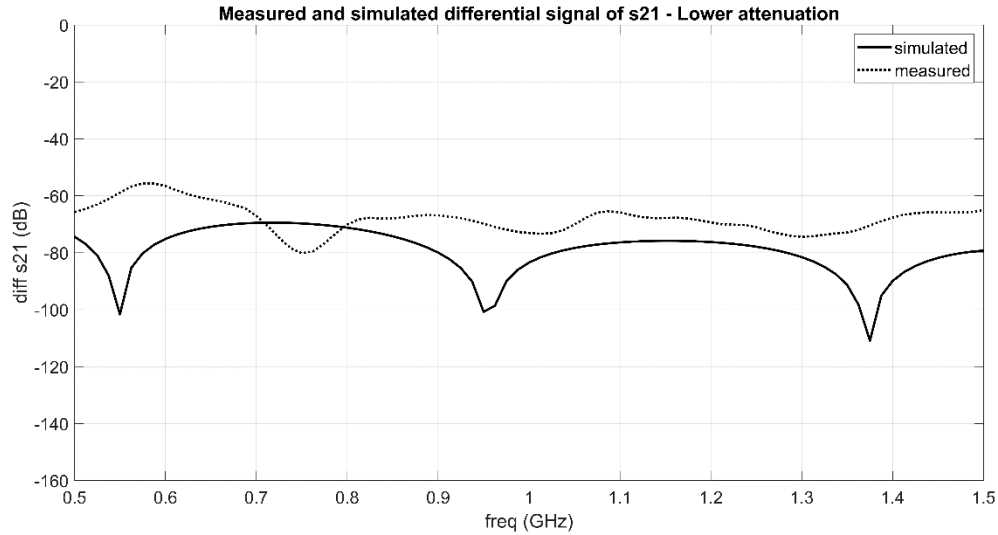
Figure 7.19 Comparison of the simulated and measured differential s21 signal.

7.4 Discussion

The manually produced antenna has a good match of results in the air and applied to the phantom head made of ABS. The only measure that shows a discrepancy is the one that reproduces the antenna in direct contact with the brain. Thus, it has been analyzed and it has been concluded that it is an acceptable discrepancy since the antenna has proved to be, both in simulation and in measurement, very sensitive to what is in its near field. Therefore, an imperfect reproduction of the condition of direct contact with the entire volume of the brain generates results that do not correspond to the simulated ones. Furthermore, the non-perfect coincidence is attributable to the inaccuracies that could have been committed in the construction phase of the individual antenna components and in the preparation of the mixture of the substrate and of the liquid that simulates the brain. It is believed that the antenna designed is able to detect the presence of objects with different permittivity than the surrounding liquid, thanks to an s21 of about -50 dB in the range of interest (0.5-1.5 GHz). The differential signal of s21, between the case of presence and absence of the metallic sphere, is also very promising, being below -100 dB.

8. Conclusion and Future Developments

In this master thesis work two antenna prototypes has been designed, one with a graphite-loaded urethane rubber substrate and the other with a Polyimide substrate. Both antennas have been successfully designed to work at 1 GHz, optimal center frequency for brain imaging, and both have shown in simulation to have performance preservation even under flexion. However, the second prototype (PI) has met an important problem, namely that of no longer being able to radiate the electromagnetic field when the antenna is placed on a head phantom made of plastic material, i.e. ABS. Furthermore, the antenna has a quite narrow bandwidth. Therefore this type of antenna has not been realized, considering that for the brain stroke imaging it is better to use antennas that have a substrate that increases the impedance matching of the antenna with the brain tissue. As in the case of the first prototype. The antenna designed was made in the laboratory, demonstrating good agreement between the measured and simulated data.

The future work could consist in the impovement of the antenna construction procedure and in a further study of the materials.

9. Bibliography

[1] [Online]. Available: https://www.stroke.org/en/about-stroke.

[2] [Online]. Available: https://www.medicalnewstoday.com/articles/7624.php.

[3] G. Donnan, M. Fisher, M. Macleod and S. Davis, "Stroke," *The Lancet,* vol. 371, no. 9624, p. 1612–1623, 2008.

[4] A. Cavallini, G. Micieli, S. Marcheselli and S. Quaglini, "Role of monitoring in management of acute ischemic stroke patients," *Stroke,* no. 34, pp. 2599-2603, 2003.

[5] A. Rocco, M. Pasquini, E. Cecconi and G. Sirimarco, "Monitoring after the acute stage of stroke: a prospective study," *Stroke,* no. 38, p. 1225–1228, 2007.

[6] J. Gubbi, A. Rao, K. Fang, B. Yan and M. Palaniswami, "Motor recovery monitoring using acceleration measurements in post acute stroke patients," *Biomed Engineering OnLine ,* vol. 12, no. 33, 2013.

[7] R. Scapaticci, M. Bjelogrlic, J. Tobon, F. Vipiana, M. Mattes and L. Crocco, "Microwave technology for brain imaging and monitoring: Physical foundations, potential and limitations," in *Emerging Electromagnetic Technologies for Brain Diseases Diagnostics, Monitoring and Therapy*, Cham, Springer, 2018, pp. 7-35.

[8] P. deAzevedo-Marques, A. Mencattini, M. Salmeri and R. Rangayyan, Medical Image Analysis and Informatics: Computer-aided Diagnosis and Therapy, Boca Raton: CRC Press, 2017, pp. 451-466.

[9] I. Sarwar, G. Turvani, M. Casu, J. Tobon, F. Vipiana, R. Scapaticci and L. Crocco, "Low-Cost Low-Power Acceleration of a Microwave Imaging Algorithm for Brain Stroke Monitoring," *Journal of Low Power Electronics and Applications,* vol. 8, p. 43, 2018.

[10] M. Cayoren and I. Akduman, "Continuous monitoring of hemorrhagic strokes via differential microwave imaging," in *Emerging electromagnetic technologies for brain diseases diagnostics, monitoring and therapy*, Cham, Springer, 2018, pp. 37-57.

[11] A. Alqadami, N. Nguyen-Trong, . B. Mohammed, M. Tobias and A. Abbosh, "Compact Unidirectional Conformal Antenna Based on Flexible High Permittivity Custom-made Substrate for Wearable Wideband Electromagnetic Head Imaging System," *Transactions on Antennas and Propagation,* 2019.

[12] M. Persson, A. Fagher, H. Trefna, Y. Yu, T. McKelvey, G. Pegenius, J.-E. Karlsson e M. Elam, «Microwave-Based Stroke Diagnosis Making Global Prehospital Thrombolytic Treatment Possible,» *IEEE TRANSACTIONS ON BIOMEDICAL ENGINEERING,* vol. 61, n. 11, p. 2806–2817, 2014.

[13] "EMTensor," 2018. [Online]. Available: http://www.emtensor.com/applications/bedside-brain-imaging/.

[14] R. Orta, "Lecture Notes on Transmission Line Theory - Department of Electronics and Telecommunications," Politecnico di Torino, 2017.

[15] [Online]. Available: https://nptel.ac.in/content/storage2/courses/117101057/downloads/lec16.pdf.

[16] [Online]. Available: https://en.wikipedia.org/wiki/Monopole_antenna.

[17] I. Saied e T. Arslan, «Wideband Textile Antenna for Monitoring Neurodegenerative Diseases,» in *IEEE 29th Annual International Symposium on Personal, Indoor, and Mobile Radio Communications (PIMRC)*, 2018.

[18] H. Bahramiabarghouei, E. Porter, A. Santorelli, B. Gosselin, M. Popovic e L. Rusch, «Flexible 16 Antenna Array for Microwave Breast Cancer Detection,» *IEEE TRANSACTIONS ON BIOMEDICAL ENGINEERING,* vol. 62, n. 10, 2015.

[19] R. Scapaticci, L. DiDonato, I. Catapano and L. Crocco, "A FEASIBILITY STUDY ON MICROWAVE IMAGING FOR BRAIN STROKE MONITORING," *Progress In Electromagnetics Research ,* vol. 40, pp. 305-324, 2012.

[20] J. Tobon, R. Scapaticci, G. Turvani, G. Bellizzi, N. Joachimowicz, B. Duchene, E. Tedeschi, M. Casu, L. Crocco and F. Vipiana, "Design and Experimental Assessment of a 2-D Microwave Imaging System for Brain Stroke Monitoring," *International Journal of Antennas and Propagation,* 2019.

[21] R. Scapaticci, J. Tobon, F. Vipiana, G. Bellizzi and L. Crocco, "Design and Numerical Characterization of a Low-Complexity Microwave Device for Brain Stroke Monitoring," *IEEE TRANSACTIONS ON ANTENNAS AND PROPAGATION,* vol. 66, no. 12, pp. 7328-7338, 2018.

[22] J. Tobon, R. Scapaticci, G. Bellizzi, G. Turvani, N. Joachimowicz, B. Duchene, E. Tedeschi, M. Casu, L. Crocco and F. Vipiana, "Design, Realization and Experimental Testing of a Microwave Brain Scanner for Cerebrovascular Diseases Monitoring," in *Riunione GTTI-SIEm*, Pavia, 2019.

[23] S. Semenov and D. Corfield, "Microwave Tomography for Brain Imaging: Feasibility Assessment for Stroke Detection," *International Journal of Antennas and Propagation ,* 2008.

[24] [Online]. Available: http://www.misumiusa.com/categoryimages/metric_2009_pdf/p1483.pdf.

[25] N. Joachimowicz, B. Duchêne , C. Conessa and O. Meyer , "Anthropomorphic Breast and Head Phantoms for Microwave Imaging," *Diagnostics,* vol. 8, no. 85, 2018.

[26] J. Liu, F. Dai, Y. Zhang and X. Yu, "Monopole quasi-Yagi antenna on polyimide substrate for flexible electronics," in *Proceedings of SPIE*, Nanjing, 2019.

[27] H. Khaleel, H. Al-Rizzo and A. Abbosh, "Design, Fabrication, and Testing of Flexible Antennas," in *Advancement in Microstrip Antennas with Recent Applications*, 2013.

[28] [Online]. Available: https://www.healthlinkbc.ca/health-topics/TP12720.

[29] World Health Organization, "Global Health Estimates 2016: Deaths by Cause, Age, Sex, by Country and by Region, 2000-2016," Geneva, 2018.

[30] [Online]. Available: https://www.starimagingindia.com/blog/difference-between-mri-scan-and-a-ct-scan/.

[31] [Online]. Available: https://ietbuildinghealth.com/blog/emf-rf-radiation/.

[32] A. Hamidipour, T. Henriksson, M. Hopfer, R. Planas and S. Semenov, "Electromagnetic tomography for brain imaging and stroke diagnostics: progress towards clinical application," in *Emerging electromagnetic technologies for brain diseases diagnostics, monitoring and therapy*, Cham, Springer, 2018, pp. 59-85.